

**Structure-Function-Analysis of Pathogenicity Associated
Proteins YopP of *Yersinia enterocolitica* and Rv2140c of
*Mycobacterium tuberculosis***

DISSERTATION

zur Erlangung des akademischen Grades eines Doktors der
Naturwissenschaften (Dr. rer. nat.) am

Fachbereich Chemie

der Universität Hamburg

vorgelegt von

Dipl. Chem. Georg Graf zu Eulenburg
Aus Marburg/Lahn, Deutschland

Hamburg, Oktober 2013

Die Wissenschaft fängt eigentlich erst da an interessant zu werden, wo sie aufhört.

Justus Liebig

Diese Arbeit wurde von Dezember 2009 bis Juli 2013 an der Hamburger Außenstelle des Europäischen Labors für Molekularbiologie (EMBL) in der Arbeitsgruppe von Dr. M. Wilmanns durchgeführt. Die Arbeit wurde von Prof. Dr. Ch. Betzel vom Fachbereich Chemie der Universität Hamburg betreut.

1. Gutachter: **Prof. Ch. Betzel**

2. Gutachter: **Dr. M. Wilmanns**

Tag der Disputation: 8.11.2013

Abstract

YopP

Human pathogenic *Yersinia* spp. translocate the acetyltransferase *Yersinia* Outer Protein P (YopP) in host immune cells, where it suppresses the expression and secretion of pro-inflammatory cytokines and contributes to the induction of apoptosis. YopP is activated through binding to the host factor IP6 and uses acetyl-CoA as a cofactor to acetylates serine and threonine residues in the activation loop of kinases, which prevents phosphorylation of these residues and the activation of the kinases.

Binding constants of YopP to its activator IP6 as well as to CoA were determined to be in the low μM range and the energetic profile of the YopP/CoA/IP6 interaction suggests cooperativity in binding events if both ligands are present. The C-terminus of YopP was found to undergo self-degradation. Binding of IP6 to YopP protects the C-terminus of YopP partially from limited proteolysis, suggesting that the C-terminus is partially intrinsically disordered prior to IP6 binding. Attempts to crystallize YopP in order to get a high resolution X-ray crystal structure failed. Full length YopP as well as several truncated constructs tended to aggregate and precipitate easily. Despite numerous efforts aggregation and precipitation of YopP could not be prevented by binding to its ligands or by use of optimized buffers. A homologous protein, *Salmonella enterica* AvrA also failed to form protein crystals.

The poor stability of YopP suggests that further bacterial and/or host factors are required to stabilize YopP. Bacterial proteins SycO and orf91a were tested for their possible interaction with YopP, but no interaction with YopP was observed under the conditions tested. It was also determined that YopP does not form a stable complex with its human kinase target MEK2.

A colorimetric assay, which allows the investigation of the kinetics of the acetylation reaction of MEK2 by YopP was established. It was shown that YopP undergoes auto-acetylation in presence of acetyl-CoA independent of the kinase substrate. The auto-acetylation step is accelerated significantly by IP6. The acetyl

transfer from YopP to the kinase does not follow simple Michaelis-Menten kinetic mechanism; instead it appears to follow a complicated multi substrate reaction mechanism. The assay suggests that a slow monoacetylation MEK2 precedes a faster acetylation of the second acetylation site. The physiological relevance and consequences of monoacetylated kinases remains to be determined.

Rv2140c

Expression of *Mycobacterium tuberculosis* (Mtb) protein Rv2140c is up-regulated in the phagocytosed Mtb. A crystal structure revealed that Rv2140c could be a phosphatidyl-ethanoamine (PE) binding protein and NMR experiments suggest, that it binds to the cell migration inhibitor locostatin. Binding studies with a number of short chain PE analogues revealed a low mM affinity of the Rv2140c/PE interaction, which confirmed that Rv2140c is a PE binding protein. To investigate the *in vivo* significance Rv2140c, a mutant strain of *Mycobacterium smegmatis* was generated, where the homologue of Rv2140c, MSMEG_4199 was deleted. The growth of *M. smegmatis* is not impaired by the deletion of MSMEG_4199 and addition of locostatin affects both the growth of wild type and mutant strain in the same manner, suggesting that locostatin has other mycobacterial interaction partners, which overrule the effect of locostatin on MSMEG_4199.

Zusammenfassung

YopP

Humanpathogene *Yersinia* spp. translozieren die Acetyltransferase *Yersinia* Outer Protein P YopP in humane Immunzellen. YopP verhindert die Expression und Sekretion von entzündungsfördernden Zytokinen durch Immunzellen und trägt zur Induktion von Apoptose in diesen Zellen bei. YopP wird durch das Wirtsmolekül IP6 aktiviert und verwendet Acetyl-CoA als Ko-Faktor um Serin und Threonin Seitenketten in der Aktivierungsschleife von Kinasen zu acetylieren. Die Acetylierung dieser Aminosäuren verhindert deren Phosphorylierung und somit die Aktivierung dieser Kinasen.

Die Bindungskonstanten von YopP zu seinem Aktivator IP6 sowie zu CoA wurden bestimmt und liegen im Bereich von wenigen μM . Das energetische Profil der YopP/CoA/IP6 Wechselwirkung deutet auf eine Kooperativität der Bindung der beiden Liganden hin. Der carboxyterminale Bereich von YopP scheint intrinsisch ungeordnet zu sein und degradiert über einen Zeitraum. Das Binden von IP6 an YopP verhindert weitgehend den carboxyterminalen Abbau von YopP durch Proteasen. Versuche YopP zu kristallisieren um eine hochauflösende Röntgenkristallstruktur zu erhalten waren nicht erfolgreich. Sowohl das Vollängenprotein, als auch verschiedene verkürzte Proteinkonstrukte erwiesen sich als hochgradig instabil und neigten zu Aggregation und Präzipitation. Weder Bindung zu Liganden noch die Verwendung von verschiedenen Puffersystemen konnte YopP stabilisieren. Ebenso schlugen Versuche fehl, *Salmonella enterica* AvrA, ein homologes Protein zu kristallisieren.

Die Instabilität von YopP könnte bedeuten, dass weitere bakterielle- oder Wirtsfaktoren benötigt werden, um YopP zu stabilisieren. Die bakteriellen Proteine SycO und orf91a wurden auf eine mögliche Interaktion mit YopP untersucht, aber unter den experimentellen Bedingungen konnte keine Wechselwirkung festgestellt werden. Ebenso wurde festgestellt, dass YopP keinen stabilen Komplex mit der humanen Kinase MEK2 bildet.

Es wurde eine kolorimetrische Methode etabliert, die es erlaubt, die Kinetik der Acetyltransferasereaktion zu untersuchen. Dabei wurde herausgefunden, dass IP6 die Selbstacetylierung von YopP, welche dem Acetyltransfer auf die Kinase vorausgeht, hochgradig beschleunigt. Die Acetylierung der Kinase folgt nicht einem Michaelis-Menten Mechanismus, stattdessen legen die Ergebnisse nahe, dass es sich um einen komplizierteren Mehrsubstratmechanismus handelt. Darüber hinaus deuten die Ergebnisse an, dass die erste und die zweite Acetylierung der Kinase durch YopP mit unterschiedlichen Reaktionsgeschwindigkeiten erfolgen und zuerst eine vollständige Monoacetylierung von YopP erfolgen muss, bevor die Acetylierung des zweiten Serins erfolgt. Die physiologische Bedeutung und Aktivität einer monoacetylierten Kinase muss sich in der Zukunft erweisen.

Rv2140c

Das Protein Rv2140c von *Mycobacterium tuberculosis* erscheint in Bakterien, die von Immunzellen aufgenommen wurden hochreguliert. Eine Kristallstruktur von Rv2140c legt nahe, dass Rv2140c ein Phosphatidylethanolamin (PE) bindendes Protein sein könnte und NMR Bindungsstudien deuten darauf hin, dass Rv2140c mit Locostatin, einem Zellmigrationsinhibitor wechselwirkt. In ITC Bindungsstudien von Rv2140c mit einer Reihe von PE Analogen wurde gezeigt, dass Rv2140c diese mit einer geringen mM Affinität binden kann und somit bestätigt, dass Rv2140c ein PE bindendes Protein ist. Um die Bedeutung von Rv2140c besser zu verstehen, wurde eine Deletion des homologen Gens MSMEG_4199 des verwandten *Mycobacterium smegmatis* durchgeführt. Dabei zeigte sich, dass das Wachstum von *M. smegmatis* unter den getesteten Bedingungen nicht von der Deletion von MSMEG_4199 beeinträchtigt wird und dass bei Zugabe von Locostatin das Wachstum des Wildtyps und der Deletionsmutanten in gleicher Weise beeinträchtigt sind. Das deutet darauf hin, dass der Effekt von Locostatin auf MSMEG_4199 durch andere Effekte von Locostatin auf *M. Smegmatis* überdeckt sein könnte.

I. Table of contents

Abstract	vi
Zusammenfassung	viii
I. Table of contents	x
II. Abbreviations	xiii
1 Introduction	1
1.1 Yersinia spp.	1
1.2 Clinical disease	1
1.2.1 Bubonic plague	1
1.2.2 Enterocolitis	1
1.3 Immune response towards bacteria	2
1.3.1 Innate immune response	3
1.3.2 Adaptive response	4
1.4 Virulence	5
1.4.1 Adhesion and translocation of <i>Yersinia</i> cells.....	5
1.4.2 Type Three Secretion System (TTSS).....	5
1.4.3 Mechanism of Translocation	7
1.4.4 Effector proteins.....	8
1.5 YopP	11
1.5.1 Downregulation of Cytokines.....	11
1.5.2 Disruption of MAPK/NF- κ B Signalling Networks	11
1.5.3 Mechanism	11
1.5.4 Induction of cell death by YopP.....	13
1.5.5 Induction of barrier dysfunction	15
1.5.6 Effect on adaptive immune response	15
1.6 Conclusion and open questions	15
1.7 Rv2140c	16
1.7.1 Mycobacterium tuberculosis.....	16
1.7.2 Clinical manifestation	17
1.7.3 Virulence factors.....	17
1.7.4 Latency and reactivation.....	18
1.7.5 Drug discovery.....	18
1.7.6 Rv2140c.....	18
2 Aim of the Work	20
3 Materials and Methods	22
3.1 Materials	22
3.1.1 Chemicals, Consumables, Equipment.....	22
3.1.2 Plasmid Vectors.....	23
3.1.3 Bacterial strains	24
3.1.4 Oligonucleotide primers.....	25
3.2 Media, Buffers and Stock solution	26
3.2.1 Media	26
3.2.1.1 <i>E. coli</i> media	26
3.2.1.2 <i>M. smegmatis</i> media.....	27
3.2.2 Buffers	28
3.2.3 Protein purification buffers	28
3.2.4 Southern blot buffers.....	28

Table of contents

3.2.5	Stock solutions 1000x	29
3.3	Methods.....	30
3.3.1	Molecular Biology.....	30
3.3.1.1	Polymerase Chain Reaction (PCR)	30
3.3.1.2	Ligase Independent cloning (LIC)	31
3.3.1.3	Site directed mutagenesis.....	32
3.3.1.4	Restriction free cloning.....	32
3.3.2	Production and purification of protein.....	33
3.3.2.1	Production of recombinant protein.....	33
3.3.2.2	Protein purification	33
3.3.2.2.1	IMAC	33
3.3.2.2.2	Size-exclusion chromatography	34
3.3.2.2.3	Ion exchange chromatography.....	34
3.3.3	Reductive methylation of Protein	34
3.3.4	Protein characterization.....	34
3.3.4.1	Estimation of protein concentration.....	34
3.3.5	SDS-PAGE.....	35
3.3.6	N-terminal sequencing.....	35
3.3.7	Dynamic Light scattering.....	35
3.3.8	Protein crystallisation.....	35
3.3.9	Creation of <i>M. smegmatis</i> knockout strain	37
3.3.9.1	Creation of the KO vector	37
3.3.9.2	Transformation of <i>M. smegmatis</i> -wt with KO vector	37
3.3.10	Southern Blot.....	38
3.3.10.1	Preparation of the hybridization probe	39
3.3.11	Unmarking of the MSMEG Δ 4199	39
3.3.12	Growth curve of MSMEG 4199.....	39
3.4	Biophysical Methods.....	39
3.4.1	Isothermal Titration Calorimetry (ITC).....	39
3.4.2	Circular Dichroism Spectroscopy.....	41
3.4.3	Acetylation assays.....	41
3.4.3.1	Michaelis-Menten Kinetics	42
4	Results.....	44
4.1	YopP.....	44
4.1.1	Expression and purification of YopP.....	44
4.1.2	Self-degradation.....	45
4.1.3	Biophysical and biochemical characterization of YopP	46
4.1.3.1	CD-Spectroscopy	46
4.1.3.2	Investigation of Binding to Ligands.....	48
4.1.3.2.1	Binding of YopP with IP6.....	48
4.1.3.2.2	Binding of YopP with CoA.....	49
4.1.3.2.3	Binding YopP/Co-A with IP6.....	50
4.1.3.3	Limited proteolysis.....	51
4.1.3.4	N-terminal sequencing.....	52
4.1.4	Crystallization experiments with YopP	54
4.1.4.1	Bioinformatic analysis.....	54
4.1.4.2	Crystallization trials with full length YopP.....	57
4.1.4.3	Co-crystallisation of YopP and small molecule ligands.....	58
4.1.4.4	Investigation of YopP aggregation by DLS.....	59
4.1.4.5	Buffer optimization.....	60
4.1.4.6	Reductive Methylation of YopP-1-288.....	61
4.1.4.7	Crystallization trials with truncated constructs of YopP	63
4.1.4.8	Crystallization of proteolysed YopP	64
4.1.4.9	In situ crystallisation.....	65
4.1.4.10	Crystallization trials with YopP homologue AvrA.....	65
4.1.5	Interaction with Chaperones.....	67

Table of contents

4.1.5.1	Expression and purification of potential chaperones.....	68
4.1.5.1.1	Expression and purification of orf91a	68
4.1.5.1.2	Expression and purification of orf155a (SycO).....	69
4.1.5.2	Co-expression of YopP and and potential chaperones.....	70
4.1.5.2.1	Co-expression of YopP with SycO	70
4.1.5.2.2	Co-expression of YopP orf91a	72
4.1.6	Investigating the YopP/MEK2 interaction	73
4.1.6.1	Expression and Purification of MEK2	73
4.1.6.2	YopP/MEK2 interaction.....	74
4.1.7	Co-crystallisation trials with YopP and MEK2.....	76
4.1.8	Co-expression of YopP and MEK2	77
4.1.8.1	Up-scaling of Co-expression.....	78
4.1.8.1.1	YopP-wt/MEK2S222/226A.....	79
4.1.8.1.2	YopP-C172A/MEK2-wt	79
4.1.9	Mass spectrometric analysis of the acetylation of MEK2 by YopP.....	80
4.1.10	Kinetic analysis of the acetlyation reaction.....	81
4.1.10.1	The effect of Elmann’s reagent on YopP/MEK2/acetyl-CoA mixtures	81
4.1.11	Steady state kinetic analysis of YopP/MEK2 acetylation	82
4.1.12	Lineweaver-Burk plot.....	85
4.1.13	Dissecting the reaction mechanism.....	86
4.1.14	Reaction of YopP with acetyl-CoA	86
4.1.15	Time Course Analysis of MEK2 Acetylation	90
4.2	Rv2140c.....	92
4.2.1	Interaction of Rv2140c with PE analogues and Locostatin	92
4.2.2	Influence of locostatin and the Rv2140c homologues MSMEG_4199 on <i>M. smegmatis</i> growth.....	95
4.2.2.1	Creation of a Δ MSMEG_4199 knock out mutant	95
4.2.3	Growth curves of of wt <i>M. smegmatis</i> and Δ MSMEG_4199 knock out in presence and absence of locostatin.	99
5	Discussion.....	101
5.1	YopP.....	101
5.1.1	Binding to Ligands IP6 and CoA.....	101
5.1.2	Self degradation and N-terminal sequencing.....	102
5.1.3	Crystallization.....	102
5.1.4	Interaction with Chaperones.....	105
5.1.5	YopP/MEK2 interaction	106
5.1.6	Acetylation reaction	107
5.2	Discussion Rv2140c	111
III.	Literature	112
IV.	Risk and Safety Statements.....	xiii
V.	Appendix.....	xiii
	Acknowledgements	xiii
	Curriculum Vitae	xv
	Publications:	xvi
	Conferences, Poster Presentations and Talks.....	xvi
	Erklärung	xviii

II. Abbreviations

aa	amino acid
acetyl CoA	acetyl coenzyme A
ADC	albumin dextrose catalase
BID	BH3 interacting-domain death agonist
bp	base pair
CARB	carbenicillin
CD	circular dichroism
CHX	cycloheximide
CREB	cAMP response element-binding protein
Cryo-EM	cryo-electron-microscopy
Da	dalton
DAMP	danger associated molecular pattern
dATP	deoxyadenosine triphosphate
ddH ₂ O	double distilled water MilliQ quality
DHPA	1,2-dihexanoyl-sn-glycero-3-phosphate
DHPE	1,2-dihexanoyl-sn-glycero-3-phosphoethanolamine
DHPG	1,2-dihexanoyl-sn-glycero-3-phospho-(1'-rac-glycerol)
DHPS	1,2-dihexanoyl-sn-glycero-3-phospho-L-serine
DIG	digoxigenin
DMSO	dimethyl sulfoxide
DNA	deoxyribonucleic acid
DNase	deoxyribonuclease
DTNB	5,5'-dithiobis-(2-nitrobenzoic acid)
dTTP	deoxythymidine triphosphate
EDTA	ethylenediaminetetraacetic acid
ERK1	extracellular signal-regulated kinase 1
FADD	fas-Associated protein with Death Domain
fw	forward
GST	glutathion-S-transferase
GTPase	guanosin triphosphate hydrolase

Abbreviations

	nuclear factor of κ light polypeptide gene enhancer in B-
I κ B α	cells inhibitor α
IKK- β	inhibitor of nuclear factor κ -B kinase subunit β
IL	interleukin
IMAC	immobilized metal ion affinity chromatography
Inv	invasin
IP6	inositolhexakisphosphate, phytic acid
IRAK	interleukin-1-receptor-associated-kinase
ITC	isothermal titration calorimetry
JNK	c-Jun N-terminal kinase
KAN	kanamycin
LcrF	thermoregulator LcrF (Low calcium response)
LcrV	virulence-associated V antigen
LPS	lipopolysaccharide
LRR	leucine rich repeat
M-cell	microfold cell
MAPK	mitogen activated protein kinase
MDP	muramy-dipeptide
MyD88	myeloid-differentiation primary-response-gene-88
	nuclear-factor- κ -light-chain-enhancer-of-activated-B-
NF- κ B	cells
NMR	nuclear magnetic resonance
	nucleotide-binding oligomerization domain-containing
Nod2	protein 2
NTA	nitrilotriacetic acid
p38	P38 mitogen-activated protein kinase
PAGE	polyacrylamide gel electrophoresis
PAMP	pathogen associated molecular pattern
PCR	polymerase chain reaction
pI	isoelectric point
pYV	plasmid of Yersinia virulence
rev	reverse

Abbreviations

RICK	receptor-interacting serine/threonine-protein kinase
RNA	ribonucleic acid
RovA	regulator of virulence protein A
SDS	sodium dodecyl sulfate
SEC	size-exclusion chromatography
SNP	single nucleotide polymorphism
SUMO	small ubiquitin like modifier
TAB	TAK1 binding protein
TAK1	transforming-growth-factor- β -activated-kinase-1
TET	tetracyclin
TLR	toll like receptor
TNF α	tumor necrosis factor α
TRAF6	TNF-receptor-associated-factor-6
TRIF	toll/IL-R domain-containing adaptor-inducing IFN- β
Tris	tris(hydroxymethyl)aminomethane
TTSS	type three secretion system
Ulp1	ubiquitin like protease 1
YadA	<i>Yersinia</i> adhesin A
YE	<i>Yersinia enterocolitica</i>
YmoA	<i>Yersinia</i> modulator A
Yop	<i>Yersinia</i> outer protein
YP	<i>Yersinia pestis</i>
YPT	<i>Yersinia pseudotuberculosis</i>
Spp	species
NLR	Nod-like-receptor

1 Introduction

1.1 *Yersinia* spp.

The genus *Yersinia* comprises 17 species (spp) of gram-negative bacteria belonging to the enterobacteriaceae family [1], [2]. The three human pathogenic *Yersinia* spp. are *Y. pestis* (YP), *Y. pseudotuberculosis* (YPT) and *Y. enterocolitica* (YE). YP is the causative agent of the bubonic plague, whereas YPT and YE are responsible for predominantly nonfatal self-limiting enteritis, which usually does not require a treatment with antibiotics. Despite the fact that they cause a disease with similar symptoms, YE and YPT are genetically diverse, the last common ancestor was estimated to have existed 0.4 -1.9 million years ago [3]. YP is genetically much less diverse than YE and YPT and has apparently emerged 1500 to 20000 years ago from a YPT [4], [5] and can be considered a subspecies of YPT. YP has acquired a few genes which allow the colonization of – and transmission from its flea vector [6]. Despite the different mode of proliferation, all three human pathogenic *Yersinia* spp. share a tropism for lymphatic tissue.

1.2 Clinical disease

1.2.1 Bubonic plague

YP caused several pandemics of the bubonic plague, the most notable were the Justinian Plague, starting in 542 and the Black Death starting in 1346. Each pandemic lead to a reduction of the population of up to 50% in the affected regions [7].The Third Pandemic started in 1855 in China. It quickly spread throughout the country, and reached Hong Kong in 1894 where YP was first isolated by Alexandre Yersin [8] and Shibasaburo Kitasato [9]. Without antibiotic treatment the Bubonic Plague has a mortality rate of 95% of infected individuals [10]. Since the 1990s thousands of cases occurred mainly in developing countries with mortalities between 1 and 17% [11].

1.2.2 Enterocolitis

YPT and YE are foodborne pathogens usually taken up with contaminated food or water [12]. However, contact with infected animals [13] was also reported to

cause human infections. YE and YPT can be divided into six and four biotypes respectively [14], depending on their ability to ferment different carbohydrates and numerous serotypes [15], depending on variations within their lipopolysaccharides (LPS) and flagellar apparatus. The pathogenicity [16] and geographical distribution of YE and YPT is highly dependant on the respective bio- and serotype [17] with YE biotype 1b serotype O:8 being the agent of the most severe disease. The manifestations of a YE or YPT infection of the gastrointestinal tract are enterocolitis, terminal ileitis, mesenteric lymphadenitis, pseudoappendicitis and less often bacteremia [18]. In healthy individuals YE and YPT infections are self-limiting and cleared with an inflammatory response, which can include fever, abdominal pain, vomiting and bloody diarrhoea [16]. In immunocompromised patients however, septicemia and systemic infections show mortality rates of up to 50% [18].

Interestingly, YE and YPT colonize predominantly the Peyer's Patches (PP), an assembly of lymphoid follicles in the terminal ileum [19] and the underlying lymphatic tissue, even though these follicles are guarded by a large number of immune cells. YE forms visible colonies in the PP within 19 h post infection and colonizes the entire patch within 4 days [20]. Over the last 30 years significant progress has been made towards uncovering the molecular basis of *Yersiniae* pathogenicity and interaction with the host.

1.3 Immune response towards bacteria

After crossing the intestinal epithelial cell barrier and entering the lamina propria, commensal and pathogenic bacteria are confronted with a variety of immune cells such as macrophages [21] and dendritic cells [22], which attempt to phagocytose [23] and kill the intruders and to launch the innate and adaptive immune response. Contact with pathogenic bacteria triggers a comprehensive activation program [24] in macrophages and dendritic cells to mount the immune response. This involves the expression and secretion of a broad range of cytokines, inducible enzymes and survival factors as well as the induction of cell death programs. Cytokines and their subaltern effects constitute a complex signaling network, which allows the immune cells to communicate with each other, to amplify or reduce inflammatory signals, to launch a localized

inflammation and to end the inflammation after the pathogens are eliminated [25], [26]. The expression of cytokines is regulated by mitogen-activated-protein-kinases (MAPK) and nuclear-factor- κ -light-chain-enhancer-of-activated-B-cells (NF- κ B) signalling, which is embedded in large dynamic regulatory complexes, located at the cytosolic side of the cell membrane [27].

1.3.1 Innate immune response

Macrophages and other immune cells detect bacteria with several pattern recognition receptors such as Toll-like-receptors (TLR) and nucleotide-binding oligomerization-domain-containing-protein (NOD) like receptors (NLR), which sense pathogen associated molecular patterns (PAMPs) such as lipopolysaccharide (LPS), flagellin, Type Three Secretion System (TTSS) components such as the YopB/YopD pore complex, muramyl-dipeptide (MDP) [28]–[30]. Binding of extracellular PAMPs to TLR leads to recruitment of myeloid-differentiation primary-response-gene-88 (MyD88) to the intracellular domain of the TLR. MyD88 in turn recruits interleukin-1-receptor-associated-kinase-4 (IRAK4) and IRAK1. IRAK1 binds the E3 ubiquitin ligase TNF-receptor-associated-factor-6 (TRAF6), they dissociate from the receptor complex and associate with transforming-growth-factor- β -activated-kinase-1 (TAK1), TAK1 binding proteins 1 and 2 (TAB1)(TAB2) as well as E1 and E2 enzymes. Auto-polyubiquitination of TRAF6 activates TAK1, which in turn phosphorylates and activates MAPKKs and IKK- β . MAPKKs and IKK- β phosphorylate MAPKs respectively I κ B α [28](Figure 1 B).

Degradation of phosphorylated I κ B α allows NF- κ B release and its migration to the nucleus, where it induces pro-inflammatory cytokines, chemokines, inducible enzymes and survival factors [31]. TNF α and IL-1 are recognized by other immune cells and induce MAPK/NF- κ B signaling, which leads to an amplification of the signal [26], [32]. The chemokine IL-8 recruits further immune cells to the site of infection [33]. Inducible enzymes such as iNOS and Cox2 control the nitric oxide (NO) level in macrophages, which is important for the efficient killing of phagocytosed bacteria [34] and subsequently for the synthesis of anti-inflammatory oxo-derivates of omega-3-fatty acids [35]. Survival factors such as

Bcl-2 regulate pro-inflammatory caspase-1 activation and contribute to the control of cell death programs [36]. MAPK signalling via p38 and ERK1/2 leads to phosphorylation and activation of transcription factors such as CREB, which modulate NF- κ B activity and control IL-2, IL-6, IL-10, and TNF α expression [37]. Besides phagocytosis and secretion of signaling molecules, macrophages undergo apoptosis and other forms of programmed cell death, which can also provide pro-inflammatory signaling to eliminate the bacterial infection [38], [39].

Another important module of the innate immune system is the inflammasome [40]. Inflammasomes are multiprotein complexes composed of NLRs that act as a cytosolic complement to the extracellular TLRs. Activation of the inflammasome results in caspase-1 activation and secretion of proinflammatory cytokines IL-1 β and IL-18. Unlike TLRs which detect exclusively PAMPs, inflammasomes are activated by proposed danger-associated-molecular-patterns (DAMPs) [40], [41], which consist of PAMPs and also molecules which originate from cell injury due to pathogen activity such as ion flux due to loss of membrane integrity through exotoxins, effector protein induced actin depolymerization or maybe even direct contact to effector proteins, as it occurs in plant immunity [40], [42]. Interestingly, deletion of the IKK- β gene in macrophages does not result in the suppression of the inflammatory response. Instead it triggers the activation of an inflammasome, which indicates that disruption of central signaling pathways can also be regarded as a DAMP [43].

1.3.2 Adaptive response

Migrating dendritic cells connect innate and adaptive immune response [44]. They phagocytose intruding bacteria, migrate to mesenteric lymph nodes and present antigens mounted onto MHCII receptor to B- and T-cells [45]. B- and T-cell activation marks the initiation of the adaptive immune response. The use of *de novo* generated antigen receptors allows the specific detection and elimination of pathogens by the adaptive immune system [46].

1.4 Virulence

The virulence of the *Yersinia* spp. is dependant on several chromosome and plasmid encoded virulence factors. Virulence factors allow *Yersinia* spp. to (i) attach to host intestinal epithelial cells, (ii) translocate to the underlying tissue, (iii) build a type three secretion system, (iv) translocate effector proteins to host cells, (v) prevent phagocytosis and secretion of pro-inflammatory cytokines and to (vi) induce programmed cell death in immune cells.

1.4.1 Adhesion and translocation of *Yersinia* cells

YE and YPT present Invasin (Inv), *Yersinia* adhesin A (YadA) and other adhesins on their surface, which enable them to adhere to epithelial cells of the intestinal mucosa (Figure 1 A) [47]. The expression of adhesins and other virulence factors is orchestrated by sophisticated thermosensing proteins such as RovA, which allows the resource efficient expression of virulence factors and keeps YE and YPT in an adhesion competent state prior to uptake by the host [48]. High DNA affinity of plasmid encoded RovA at ambient temperatures leads to a high expression of chromosome encoded Inv; reduced DNA binding at 37°C due to uptake by the host leads to RovA degradation and repression of Inv [49], [50]. During the initial steps of the infection, Inv binds directly to host β 1-integrins [51] present on the surface of M-cells, which are located in epithelial layer of the Peyer's Patches in the terminal ileum. Inv binding also triggers remodelling of the actin cytoskeleton of the M-cells, which leads to the uptake of YE and YPT into intracellular vesicles [52] and subsequent translocation across the Peyer's Patches intestinal epithelium [53]. In contrast, expression of virulence plasmid encoded adhesin YadA is suppressed at ambient temperatures and induced at 37°C by the LcrF/YmoA system [54]. YadA confers adherence to the extracellular matrix components collagen [55], [56] and fibronectin [57] as well as adherence to phagocytes, but prevents phagocytosis in concert with type three secreted effectors [58], [59].

1.4.2 Type Three Secretion System (TTSS)

All human pathogenic *Yersinia* spp. share a ~70 kb plasmid of *Yersinia* virulence (pYV) [60], [61], which encodes the Yop secretion c (Ysc) TTSS [62]–[64] and five to six secreted *Yersinia* Outer Proteins (Yop) effector proteins [65]. Besides

ysc, *Yersinia* can have up to two chromosomally encoded TTSS *ysa* and *ysb*, which can also translocate pYV effectors [66].

Expression of the *ysc* secretion system and of the effector proteins is resource intense – induction of secretion in medium leads to growth arrest – for *Yersinia* and is therefore only expressed upon host contact under the control of the transcriptional activator LcrF [54]. LcrF itself is under the control of the thermosensing *Yersinia* modulator A (YmoA), which binds downstream of the transcription initiation site of *lcrf* and hence blocks transcription at ambient temperatures. At host temperatures, YmoA is being degraded rapidly which allows transcription of *lcrf*. Besides that, a cis-acting RNA element within the *lcrf* transcript forms two stemloops at ambient temperature, which prevent ribosome binding and translation of LcrF. At 37°C, the loops unfold and LcrF is translated, allowing the build-up of the TTSS and synthesis of the effectors [67].

The TTSS is a ~3.5 MDa multi-protein complex, composed of more than 30 different proteins [63], [64], [68]. It enables pathogenic gram negative bacteria to counteract the host immune response, but it also enables symbiotic bacteria to interact with their host [69]. YE builds 30 to 100 secretion needles per bacterium to translocate effectors to host cells [70]. Cryo-EM characterization of the *Salmonella* and *Shigella* TTSS needle complexes in combination with high resolution X-ray-protein-crystal- and protein-NMR structures of individual subunits revealed an overall structure [71]–[74] which resembles the shape and the dimensions of the bacterial flagellum and indeed, most components of the TTSS have homologues in the flagellum [75]. Large scale sequence analysis of TTSS and bacterial flagella revealed that a common ancestor of all TTSS evolved from the flagellum, followed by rapid adaption via lateral gene transfer to multiple pathogens such as *Yersinia*, *Salmonella*, *Shigella* and diverse host systems such as mammals [76] and plants [77]. The TTSS consists of a basal body, which resides in the bacterial membranes, a large, needle like filament, which extends to the extracellular space and a translocon pore, which allows connection to the host cell membrane. The basal body is composed of an inner membrane ring with a heterogeneous 19-22 fold rotational symmetry and an outer membrane ring with a 12 – 14 fold rotational symmetry, which are

connected by a neck, spanning through peptidoglycan layer and the periplasm [71]. After the assembly of the basal body, YscF is secreted and around 140 copies of YscF [78] form a 60 nm long [79], needle like structure with a helical architecture [80], an outer diameter of 80 Å and a 25 Å axial lumen [81]. The tip of the injection needle is composed of a pentameric LcrV complex [82], [83]. The structure of the TTSS provides a central channel with a diameter of 20 to 40 Å, spanning from the basal body to the tip of the needle filament, thus providing a conduit through which unfolded proteins can be secreted [71].

1.4.3 Mechanism of Translocation

The secretion of the effector proteins is regulated by secretion chaperones, which are encoded adjacent to the respective effectors. Most of the effector proteins contain a 15 to 20 aa N-terminal signal sequence [84], followed by a chaperone binding domain (cbd). Specific class Ia secretion chaperones bind the cpd and keep it in an extended conformation [85], [86], which allows loading of the effectors to a sorting platform, which is connected to the TTSS [87]. Two mutually non exclusive mechanisms, as outlined below, have been proposed [88]. Both mechanisms share a decisive role for the translocators YopB/YopD which form a transient pore in the host cell membrane [89].

The one-step model suggests a direct connection between the bacterial cytosol and the host cell cytosol [90] via a continuous channel from the TTSS base, the injection needle and a proposed YopB/YopD/LcrV translocon pore in the host cell membrane (Figure 1 B). According to this model, LcrV acts as an assembly and folding platform for the insertion of translocators YopB/YopD into the host cell membrane [78]. *In vivo* and *in vitro* experiments with respective homologues of LcrV and YopB from *Shigella* show a recruitment of the YopB homologue to LcrV, which is induced by LcrV binding to deoxycholate, an abundant bile salt in the ileum. [83], [91], [92]. Under *in vitro* conditions, YPT YopD binds LcrV [93] and YP YopD can be found in TTSS needle preparations [94]. This indicates an interaction between the LcrV needle tip and the YopB/YopD translocators. However, there is no direct evidence yet that the effector proteins are “injected” into the host cells.

The two-step model proposes that secretion and translocation are two independent processes and that translocation occurs via an AB toxin related mechanism [88]. Under Ca^{2+} deficient conditions, *Yersinia* secretes effector proteins into the medium [95], [96]. Lack of Ca^{2+} is believed to mimic a phagosome-like environment within macrophages. Under such conditions, YopB/YopD/YopE complexes in a 1:2:1 ratios were recovered from the supernatant of *Yersinia* cultures [97]. YP YopD as well as effectors YopH and YopE are secreted prior to host cell contact even under Ca^{2+} rich conditions and attached to the bacterial surface. Upon host cell contact these surface localized effectors were translocated into the host cells where they induced their physiological response [98].

1.4.4 Effector proteins

In the host cell, the *Yersinia* effectors YopH, YopT, YopE, YopO mainly engage the regulation of the actin cytoskeleton, which leads to actin depolymerisation and rounding of the immune cells and inhibits phagocytosis, whereas YopM, YopQ and YopP act on the signalling networks which induce the expression of cytokines [99]–[102].

YopH is a phosphatase, which binds and dephosphorylates proteins. Among its targets are p130-kD Crk associated substrate (p130Cas) [103] and Fin-binding protein (FYB) [104], which both have a role in β 1-integrin signalling and phagocytosis [105].

YopE is a GTPase activating protein, which targets small G-proteins Rho1, Rac1 and CDC42. Deactivation of these proteins leads to an unregulated depolymerisation of actin fibres. Host cells counteract YopE by polyubiquitination and targeting to the proteasome [106], [107].

YopT is a cysteine protease, which cleaves close to the C-terminus of membrane anchored small G-proteins Rho1, Rac1 and CDC42. This leads to a detachment of the proteins from the membrane and contributes to the disruption of the actin cytoskeleton [108].

YopM is a scaffolding protein with a horseshoe-like structure [109], which contains 13 to 20 leucine-rich repeats. It binds and activates [110] PKN2 and RSK1 kinases by preventing their dephosphorylation [111]. Recently YopM was found to directly bind caspase-1, thus preventing the formation of the mature inflammasome [112] and the induction of pyroptosis.

YopO (*Yersinia* protein kinase A (YpKA) for YP and YPT) contains an N-terminal serine/threonine kinase domain with a remarkable homology to eukaryotic kinases [113], followed by a RhoGTPase-binding domain [114] and a C-terminal actin-binding domain, which is also required for its activation within the host cell [115]. The crystal structure of its RhoGTPase binding domain in complex with host factor Rac1 revealed a structural mimicry of host guanidine nucleotide dissociation inhibitors (GDI) of host Rho GTPases. The kinase domain phosphorylates actin [115] and the G α Q subunit of heterotrimeric G proteins *in vitro*.

YopQ (YopK for YP and YPT) modulates the function of the translocon pore, and the secretion of effectors. It interacts with the host signalling component RACK1 [116]. Moreover, YopQ also seems to modulate YopP dependent apoptosis and has an effect on the inflammasome recognition [117]. YopQ is exclusively found in *Yersinia* spp. and has no homology to any known protein.

YopP (YopJ for YP and YPT), is a 32 kDa protein located within the SycO/YopO/YopP operon [118], [119]. YopP causes a comprehensive suppression of pro-inflammatory cytokines secretion in macrophages and induces apoptosis in macrophages [120] and dendritic cells [121]. YopP modulated cytokine secretion enhances the permeability of intestinal epithelial cells towards pathogens [122], [123].

Introduction

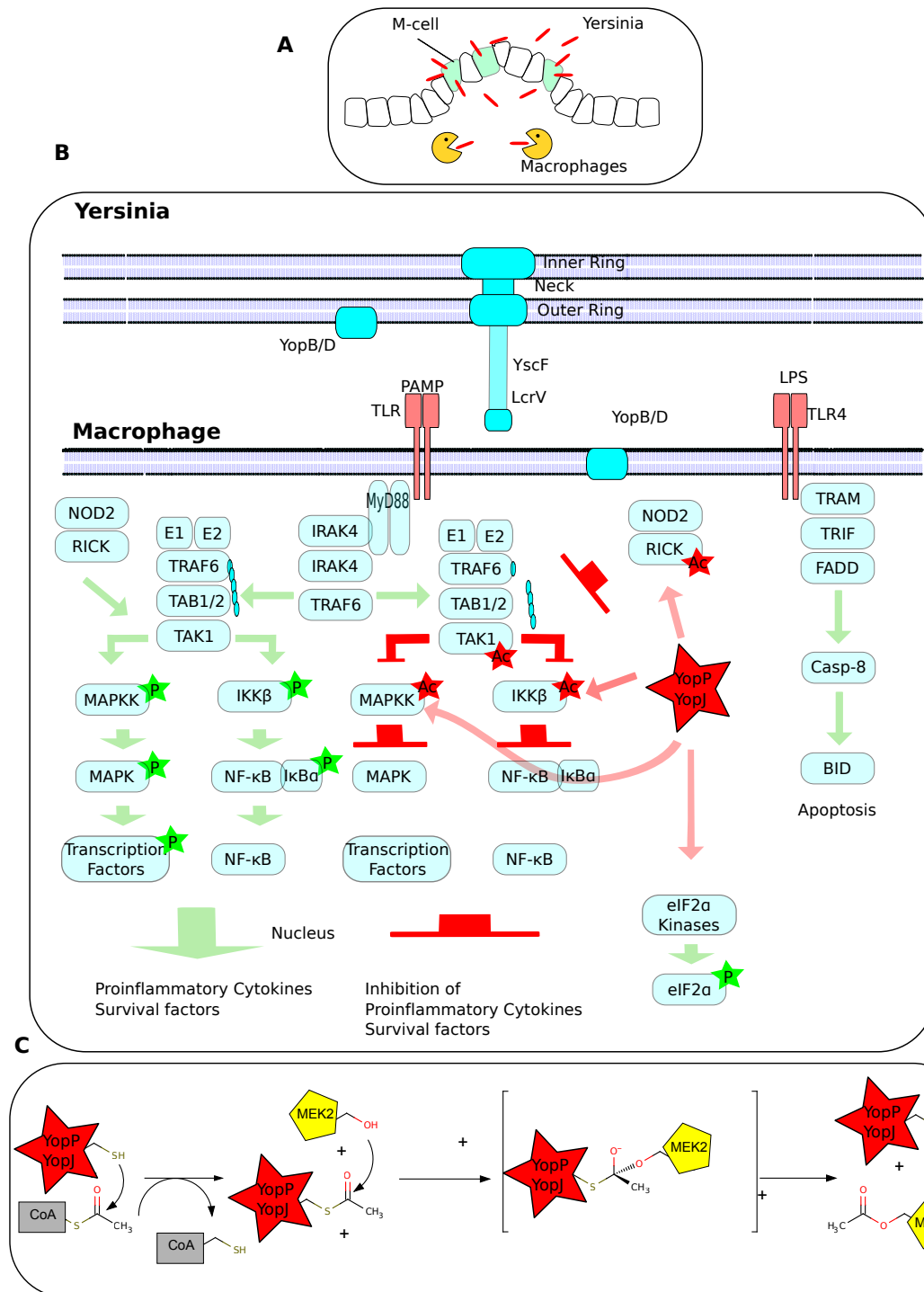


Figure 1 (A) Peyer's Patches and the underlying tissue (B) Innate immune recognition of pathogenic bacteria and induced signalling events. YopP's effect on MAPK/NF- κ B signalling. (C) Proposed reaction mechanism of YopP.

1.5 YopP

1.5.1 Downregulation of Cytokines

It was noticed that *Yersinia* spp. suppresses the secretion of pro-inflammatory cytokines of macrophages such as TNF α in a virulence plasmid dependent manner [124], [125]. The translocation of YopP to the host cells was later identified to cause the downregulation of pro-inflammatory cytokines such TNF α [126]–[128] IL-8 [129] IL-8 α [130], IL-1b [131] and many more, which effectively suppresses the inflammatory response in the initial phase of *Yersinia* infections. The impact of YopP on the suppression of cytokines is also reflected in microarray-based experiments, where only YopP but none of the other effectors had a significant impact on the transcription of immune response related genes [132].

1.5.2 Disruption of MAPK/NF- κ B Signalling Networks

The connection between MAPK/NF- κ B, cytokine secretion and inflammation [133] led to the discovery that YopP interferes with the MAP kinase signalling network upstream of the MAPK level by preventing the phosphorylation and activation of the kinases ERK1/2, p38 and JNK [126], [127], [134]. Therefore, critical MAPK-related transcription factors such as CREB cannot be activated [135]. In a similar fashion, NF- κ B activation is prevented by inhibition of phosphorylation of IKK- β [128], [129]. YopP also interferes with the MAPK/NF- κ B regulation at the MAPKKK level by preventing the phosphorylation and activation of TAK1, which is an activator of both NF- κ B and MAPK signalling [136]–[138]. In experiments aiming to narrow down at which level YopP interferes with MAPK signal transduction, an activated Rac1 GTPase mutant failed to restore the MAPK signalling, indicating that YopP has to act downstream of Rac, that is to say either at the MAPKKK or MAPKK level [139].

1.5.3 Mechanism

The comprehensive downregulation of MAPK and NF- κ B networks suggested that YopP has to interact directly or indirectly with the kinases, to function as a “MAP kinase poison” [139]. In a series of yeast two-hybrid, co-

immunoprecipitation and GST-pulldown assays, it was shown that YopJ can bind to human MAP kinases MKK1, MEK2, MKK3, MKK4, MKK5 and IKK- β , which suggested that this binding prevented the phosphorylation and activation of the MAPKKs [140]. The discovery of a conserved catalytic triad (histidine 109/(aspartate)glutamate 128/cysteine 172) and sequence homology to adenovirus proteases and *S. cerevisiae* ubiquitin like protease 1 (Ulp1) led to the hypothesis that YopP is a cysteine protease, which specifically cleaves ubiquitin or small ubiquitin like protein (SUMO) from proteins associated with TLR/MAPK/NF- κ B signalling network and hence causes its inhibition [141]. The YopP protease hypothesis was supported by the loss of inhibitory activity of catalytically inactive C172A mutants and a reduction of the overall SUMOylation and ubiquitination levels of proteins in YopP overexpression assays [138], [141], [142]. In particular deubiquitination of polyubiquitinated TRAF6 was believed to cause the suppression of cytokine secretion and the disruption of MAPK/NF- κ B signalling, since only polyubiquitinated TRAF6 can activate TAK1, which then activates MAPKKs and IKK- β [143]. However, since all deubiquitination assays were performed with YopP over-expression in the host cell, it could not be ruled out that the changes in ubiquitination levels were not due to an effect of YopP on the translation of ubiquitin or SUMO [120]. So, it could not be clearly determined if and to what extent the protease activity contributes to the disruption of the MAPK/NF- κ B signalling network. However, a different enzymatic activity of YopP provides an attractive explanation of YopP's effect on the host cell: YopP acts as an acetyltransferase, which uses acetyl-coenzymeA (acetyl-CoA) as a cofactor to acetylate critical serine and threonine residues in the activation loop of MAPKKs and IKK- β [144], [145] as well as TAK1 and RICK [122], [123] (Figure 1 C). Acetylation of these residues prevents phosphorylation and activation by the upstream MAPKKK and inhibits phosphorylation and activation of the downstream MAPK. This model elegantly explains the disruption of the MAPK/NF- κ B signalling network by YopP. Acetylated kinases were detected both *in vivo* and *in vitro* by mass spectrometry based assays [122], [144], [145] and acetylation of the kinases was shown to inhibit their ability to phosphorylate the downstream kinases [146]. The

acetyltransferase activity of YopP and the proposed reaction mechanism also explains the significance of C172: YopP binds acetyl-CoA, C172 attacks the acetyl-CoA thioester and the acetyl-group is transferred to C172. Acetylated YopP then binds the kinase respectively IKK- β . The hydroxyl groups of the serine and threonine sidechains then react via nucleophilic attack with the carboxyl-carbon-atom of the thioester at C172 and the acetyl-group is transferred to the serine and threonine of the kinase [147]. YopP acts as a leaving group and can enter further reaction cycles. Yeast-based assays identified the host kinase G α helix as important for the YopP/Kinase interaction [148]. YopP is activated by the host cell factor inositolhexakisphosphate (IP6), which could also explain how YopP is kept in a quiescent state in the bacterium, since bacteria lack the capacity to synthesize IP6 [149].

1.5.4 Induction of cell death by YopP

The induction of apoptosis [150]–[152] by *Yersinia* is dependent on YopP and its ability to suppress NF- κ B activation [128], [129]. Macrophages transfected with a YopP expression vector also undergo apoptosis, but only co-stimulation of the macrophages with LPS restores the apoptosis rate of macrophage infected with *Yersinia* [153]. LPS is an inducer of a macrophage activation program [24], which results in the secretion of cytokines and sensitization of naïve macrophages with LPS provides protection against *Yersinia*-mediated apoptosis [154]. LPS triggers MAPK/NF- κ B activation via TLR2 and TLR4, but only TLR4 is responsible for the LPS augmentation in YopP-mediated apoptosis [155]. Besides the MAPK/NF- κ B activation via MyD88, TLR4 triggers an NF- κ B independent apoptotic signal via Toll/IL-R domain-containing adaptor-inducing IFN- β (TRIF), Fas-Associated protein with Death Domain (FADD) and activation of caspase-8 and BH3 interacting-domain death agonist (BID), which results in cytochrome-C release from mitochondria and activation of caspases-3, -8, -9 [156]–[159]. In this way, YopP interferes with a conserved macrophage activation program, which involves MAPK/NF- κ B induction of pro-inflammatory and pro-survival genes on one hand and pro-apoptotic caspase-8 signalling on the other hand. By selectively suppressing the pro-inflammatory/pro-survival branch through YopP, the pro-apoptotic branch predominates and the

macrophages undergo apoptosis [158]. Apoptotic macrophages trigger production of anti-inflammatory cytokines IL-10 and TGF- β and is considered to be silent for the immune system [38], [160]. In activated macrophages however, *Yersiniae* cause so-called pyroptosis, a cell death program independent of YopP, which involves inflammasome activation and processing of caspase-1, release of pro-inflammatory cytokines IL-1 β and IL-18 and eventually lysis of the macrophages and release of pro-inflammatory intracellular content [160], [161]. Prevention of pyroptosis and suppression of inflammatory response by YopP could be crucial for *Yersiniae's* ability to colonize the Peyer's Patches without an initial immune response [38], [162], [163].

The genetic variability of the *Yersinia* spp. and the various bio- and serotypes is also reflected by a number of single nucleotide polymorphisms (SNP) within the *yopp/yopj* gene [131], [153], [164], [165]. These SNPs result in differences in type three secretion efficiency as well as in a different ability to inhibit NF- κ B and MAPK signalling [38]. Even though the different YopP/YopJ isoforms have sequence identities of more than 95%, they cause distinct forms of programmed cell death, ranging from apoptosis to necrosis and are all associated with caspase-1 activation [131], [166], [167]. The degree of caspase-1 activation correlates with the extent of YopJ mediated NF- κ B inhibition [131], indicating that NF- κ B inhibition could act as a DAMP, which contributes to the activation of a specific inflammasome, which then processes caspase-1 and triggers IL-1 β and IL-18 secretion. The activation of the inflammasome could also explain that highly active YopP/YopJ is not by definition beneficial for the pathogen. Expression of YE O8 YopP in YPT and YP for example causes attenuation of the infection in the mouse model [165], [168]. Thus the activity of YopP of a particular strain has to be balanced in respect to the activity of the other effectors and to the innate immune stimulation by its PAPMS to suppress cytokine secretion and to avoid the inflammatory response.

Given the impact of YopP on NF- κ B/MAPK signalling, the large number of inflammatory diseases and the mechanistic similarities between forms of cancer and inflammation [31], it is not surprising that numerous patents involving

YopP have been granted [169]–[171]. It remains to be seen if recombinant YopP can be applied in a cell type specific way to treat cancer or chronic inflammation.

1.5.5 Induction of barrier dysfunction

Besides the effect of YopP on the MAPK/NF- κ B network at the level of MAPKK, YopJ also acetylates the upstream kinases TAK1 and RICK and prevents their phosphorylation [122], [123]. Acetylation of RICK by YopJ reduces RICKs affinity for Nod2 and allows Nod2 mediated activation of caspase-1 and subsequently IL-1b secretion, which causes barrier dysfunction in the Peyer's Patches and hence could help *Yersinia* to colonize the Peyer's Patches [172].

1.5.6 Effect on adaptive immune response

Besides the suppression of cytokines in macrophages and the indirect effect on the adaptive immune system, YopP also suppresses cytokines and induces apoptosis in dendritic cells [121]. Moreover, it also interferes with the MAPK-regulated antigen uptake and degradation in dendritic cells, which impairs the activation of B- and T-cells [173], [174].

1.6 Conclusion and open questions

The investigation of *Yersiniae* virulence and YopP's contribution has led to a better understanding of bacterial virulence, innate immune response and signal transduction regardless of the actual reaction mechanism. The acetyltransferase activity of YopP however, gives rise to several questions:

In many cases, effector proteins from pathogens mimic functions of host proteins. YopO, for example, mimics the function of a eukaryotic kinase and a GTPase. Is serine/threonine O-acetylation only performed by bacterial pathogens or does the host also use serine/threonine acetyltransferases to regulate kinase activities?

Are there further substrates of YopP in the host? The MAPK/NF- κ B network is embedded in a dynamic regulatory complex, composed of hundreds of proteins, many of which contain serine/threonine kinases domains [175].

Is there a preferred localization for YopP within the host cell? A homologue of YopP from a plant pathogenic bacterium was shown to interact with a host 14-3-

3 scaffold protein [176]. MAPK as well as NF- κ B are constrained in scaffolds and the recruitment of YopP to such a scaffold would allow faster inhibition of signalling events compared to a free diffusion of YopP in the cell [175].

What is the relationship or crosstalk between serine/threonine acetylation and other PTM? Besides the ubiquitous phosphorylation and ubiquitination, the dynamics of protein complexes are influenced by lysine acetylation [177] and other modifications. IKK β Cys179 for example, can be nitrosylated, and Thr180 can be acetylated by YopP [178].

Is there a differential inhibition of individual components of the MAPK/NF- κ B network, for example does YopP have a preference to acetylate particular kinases before others?

Even though YE and YPT do not pose an eminent threat and YP infections are under control at the moment, sudden outbreaks of foodborne diseases due to the rapid acquisition of new virulence factors like the recent EHEC case in Hamburg [179] underlines the importance of basic research in host/pathogen and host/commensal interaction. Furthermore, host pathogen interactions and the effector proteins provide a sophisticated toolbox to study fundamental signalling processes in the host, which allow a better understanding of cancer and chronic inflammation [180].

1.7 Rv2140c

1.7.1 Mycobacterium tuberculosis

Mycobacterium tuberculosis (Mtb) causes tuberculosis (TB), which kills more humans than any other infectious disease and accounts for the death of 1.4 million people annually [181]. Each year, 8.7 million new cases of active TB are reported and up to 1/3 of the worlds population could be infected with latent TB [181], [182].

TB is an ancient disease. Traces of Mtb DNA could be recovered from human bones from the Neolithic age [183]. Recent phylogenetic analysis indicates that Mtb has accompanied people since the first humans left Africa [184].

1.7.2 Clinical manifestation

In most cases, Mtb infects the lungs and causes pulmonary TB. However in 10 to 20% of the cases Mtb can also infect other organs like bones and the central nervous system [185]. Transmission occurs usually through inhalation of Mtb containing aerosols of infected individuals. After 8 weeks Mtb starts spreading throughout the lung and in the following month the first symptoms such as chest pain can occur [186]. In the last stage pulmonary lesions and extrapulmonary lesions in bones may occur. However, progression of the disease stops in most individuals, and only 3 to 5% develop TB in the first year and 3 to 5% develop TB later in life through a reactivation of a pre-existing infection [185].

1.7.3 Virulence factors

The virulence of MTB is dependant on several virulence factors, which include a cell wall composed of mycolic acids, secretion of proteins through a Type VII secretion system and dormant cells, which can be inactive for decades and suddenly reactivate the infection.

After inhalation Mtb encounters macrophages and immune cells which induce the innate and adaptive immune response [187]. Phagocytosed Mtb shows resistance against reactive oxygen species, whereas it is susceptible to reactive nitrogen species [188]. Mtb can inhibit the phagosome lysosome fusion [189] and prevent the acidification of the lysosome [190]. The Mtb cell wall comprises a waxy layer composed of mycolic acids [191], which is an effective permeability barrier against small molecule drugs [192], [193]. Mtb encodes several Type Seven Secretion Systems [194], which allows secretion of a broad range of PE/PPE proteins, named after conserved proline/glutamate, proline/proline/glutamate residues [195]. Many of these proteins are essential for Mtb virulence. They have a strong effect on the secretion of cytokines [195] and enable Mtb to leave the myeloid cell phagosome and enter the cytosol [196]. However, unlike the case of gram negative pathogens such as YE, the molecular basis of the host pathogen interaction is not known [194].

1.7.4 Latency and reactivation

As a result of the immune response towards TB, Mtb-infected macrophages are encapsulated in a granuloma by recruited immune cells, which effectively shuts off the blood and nutrient supply [197]. Mtb stops replicating and reduces its metabolism to a minimum. It can then remain in this state of latency for decades. Since most antibiotics target only replicating bacteria, they are ineffective against Mtb [198]. In case of immuno-compromisation, in particular due to HIV/AIDS, reactivation of TB occurs probably as a consequence of dormant cells reactivating and replicating [199].

1.7.5 Drug discovery

The main drugs against TB are isoniazid and rifampicin. The standard treatment for active pulmonary TB is a combinational application of high doses of isoniazid, rifampin, pyrazinamide and ethambutol for up to nine months [200]. Despite the severe side effects of isoniazid, which can damage the liver [201] and the central nervous system [202], isoniazid has been the workhorse of TB treatment for more than 50 years.

The rising number of multi-drug resistant Mtb strains underlines the importance of drug discovery [203] and vaccine development [204], which goes along with enhanced fundamental research on Mtb, its genetics and host pathogen interaction, as well as an comprehensive integration of the research towards a systems biological understanding of TB [199].

Of the more than 4000 Mtb protein coding genes, more than a thousand have been annotated as hypothetical proteins [205]. Structural and functional characterization of such proteins can give a hint towards their physiological function, as well as their potential to serve as a drug target [206].

1.7.6 Rv2140c

The Mtb ORF Rv2140c encodes a conserved hypothetical protein [207]. Up-regulation of Rv2140c of Mtb grown in interferon- γ -activated macrophages compared to non-activated macrophages suggested the importance of Rv2140c for Mtb within the phagolysosomal environment. In a transposon-based mutagenesis assay, Rv2140c was identified to be essential for the survival of Mtb

in mouse lungs [208]. Even though no secretion signal has been identified within its sequence, Rv2140c is found in supernatants of Mtb culture filtrates [209], [210]. Rv2140c induces a robust IFN- γ release in Mtb-infected mice, corresponding to ~20% of IFN- γ release of the total preparation of culture filtrate [211]. Subsequently, Rv2140c has been patented as an antigen in a novel BCG tuberculosis vaccine [212]. Use of secreted Mtb proteins such as ESAT-6 and CFP-10 gave rise to vaccines, which provide protective immunity in animal models of TB infection [213].

Sequence homology and the crystal structure suggest that Rv2140c belongs to the family of phosphatidylethanolamine binding proteins (PEBP) [214]. Eukaryotic PEBPs were first isolated as a cytosolic component of brain material [215] and were shown to bind organic cations and phosphatidylethanolamine (PE) [216], [217], a major component of many cell membranes. PEBPs are found in all kingdoms of life. The roles of PEBPs in eukaryotes include protease inhibition [218], a mammalian peptide neurotransmitter [219], and both intra- and extracellular odorant receptors [220]. Modulation of MAP-kinase and NF- κ B signalling in mammals, plants and yeast, which corresponds to their function as a Raf-kinase inhibiting protein (RKIP) is the best investigated process [221]. PEBP/RKIP appears to bind Raf1, MEK2, as well as IKK α and hence modulate activation of signalling events. Reduced expression of PEBPs has been linked to various forms of cancer [222] and most notably, high expression of PEBPs can prevent cancer metastasis [223].

Locostatin is a 3,2 disubstituted oxazolidinone with a α,β -unsaturated N-acyl group, which has an inhibitory effect on epithelial cell sheet migration [224]. This effect was thought to be mediated by binding to PEBP/RKIP [225] and interference with Raf inhibition. Recent findings indicate that even though locostatin binds PEBP/RKIP, this binding does not impair its interaction and inhibition of Raf-kinase. Instead PEBP/RKIP seems to protect cells from locostatin effects by an unknown mechanism, which rather indicates a function of PEBP in detection and counteracting effects of toxic compounds [226].

Contrary to the growing knowledge about the various roles of PEBPs in eukaryotes, little is known about their functions in bacteria and archaea. YBCL of uropathogenic *E. coli* is secreted by an unknown mechanism. It suppresses transepithelial neutrophil migration[227]. One hint for the function of PEBPs within microorganisms could be that *Sulfolobus solfataricus* homologue SsCEI binds to and inhibits the function of a *S. solfataricus* serine protease [228], [229]. This indicates that bacterial PEBPs could serve similar functions as their eukaryotic counterpart.

2 Aim of the Work

Yersinia enterocolitica, the causative agent of an enterocolitis, is a foodborne pathogen. It has a unique repertoire of effector proteins, which are translocated into the cytosol of host cells. They interfere with the innate and adaptive immune recognition and induce apoptosis in immune cells. The effector proteins and their functions are highly conserved among the human pathogenic *Yersinia* spp *Y. pseudotuberculosis* and *Y. pestis*, the causative agent of the bubonic plague. *Yersinia* outer protein P (YopP) is responsible for a comprehensive downregulation of pro-inflammatory cytokine secretion as well as for the induction of apoptosis in macrophages and dendritic cells. YopP is an acetyltransferase, which acetylates critical serine and threonine residues in the activation loop of MAPKKs and IKK- β . This effectively disrupts the signal transduction through the MAPK/NF- κ B signalling network. Compared to the rich body of knowledge concerning the impact of YopP on apoptosis and cytokine secretion, little is known about the molecular basis of YopP's activity and the reaction mechanism of this novel post-translational modification. This thesis aims to investigate YopP and its interaction with host kinases through an interdisciplinary approach, which attempts to crystallize YopP in order to obtain a high-resolution x-ray crystal structure and to perform a kinetic analysis of the acetylation reaction. In order to crystallize YopP, a detailed biophysical and biochemical characterization of YopP and its interaction with host and pathogen co-factors is required.

The second aim of this thesis is the biophysical and *in vivo* characterization of Rv2140c, a protein of *Mycobacterium tuberculosis*, which was found to be upregulated in Mtb-infected immune cells. Contrary to the situation with YopP, a high resolution X-ray crystal structure is available, but only limited knowledge about Rv2140c role in infection. The structure suggests that Rv2140c is a phosphatidylethanolamine binding protein and could therefore also play a role in the recognition of locostin, a cell migration inhibitor, which is known to bind to and modulate the activity of eukaryotic PEBPs and to also interact with Rv2140c *in vitro*. To validate that Rv2140c is a PEBP, the binding of Rv2140c to various PE analogues should be characterized. To characterize the role of Rv2140c and its interaction with locostin *in vivo*, the homologous gene of *Mycobacterium smegmatis* should be deleted and the knock out mutant should be characterized.

3 Materials and Methods

3.1 Materials

3.1.1 Chemicals, Consumables, Equipment

Table 1 Chemicals

Chemical	Supplier
Tet	Roth
Hyg	Roth
Carb	Roth
Kan	Roth
Silicone / Paraffin oil	Hampton research
Iodoacetamide	Sigma
TECP	Sigma
Acetyl-coA	Sigma
Agarose	Serva
coA	Sigma
DHPA	Avanti Polar Lipids
DHPE	Avanti Polar Lipids
DHPG	Avanti Polar Lipids
DHPS	Avanti Polar Lipids
DIG Molecular weight marker	Roche
Dimethylamine borane	Fluka
DNA Ladder mix 1kb plus	NEB
Glycine amide (GlyAd)	Sigma
Glycine ethyl ester (GlyEE)	Sigma
IP6	Sigma
Locostatin	Sigma
Ni-NTA agarose	Qiagen
Proline amide (ProAd)	Iris Biotech
Rotimark 10-150	Carl Roth
Tween 80	Roth
Synthetic Peptide (GQLIDSMANSFVGTR)	Abgent

Table 2 Consumables

Consumables	Supplier
NucleoSpin Plasmid	Macherey & Nagel
DIG-High Prime DNA Labeling and Detection Starter Kit I	Roche
Centrifuge filters 0.6 mL (0.2/0.45 µm)	Millipore
Centrifugal concentrators 6 mL, 20 mL	Millipore

Nylon membrane	Roche
24 well platereader plate(no. 662960)	Greiner
384 well platereader plate	Greiner
PCR tubes	Saarstedt
96 well sitting drop/vapour diffusion	Greiner/Inovadyne
96 well plate under oil	Jena Bioscience, Douglas Instruments
Limbro 24 well crystallisation plate	Crystalgen / Molecular dimensions
Siliconized glass cover slides	Hampton research
PVDF Membrane	Roth
Plastic tubes (1.5 – 50 mL)	Saarstedt
Syringe filters (0.45, 0.22 µm)	Satorius

Table 3 Technical equipment

Item	Supplier
Äkta Purifier	GE healthcare
Äkta Explorer	GE healthcare
VP-ITC	Microcal
Plate reader	TECAN M100
CD spectrometer	JASCO
Nanodrop	PEQlab
SDS-PAGE electrophoresis System	Biorad
DNA Eletrophoresis System	Biorad
Hybridization oven	Thermo Fisher Scientific
DLS	SpectroSIZE 300 (Nabitec, Germany)
Columns	
SuperdexS75 16/60	GE Healthcare
SuperdexS75 200/60	GE Healthcare
SuperdexS75 HR 10/300	GE Healthcare
SuperdexS200 HR 10/300	GE Healthcare
MonoQ HR 10/10	GE Healthcare

3.1.2 Plasmid Vectors

YopP, MEK2, orf155, orf91a

pGEX-4T3 (Amersham/GE): Ampicillin resistance, N-terminal GST-tag and thrombin cleavage site.

pET-Z21a/Lic (EMBL in house vector/Arie Geerlof): based on pET-24d with an N-terminal 10 kDa His6-Z-tag and TEV-protease cleavage site.

pCDF-13 (EMBL in house vector/Arie Geerlof): Co-expression vector with a C-terminal His-tag

Rv2140c

pETM-11: Expression vector for Rv2140c. KanR, N-terminal 6His-tag and a TEV-protease cleavage site.

pJV53 (Elke Noens) genes Ch9c recombination genes 60-61 recombinase expression vector.

pYUB854 : HygR, flanked by $\gamma\delta$ -resolvase sites.

pHG542 (Elke Noens) $\gamma\delta$ -resolvase , TetR

3.1.3 Bacterial strains

E. coli **DH5 α** (Invitrogen) was used for cloning, isolation and propagation of recombinant DNA

E. coli **BL21(DE3)** (Stratagene) was used for IPTG induced expression of genes and production of recombinant proteins

E. coli **Origami (DE3) pLysS** (Novagene) was used for the co-expression of MEK2S222/226C mutants and YopP-wt

E. coli **HB101** Chemically competent cells (Promega) were used for the creation of the pYUB854 derived MSMEG_4199 knock out vector.

M. smegmatis **mc²155** was used for growth curve experiments, DNA extraction of genomic DNA and generation of a *M. smegmatis* Δ _MSEMG_4199 knock out mutant. *M. smegmatis* is intrinsically resistant against carbenicillin.

M. smegmatis Δ _MSEMG_4199 knock out mutant was used for growth curve experiments.

3.1.4 Oligonucleotide primers

All oligonucleotides were purchased from Eurofins MWG Operon. The lyophilized oligonucleotides were diluted in ddH₂O to a concentration of 10 pmol/μL and stored at -20°C.

Table 4 LIC overhangs are highlighted in red, mutation sites in green and restriction sites in blue

YopP-LIC-for-1	5'- CAGGGCGCCA TGATTGGACCAATATCACAAATAAACAGCCC-3'
YopP-LIC-for-18	5'- CAGGGCGCCA TGGAGACCAGTTCTTTAATCAG-3'
YopP-LIC-for-88	5'- CAGGGCGCCA TGAACGTCATAGAAAATGGAG
YopP-LIC-Rev-200	5'- GACCCGACGCGGT TATTTTTTTGTTAACAAACAGTACC-3'
YopP-LIC-Rev-223	5'- GACCCGACGCGGT TATTTGTAAAAAGTTACCGGGAG-3'
YopP-Lic-Rev-250	5'- GACCCGACGCGGT TAACCTTTTATATTATCTTCATG-3'
YopP-LIC-Rev-288	5'- GACCCGACGCGGT TATACTTTGAGAAGTGTTTTATATTCAGC-3'
Orf155-LIC-for	5'- CAGGGCGCCA AGTGATTAACCTTTACTGAGCTACTCCAAAAA-3'
Orf155-LIC-Rev	5'- GACCCGACGCGGT AATAACCGATTGAGTAGATTGAGTAAGAGGGGGC-3'
Orf91a-LIC-for:	5'- CAGGGCGCCA TGCTATCAATTAGAAAGAATGAATGTCCTTGCTGG-3'
Orf91a-LIC-rev	5'- GACCCGACGCGGT TATTTATCCTTATTCAGGGAATTAACAGCGGTATG-3
AvraA-LIC-for	5'- CAGGGCGCCA TGATATTTTCGGTGCAGGAGCTATCATG-3'
AvraA LIC-rev	5'- GACCCGACGCGGT TACGGTTTAAGTAAAGACTTATATTCAGCTATCC-3'
MEK2-LIC-55-for	5'- CAGGGCGCCA TGGCCTTTCTCACCCAGAAAGC-3'
MEK2-LIC-rev-400	5'- GACCCGACGCGGT TATCACACGGCGGTGCG-3'
MEK2-S222/226A	5'-GCCAGCTCATAGAC GC CATGGCCAAC GC CTTCGTGGGCACGC-3'
MEK2-S222/226C	5'-GCCAGCTCATAGACT GC CATGGCCAAC TG CTTCGTGGGCACGC-3'

Materials and Methods

MEK2-S226C	5'-GCCAGCTCATAGACTCCATGGCCAAC TGCT TTCGTGGGCACGC-3'	
MEK2-S222C	5'-GCCAGCTCATAGACT GC ATGGCCAAC TCCT TTCGTGGGCACGC-3'	
T7-promotor	5'-TAATACGACTCACTATAGGG-3'	
T7_terminator	5'-CTAGTTATTGCTCAGCGGT-3'	
MSMEG-4199-A	5'-CACAG GTACCC CGCTGCGCGACACGGCCAAC-3'	KpnI
MSMEG-4199-B	5'-CG TCTAGAG CCCCGTCGCTGACCGACTCGG-3'	XbaI
MSMEG-4199-C	5'-ACG AAGCTT GACCTGCCGGAGAACGCCACG-3'	HindIII
MSMEG-4199-D	5'-AC ACTAGT GAACTGGGGTTGGCGGGCATCG3'	SpeI
KOseq_frag1_F	5'-CGTTCATCCATAGTTGCCTGAC-3'	
KOseq_frag1_R	5'-CTTGTCCGATATTTGATTTAGG-3'	
KOseq_frag2_F	5'-CGGACGGTTGCTAGCACGC-3'	
KOseq_frag2_R	5'-GGGATTTTGGTCATGGTAATAC-3'	

3.2 Media, Buffers and Stock solution

3.2.1 Media

3.2.1.1 *E. coli* media

	SOC Medium
Yeast Extract	2.5 g
Tryptone	10 g
NaCl (5 M)	1 mL
KCl (3 M)	416 uL
MgCl ₂ (1 M)	5 mL
MgSO ₄ (1 M)	5 mL
ddH ₂ O	Adjust to 495 mL
	Autoclave
Glucose (1 M)	5 mL

LB

LB Broth Granulated	20 g
ddH ₂ O	Adjust to 1 L
	Autoclave

TB

TB Broth Granulated	47.6 g/L
Glycerol	4 mL
ddH ₂ O	Adjust to 1 L
	Autoclave

3.2.1.2 *M. smegmatis media*

7H9 Broth

Middlebrook 7H9 Powder	4.7 g
ddH ₂ O	900 mL
Glycerol (40% (v/v))	5 mL
	Autoclave
ADC	100 mL
Tween 80 (20% (v/v))	2.5
CHX	1 mL
Carb	1 mL
HygB	1 mL
Kan	0.4 mL

7H9 Induction Medium

Middlebrook 7H9 Powder	4.7 g
MQ H ₂ O	900 mL
Glycerol (40% (v/v))	5 mL
	Autoclave
ddH ₂ O	100 mL
Tween 80 (20% (v/v))	2.5 mL
Succinate (20%)	10 mL
Cycloheximide	1 mL
Carbenicillin	1 mL
Kanamycin	0.4 mL

7H10 Agar

Middlebrook 7H9 Powder	4.7 g
ddH ₂ O	900 mL
Glycerol (40% (v/v))	5 mL
Agarose	10 g
	Autoclave
ADC	100 mL
Tween 80 (20% (v/v))	2.5

Cycloheximide	1 mL
Carbenicillin	1 mL
Hygromycin B	1 mL
Kanamycin	0.4 mL

3.2.2 Buffers

3.2.3 Protein purification buffers

Lysis Buffer/Wash Buffer

NaCl	400 mM
Tris/HCl (pH 8.0)	50 mM
Imidazole	10 mM
DNase	1 μ L (1 mg/mL) / mL cell suspension
Lysozyme	1 μ L (5 mg/mL) / mL cell suspension
Protease inhibitor mix	10 μ L/
DTT	1 mM

Elution Buffer

NaCl	400 mM
Tris/HCl (pH 8.0)	50 mM
Imidazole	500 mM

Dialysis Buffer

NaCl	200 mM
Tris/HCl (pH 8.0)	50 mM

Dialysis Buffer Rv2140c

NaCl	50 mM
20 mM NaH ₂ PO ₄	20 mM

3.2.4 Southern blot buffers

Denaturation Buffer

NaCl	1.5 M
NaOH	0.5 M

Neutralization Buffer

NaCl	1.5 M
Tris/HCl (pH 7.5)	1 M

SSC Buffer 20x

NaCl	3 M
Na ₃ Citrate	0.3 M

Washing Buffer

Maleic acid /NaOH pH 7.5	0.1 M
NaCl	0.15 M
Tween20	0.3 % (v/v)

Malic acid buffer

Maleic acid / NaOH pH7.5	0.1 M
NaCl	0.15 M

Detection Buffer

NaCl	0.1 M
Tris/HCl (pH 9.5)	0.15 M

TE-buffer

Tris/HCl (pH 8.0)	10 mM
EDTA	1 mM

Blocking solution (1/10)

Malic acid buffer	90%(v/v)
Blocking solution (Roche Kit)	10% (v/v)

Antibody solution (1/5000)

Blocking solution	1 mL mL
Antibody solution (Roche)	0.2 µL

Colour Substrate solution

Detection buffer	10 mL
NBT/BCIP stock (Roche)	200 µL

3.2.5 Stock solutions 1000x

Kan	50 mg/mL
HygB	100 mg/mL
Carb	100 mg/mL
IPTG	1 M

3.3 Methods

3.3.1 Molecular Biology

3.3.1.1 Polymerase Chain Reaction (PCR)

The PCR utilizes the thermostability and temperature dependent activity of DNA polymerases of thermophiles [230] in presence of specific synthesized DNA primers and template DNA to synthesize and amplify DNA sequences of interest. One cycle of PCR involves melting of DNA, annealing of the primers, which are complementary to a specific sequence in the DNA and elongation of the sequence. Several cycles of PCR lead to an exponential amplification of the DNA template, which can be genomic DNA, vectors or cDNA. The melting temperature for the reactions was calculated according to the nearest neighbour method[231] with the manufacturers web tool[232]. The annealing temperature was calculated as the lowest melting temperature of the two primers plus 2°C. The elongation time was calculated as 15 to 30 s/kb (Phusion) and 1 min/kb (Taq).

Table 5 Sample composition for Phusion PCR

Component	Volume (μL)	Final concentration
5x Phusion HF-Buffer	10	1x
10 mM dNTPs	1	0.2 mM each
10 μM Fw.-Primer	0.5	250 nM
10 μM Rev.-Primer	0.5	250 nM
5-20 ng/ μL Template	1	0.1-0.5 ng/ μL
2 U/ μL Phusion Polymerase	0.5	0.02 U/ μL
ddH ₂ O	To 50	

Table 6 Sample composition for Taq 2X Master Mix

Component	Volume/ μL	Final concentration
10 μM For.-Primer	1	250 nM
10 μM Rev-Primer	1	250 nM
5-20 ng/ μL Template	1	0.1-0.5 ng/ μL
Taq 2X Master Mix	25	1x
DMSO (99.9%)	up to 2.5	
ddH ₂ O	To 50	

Table 7 Example of a PCR program with a PCR product of 1000 bp

Cycles	Step	Phusion		Taq	
		Temp/°C	Time/s	Temp/°C	Time/s
1	Denaturation	98	300	95	30
30	Denaturation	98	30	95	15
	Annealing	60	25	60	25
	Elongation	72	60	68	120
1	Elongation	72	300	68	600

3.3.1.2 Ligase Independent cloning (LIC)

LIC[233], [234] makes use of the 3'-5' exonuclease activity of T4 DNA polymerase. The linearized LIC-vector and the PCR product are treated separately with T4 DNA polymerase to create specific complementary overhangs, which allows efficient annealing of PCR product and vector in absence of DNA ligases.

Forward Primer 5'-**CAGGGCGCCA**TG-gene of interest
 Reverse Primer 5'-**GACCCGACGCGGT**TA-gene of interest (rev. comp.)

The PCR product and BsaI linearized vector are purified by agarose gel-electrophoresis and gel-extraction.

The purified PCR Product was incubated with T4 DNA polymerase in the presence of dATP and the linearized vector backbone was incubated with T4 DNA polymerase in the presence of dTTP for 30 min at 25°C. After 25 min heat deactivation at 75°C, the mixtures can be used for annealing reactions immediately or can be stored at -20°C.

Table 8 Preparation of LIC overhangs

	Insert	Vector
10x NEB2	2 µL	2 µL
PCR Product	0.2 pmol	
Linearized Vector		0.8 pmol
dATP (100 mM)	0.5 µL	
dTTP (100 mM)		0.5 µL
DTT (100 mM)	1 µL	1 µL
100x BSA	0.2 µL	0.2 µL
T4 DNA Polymerase (3U/µL)	0.4 µL	0.4 µL
ddH ₂ O	20 µL	20 µL

The ligation was performed with a 1:2 to 1:3 molar ratio of vector:insert.

Vector (0.8 pmol)	1 μ l
PCR product (0.02 pmol)	2 μ L
	5 min Incubation
EDTA pH 8.0 (25 mM)	1 μ L
5 min incubation	

1 μ L of the ligation reaction was typically used to transform 50 μ L DH5 α cells. Colonies were screened by colony PCR for amplicons of the desired length using T7 promoter and T7 terminator and analyzed by agarose gel electrophoresis. The positive colonies were used to inoculate 10 mL TB overnight cultures and the plasmids were isolated and sequenced.

3.3.1.3 Site directed mutagenesis

To incorporate mutations in a plasmid vector, oligonucleotide primers containing the desired mutation and complementary overhangs of 10 to 15 bp to the target sequence were designed. PCR with Phusion polymerase with 20 cycles and elongation time of 5 min in order to amplify the entire plasmid was performed. 20U DpnI were added to the reaction mixture and incubated for 1 h to digest the methylated DNA template. 50 μ L chemically competent DH5 α cells were transformed with 10 μ L of the reaction mixture. Colonies were used to inoculate 10 mL TB overnight cultures and the plasmids were isolated and sequenced.

3.3.1.4 Restriction free cloning

Z-MEK2, Z-orf155a and Z-orf91a were amplified from pETZ2-1a/Lic with T7 promoter and terminator according to the restriction free cloning method[235]. The amplicons were purified with the MN kit and used as “mega primers” in PCR reactions with the pCDF-13 co-expression vector. After 20 cycles of PCR with Phusion polymerase, DpnI was added and incubated for 1 h at 37°C. DH5 α cells were transformed with 10 μ L of the PCR reaction. Colonies were screened as described for the mutagenesis and the vectors were sequenced.

3.3.2 Production and purification of protein

3.3.2.1 Production of recombinant protein

Expression plasmids were transformed in *E. coli* BL21 (DE3) chemically competent cells and plated on LB agar with the appropriate antibiotics. Single colonies were used to inoculate 50 mL TB o/n cultures with the same antibiotics. 0.5 – 1 L TB medium was inoculated with 1% of the o/n cultures and incubated at 37°C and continuous shaking (220 rpm) until OD_{600 nm} 0.5 - 0.9 was reached. Cultures were cooled to 21°C and the protein expression induced by addition of IPTG to a final concentration of 0.2 mM. After 12 to 20 h the cells were harvested by centrifugation at 4000 x g for 25 min. The pellets were resuspended in resuspension buffer (3 mL buffer/g wet pellet), flash frozen in liquid nitrogen and stored at -80°C.

3.3.2.2 Protein purification

The recombinantly expressed proteins were purified with a combination of immobilized metal ion affinity chromatography (IMAC), size exclusion chromatography (SEC) and anion exchange chromatography if necessary.

3.3.2.2.1 IMAC

The cell pellets were thawed at 4°C and disrupted by sonification on ice. Insoluble components of the lysate were removed by centrifugation (30000 x g, 4°C, 45 min). The supernatant was filtered (45 µm) and applied onto Ni-NTA agarose packed in a gravity flow column equilibrated with wash buffer. The Ni-NTA agarose was washed with 5 to 10 column volumes of wash buffer and bound proteins were eluted with 3 volumes of elution buffer. The proteins were dialyzed over night at 4°C against dialysis buffer. In case the tag had to be removed, TEV-protease (1/100 w/w) was added to the protein prior to dialysis and the dialyzed protein solution was then applied to Ni-NTA agarose to remove the tag. The purity of the protein was controlled with SDS-PAGE and the concentration by absorption measurement at 280 nm.

3.3.2.2.2 Size-exclusion chromatography

Proteins were concentrated to 10 to 20 mg/mL, filtered (0.22 μ m) and purified by size exclusion chromatography using Superdex S75 or Superdex S200 material packed in 16/60 columns mounted on a Äkta Purifier or Äkta Explorer.

3.3.2.2.3 Ion exchange chromatography

In case the purity of the proteins was not sufficient after IMAC/SEC purification, proteins were further purified with GE MonoQ column, mounted on Äkta Purifier or Äkta Explorer. Proteins were dialyzed against 50 mL NaCl, 20 mM Tris/HCl pH 8.0 buffer and eluted with a gradient from 50 to 500 mM NaCl over 100 mL. Eluted proteins were dialyzed against dialysis buffer.

3.3.3 Reductive methylation of Protein

The reductive methylation of protein was performed according to the protocol of Walter et al[236]. Recombinant protein was purified and expressed as described. During the TEV protease cleavage of the tag, the protein was dialyzed against 50 mM HEPES pH 7.5, 250 mM NaCl and a SEC was performed with the same buffer. 20 μ L fresh 1 M dimethylamine-borane-complex (ABC) and 40 μ L 1 M formaldehyde were added per mL of a protein solution of 1 mg/mL and the reaction was incubated at 5°C for 2 h. Then another 20 μ L of the ABC solution and 40 μ L of the formaldehyde solution were added, after 2 h incubation 10 μ L of the ABC solution was added and the reaction was incubated at 5°C over night. The reaction was quenched by an addition of an equal amount of dialysis buffer then the sample was concentrated and purified by SEC in dialysis buffer.

3.3.4 Protein characterization

3.3.4.1 Estimation of protein concentration

Protein concentrations in solution were estimated by the absorption of light at 280 nm using a NanoDrop ND-1000 UV/Vis spectrophotometer. According to the Lambert-Beer law, $A = \epsilon lc$, the absorbance A of light is proportional to the path length of light l , the concentration c of the sample and a substance and wavelength specific extinction coefficient ϵ . At 280 nm, ϵ of a protein can be

calculated as the sum of number of Trp, Tyr, and disulfides, multiplied by their extinction coefficient [237]–[239]. Hence the concentration is given

$$c = \frac{A_{280\text{nm}}}{\epsilon \cdot l}$$

by $\epsilon(\text{Protein}) = n(\text{Tyr}) \cdot \epsilon(\text{Tyr}) + n(\text{Trp}) \cdot \epsilon(\text{Trp}) + n(\text{Cys}) \cdot \epsilon(\text{Cys})$

3.3.5 SDS-PAGE

SDS-PAGE [240] was used to monitor protein purity at all steps of the purification process. Proteins were denatured at 95°C in SDS-sample buffer. SDS binds in a fixed ratio to polypeptide backbones [241], thereby giving the proteins a charge, which is proportional to their Mw and allows the separation during the electrophoresis according to their Mw instead of according to the intrinsic charge of the protein. The Mw of a given protein can be estimated by comparison with Mw marker with proteins of a known length run on the same gel. Gels were run at constant 220 V for 40 to 60 min and stained with Coomassie G250 or R250.

3.3.6 N-terminal sequencing

N-terminal sequencing allows the determination of the N-terminal amino acid sequence of a given protein [242]. Unstained SDS-PAGE gels were blotted to a PVDF membrane at 4°C. N-terminal sequencing was performed by Dr. Fritz Buck, UKE Hamburg.

3.3.7 Dynamic Light scattering

Dynamic light scattering (DLS) was used to analyse the dispersity of YopP in solution. Freshly purified protein samples were ultra centrifuged and 9 µL of protein solution were transferred to an optical cuvette for the measurement.

3.3.8 Protein crystallisation

SEC-purified proteins were subjected to crystallisation trials, either using the EMBL-Hamburg high throughput crystallisation facility [243] or manually. Proteins in supersaturated solutions can undergo a phase transition and form crystallisation nuclei from which protein crystals can grow (Figure 2). In the vapour diffusion method [244], aqueous protein solution is mixed with a precipitant solution in an airtight container. The drop can be either positioned

hanging at the lid of the container or as sitting drop separated from the precipitant reservoir. Due to the different precipitant concentrations in the drop and the reservoir, an equilibration process sets in, during which the concentration of both protein and precipitant is increasing and may reach the nucleation zone and protein crystals can form (Figure 2 C). In the microbatch methods under oil, protein and precipitant solution are mixed and stored in a plate which is covered with a water impermeable oil [245](Figure 2 A). This method explores less phase space than vapour diffusion and can be modified to use a mixture of water impermeable and permeable oils which allow evaporation of water and an increase of protein a precipitant concentration over time [246] (Figure 2).

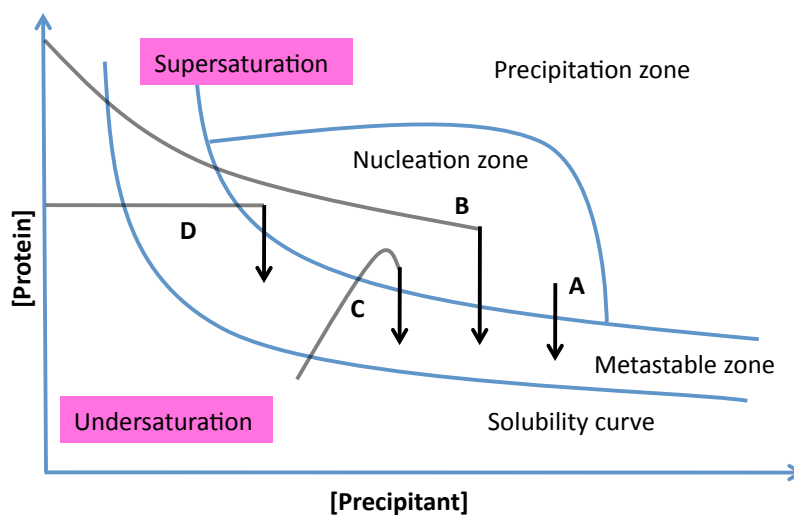


Figure 2 Protein crystallisation phase diagram in which the protein concentration is plotted against the precipitant concentration. Proteins in supersaturated solutions can form crystallisation nuclei. Supersaturation can be achieved by (A) microbatch, (B) free interface diffusion, (C) vapour diffusion or (D) microdialysis. The formation of crystallisation nuclei leads to a drop in protein concentration, which allows a transition to the metastable zone, where the existing nuclei can grow to crystals. Figure redrawn form [244].

3.3.9 Creation of *M. smegmatis* knockout strain

3.3.9.1 Creation of the KO vector

The *M. smegmatis* knockout strain Δ MSMEG_4199 was generated using the recombineering method of van Kessel and Hatful [247], [248]. Homologues AB and CD, which span from the up- and downstream regions of MSMEG_4199 to the protein coding region of MSMEG_4199 were amplified by PCR from *M. smegmatis* mc²155 genomic DNA. Amplicon MSMEG-4199-A/MSMEG-4199-B (Table 4)(AB) and pYUB854 derived pEN11 vector were both digested with XbaI/KpnI and purified by agarose-gel-extraction. The linearized vector and the fragment were ligated with T4 DNA ligase and transformed into HB101 chemically competent cells. PCR with primers AB and DNA sequencing verified the correct insertion of amplicon AB in pEN11. Vector pEN11_AB and amplicon CD were both digested with HindIII/AgeI and purified by DNA-gel-extraction. Amplicon CD and linearized pEN11_AB vector were ligated and transformed into HB101 chemically competent cells. The correct sequence of pEN11_AB_CD was verified by PCR with primers A, B, C and D, digestion with the respective endonucleases KpnI, XbaI, HindIII and AgeI and DNA sequencing. A DNA preparation from 50 mL HB101 o/n culture was performed to have a high concentration of DNA for the following transformation. pEN11_AB_CD was digested with KpnI/XbaI. The insert was separated from the vector backbone by agarose-gel-electrophoresis and the substrate was purified by gel-extraction.

3.3.9.2 Transformation of *M. smegmatis*-wt with KO vector

1.5 μ L of the linear targeting substrate (100 ng/ μ L) was added to electro-competent *M. smegmatis* mc²155 cells harbouring the pJV53 plasmid. The cells were incubated on ice for 10 min, electroporated twice with 2.5 kV, 1 k Ω , 25 mF. 1 mL 7H9 induction medium was added and the cells were allowed to recover at 37°C, 175 rpm for 4 h. The entire transformation reaction was plated on 7H9 (Kan, Hyg, Carb) agarose plates.

10 recovered colonies were each inoculated in 20 mL 7H9 broth medium (Kan, Hyg, Carb). The cultures were allowed to reach OD_{600 nm} of 2. Genomic DNA of the

Hyg resistant cells was extracted according to the protocol of van Kessel and Hatful [248] and glycerol stocks of the cultures were prepared.

3.3.10 Southern Blot

Southern blot is a method, which allows the detection of specific DNA fragments by hybridization with a complementary sequence [249]. In the work presented here, a digoxigenin-11-dUTP (DIG) labelled probe was prepared, which was visualized after the hybridization with a DIG specific antibody, conjugated to alkaline phosphatase [250]. Addition of alkaline phosphatase substrates BCIP/NBT results in the formation of a blue precipitate at the location of the hybridization. 5 µg genomic DNA of Hyg resistant *M. smegmatis* were diluted in 50 µL NEB buffer and digested over night with respective restriction endonucleases. 50 µL of ddH₂O, 1/10 (v/v) NaAc, 3 M pH 5.2, 1 µL glycogen and 3 volumes of EtOH were added consecutively to precipitate the *M. smegmatis* genomic DNA. The samples were put at -80°C for 20 min and spun at 12000 x g for 10 min. The pelleted DNA was washed with 100 µL EtOH. Afterwards, the pellets were dried, resuspended in 10 µL ddH₂O and separated with a 1% agarose TBE gel along with DIG-labeled DNA molecular weight marker VII (Roche). The gels were incubated with 0.25 M HCl for 15 min, followed by 30 min. with denaturation buffer and twice washed for 15 min. with neutralization buffer and with ddH₂O. DNA was blotted on a positively charged nylon membrane by capillary transfer with 20xSSC buffer over night [251]. The DNA was then cross-linked to the membrane by UV-light. The membranes were pre-hybridized in a 50 mL Falcon tubes with the appropriate amount of DIG Easy Hyb buffer (Roche) for 30 min. The DIG-labelled probe (See paragraph 3.3.10.1) was denatured (95°C, 5 min) and added to pre-warmed DIG easy hyb buffer. The pre-hybridization solution was discarded and the hybridization solution was added. The hybridization reaction was incubated under constant agitation for 4 h at 58°C. The membrane was put in washing buffer for 5 min, for 30 min in 100 mL blocking solution, for 30 min in antibody solution, twice for 15 min in washing buffer and for 5 min in detection buffer. Eventually the membrane was placed in 10 mL freshly prepared colour substrate solution. Placing the membrane in TE-buffer as soon as the bands became visible stopped the colour reaction.

3.3.10.1 Preparation of the hybridization probe

Hyg res cassette was obtained by restriction digest and gel-extraction of pEN11 vector. 1 μg DNA was diluted in 16 μL ddH₂O, denatured at 95°C for 10 min and put on ice. 4 μL of DIG-High prime (Roche) was added to the DNA and the reaction was incubated at 37°C over night. The reaction was stopped by adding 2 μL 0.2 M EDTA pH 8.0. The labelling efficiency was determined according to the manufacturer's manual.

3.3.11 Unmarking of the MSMEG Δ 4199

One of the Hyg-resistant, Southern-Blot positive clones was transformed with the $\gamma\delta$ -resolvase containing pGH542 plasmid (Tet resistance) and grown on Tet selective 7H10 plates. Recovered colonies were patched onto (i) Hyg (ii) Carb and (iii) Tet selective 7H10 agar plates. Only colonies which were Tet resistant and Hyg sensitive were used to inoculate 7H9 (Carb) and later plated on (i) Hyg (ii) Carb and (iii) Tet selective 7H10 agar plates. Colonies, which were Kan, Tet and Hyg sensitive, were used to prepare genomic DNA. The generation of the scar mutant was verified by PCR from genomic DNA.

3.3.12 Growth curve of MSMEG 4199

In a 24 well culture plate, 500 μL 7H9 broth medium were inoculated with 50 μL of a dense *M. smegmatis* culture. The plates were sealed with Parafilm and the growth was monitored by measurement OD_{600 nm} in a TECAN M1000 plate reader. The plates were incubated at 37°C with orbital shaking of 4 mm amplitude. The OD_{600 nm} was measured every 20 min. All experiments were performed in triplicates.

3.4 Biophysical Methods

3.4.1 Isothermal Titration Calorimetry (ITC)

ITC allows the direct determination of thermodynamic parameters such as reaction stoichiometry n , enthalpy change ΔH , and association and dissociation constant (K_a/K_d) of reactions and interaction in solution [252]. Two interacting partners are titrated against each other and the energy consumed or generated is calculated by the amount of energy, which was needed to keep the sample cell

at the same temperature as the reference cell. From the direct parameters the changes in Gibbs energy ΔG and the change in entropy ΔS can be derived using the relationship given in the Gibbs-Helmholtz equation [253], [254]

Equation 1
$$\Delta G = \Delta H - T\Delta S = -RT \ln K_a$$

with the ideal gas constant $R = 8.314 \text{ Jmol}^{-1}\text{K}^{-1}$ and the absolute temperature T in Kelvin (K). The mass action law of bimolecular reaction $A+B \rightleftharpoons AB$ defines the association constant K_a as the ratio between bound and unbound reactants.

Equation 2
$$K_a = \frac{[AB]}{[A][B]} = \frac{1}{K_d}$$

Stoichiometry n and K_a/K_d values are derived from the plotting of the energy changes against the molar ratio of the titrants.

The calorimetric experiments were performed with a VP-ITC (MicroCal). An initial injection of 3 μL (6 s duration) was followed by 27 (20 s duration) injections of 10 μL each, with 240 seconds spacing in between two injections. The stirring speed of the injection syringe was 307 rpm. Heats of dilution were determined by injecting the ligands into the buffer and subtracted from the heat of interaction prior to curve fitting. Data analysis and curve fitting was performed with Origin 7 and the MicroCal plug-in for a standard non-interacting one site model. In case of the low affinity phospholipid titrations, the inflection point of the curve becomes poorly defined. The stoichiometry parameter n was therefore fixed to 1.0 for all the fittings [255] which is consistent with the structural information and other published data [214], [256].

Titration with YopP were performed in dialysis buffer pH 8.0. CoA was dissolved in the buffer, which was used to dialyse YopP. IP6 was diluted in the buffer, which was used to dialyse YopP from a 20 mM stock solution in dialysis buffer (pH 8.0). SEC purified Rv2140c was dialyzed against 50 mM NaCl, 20 mM NaH_2PO_4 pH 6.5 and concentrated to 0.32 to 0.49 mM. Phospholipids (>98% purity) (Avanti Polar Lipids) were dissolved in the same buffer as the protein to give final concentrations of 24.3 mM for DHPE, 25.6 mM for DHPA, 21.0 mM for DHPS and 21.5 mM for DHPG. DHPE was not entirely soluble in the buffer and

the insoluble material could not be resolubilized, hence the concentration used in the experiments is likely to be lower than 25.6 mM.

3.4.2 Circular Dichroism Spectroscopy

Based on the phenomenon of different absorption of left – and right circularly polarized light by optically active molecules, CD-spectroscopy is widely used to estimate the secondary structure content of proteins due to different absorption characteristics of α -helices, β -sheet and random coil [257]. Moreover, loss of secondary structure content during temperature ramping experiments can reveal the correct folding state as well as the melting temperature of a protein. Purified protein was diluted with water to 0.1 to 0.5 mg/mL

3.4.3 Acetylation assays

Ellmann's reagent (5,5'-**dithio**bis-(2-**nitro**benzoic acid)) (DTNB) [258] was used to investigate the kinetics of the acetylation reaction. Thiol groups are oxidized by DTNB at neutral and basic pH, which leads to formation of a disulfide bond between the thiol and 2-**nitro**-5-**thio**benzoate (NTB) and the release of the other NTB, which dissociates to NTB^{2-} . NTB^{2-} has a yellow colour and an absorption peak at 412 nm. During the acetylation reaction, coenzyme-A is released by a rate depending on the kinetic parameter. The free thiol group of CoA can react with DTNB and the amount of released CoA can be studied by monitoring the absorption at 412 nm (Figure 3).

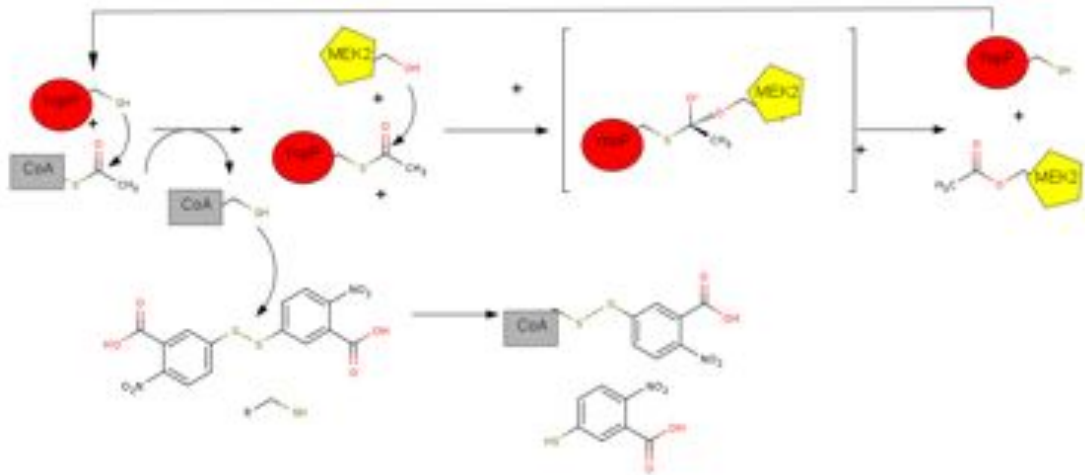
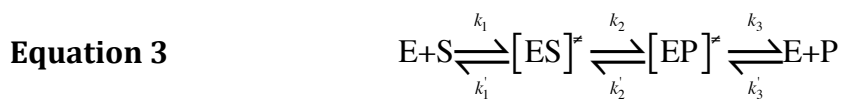


Figure 3 Reaction mechanism of YopP mediated MEK2 acetylation and subsequent reaction of CoA with DTNB.

For the kinetic experiments, serial dilutions of MEK2 and acetyl-CoA were pipetted in 0.5 mL reaction tubes and gently mixed. IP6 was diluted to the indicated concentrations from a 20 mM stock in dialysis buffer (pH 8.0). 15 μ L of the reaction mixture were transferred to 384 well Greiner plates. The plates were centrifuged at 4000 x g for 10 s and placed in the TECAN plate reader. $A_{412\text{ nm}}$ was recorded every 20 s for 1 to 24 h.

3.4.3.1 Michaelis-Menten Kinetics

The reaction of enzyme E and substrate S to the product P by the intermediate formation of enzyme/substrate and enzyme/product complexes and the eventual release of the product can be described as follows:



Assuming that $k_3 \gg k_2$ and $k_1 \gg k_2$, k_2 becomes the rate limiting step. Equation 3

can be simplified to $E+S \xrightleftharpoons[k_1']{k_1} [EX]^{\#} \xrightarrow{k_2} E+P$ with the assumption of a central

intermediate complex $[EX]^{\#}$. Under equilibrium conditions the dissociation constant K_d of the enzyme substrate complex can be described as:

Equation 4
$$K_d = \frac{k'_1}{k_1} = \frac{[E][S]}{[EX]}$$

For the case when k'_1 and $k_1[S] \gg k_2$ the rapid establishment of an equilibrium between E, S and EX occurs and with the assumption that the concentration of EX does not change over time, $d[EX]/dt=0$. The total enzyme concentration $[E]_0$ and the total substrate concentration $[S]_0$ is the sum of free and complex bound forms:

Equation 5
$$[E]_0 = [E] + [EX], [S]_0 = [S] + [EX]$$

With Equation 4, Equation 5 can be rewritten as:

$$[E]_0 = \frac{K_d [EX]}{[S]} + [EX]$$

Dividing both sides by $[EX]$ and multiplying with k_2 and applying the terms for the rate of product formation $v=k_2[EX]$ and the maximum velocity are and $V_{max}=k_2[E]_0$, we get the Michaelis-Menten-Equation [259]:

Equation 6
$$v = \frac{V_{max} [S]}{K_m + [S]}$$

The function describes the initial reaction velocities v against the substrate concentration S under the assumption that the concentration of the EX complex is constant. It approaches a maximal velocity v_{max} for high substrate concentrations. It allow indirect access to k_1 , k'_1 and K_d via the substrate concentration, at which the velocity is half maximal via $v_{max}/2$ corresponds $K_m = (k'_1+k_2)/k_1$, in the case $k_2 \ll k'_1$, $K_m=K_d$. Moreover, it allows direct access to k_2 via $k_2=v_{max}/[E]_0$.

4 Results

4.1 YopP

4.1.1 Expression and purification of YopP

Y. enterocolitica (pYVe8081) YopP-wt and YopP-C172A were kindly provided by Dr. Klaus Ruckdeschel (UKE Hamburg) in a pGEX-4T3 vector with a N-terminal GST-tag. No significant protein expression was observed with *E. coli* BL21(DE3) inducible expression strains (data not shown). YopP-wt and YopP-C172A were sub-cloned into the pETZ2-1a/Lic vector. YopP-wt and YopP-C172A showed high expression level. After IMAC and SEC purification, the yield was between 15 and 25 mg per L of culture medium. SDS-PAGE revealed that Z-YopP (Figure 4 B) as well as YopP (Figure 4 D) showed degradation pattern. Besides the intense band for the 32 kDa full length protein, at least four less intense bands of truncated species between 20 and 30 kDa (Figure 4 D) were present. Supplementing the resuspended cell pellet with protease inhibitor mix prior to cell lysis had no effect on degradation pattern. The pattern was observed for YopP-wt as well as YopP-C172A, indicating that it was not caused by a possible protease activity of YopP.

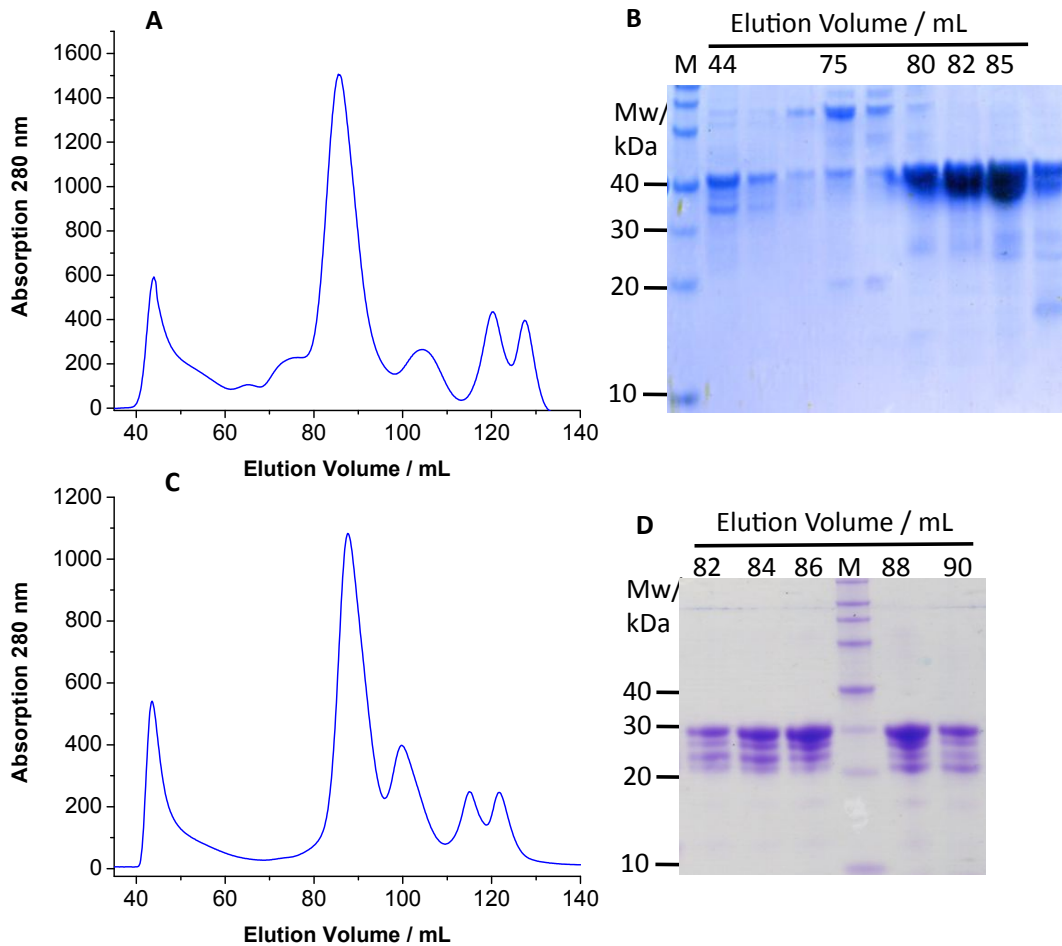


Figure 4 Purification of wt YopP₁₋₂₈₈ **(A)** SEC elution profile of IMAC purified Z-YopP₁₋₂₈₈ **(B)** SDS-PAGE (12%) of indicated fractions of (A). **(C)** SEC elution profile of YopP₁₋₂₈₈. **(D)** SDS-PAGE (12%) indicated fractions of (C). (M: Marker: RotiMark 10-150)

The identity of the native protein was verified by MALDI-TOF and indicated a protein of 32 kDa, while also there some degradation bands were visible (Figure 17). Finger print tryptic digest of SDS-PAGE revealed numerous peptides, which could be assigned to *Y. enterocolitica* YopP.

4.1.2 Self-degradation

Interestingly, upon storage of wt Z-YopP at 4°C for three weeks, the protein was truncated to a smaller fragment of approx. 20 kDa on SDS-PAGE (Figure 5 A). Attempts to characterize the identity of the truncated YopP by LC-MS/MS (carried out by the proteomics core facility in EMBL-Heidelberg) gave an ambiguous result of a YopP fragment of a maximal length of aa 18 to aa 250.

Results

Even though amino- and carboxy-terminus were not detected in the investigated sample, the coverage (Figure 5 B) over the protein sequence contained gaps and it also did not seem to reflect the approx. 20 kDa protein, which is present on the SDS-PAGE. However, the Z-tag was not detected in the 20 kDa band. Besides this intense band, lane 1 in (Figure 5 A) shows two faint bands, one at 40 kDa and another one between 40 and 30 kDa. In the lanes 2 and 3, TEV-protease was added and the two faint bands were shifted by -10 kDa, indicating that these bands correspond to degraded YopP species, which still contain the 10 kDa N-terminal Z-tag and hence the degradation must have occurred predominantly at the C-terminus. In contrast, the intense band at 20 kDa is not shifted due to addition of TEV-protease, indicating that this band corresponds to a YopP species, in which the N-terminal Z-tag as well as a part of the C-terminus are degraded.

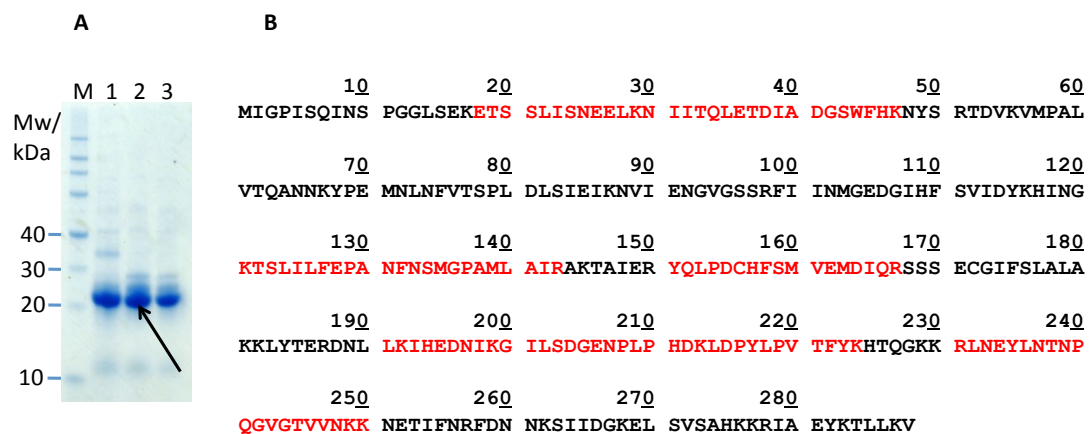


Figure 5 Self-degradation of wt Z-YopP_1-288. **(A)** SDS-PAGE (12%) of YopP. (1) Z-YopP. (2) Z-YopP +TEV (1/10). This band was analyzed by LC-MS/MS. (3) Z-YopP + TEV (1/100). **(B)** LC-MS/MS analysis of self-degraded YopP. Fragments, which were detected in band A2 are highlighted in red. (M: Marker: RotiMark 10-150)

4.1.3 Biophysical and biochemical characterization of YopP

4.1.3.1 CD-Spectroscopy

CD-spectroscopy was used to investigate the secondary structure of YopP, the folding state and the respective melting temperature. UV/Vis-CD-spectra of fl YopP-wt and of the self-degraded Z-YopP-wt were recorded and confirmed a

Results

high degree of α -helical content for both as it was expected from secondary structure prediction (Figure 12) and homology modelling (Figure 6 B, E). Temperature ramping experiments were performed at 223.5 nm and revealed marked differences in the unfolding characteristics between fl YopP-wt and degraded Z-YopP-wt. Upon temperature ramping, fl YopP showed a sigmoidal melting curve with a melting temperature of approximately 55°C (Figure 6 C). Upon cooling, the protein did not retain its secondary structure content and remained denatured. The degraded YopP-wt however, also showed a sigmoidal melting curve, but even at 95°C, the ellipticity at 223.5 nm dropped only by 50% compared to 4°C, upon cooling it returned to 60% of the start value (Figure 6 F). This indicates that the degraded YopP-wt is only partially unfolded at 95°C and most of it refolds upon cooling.

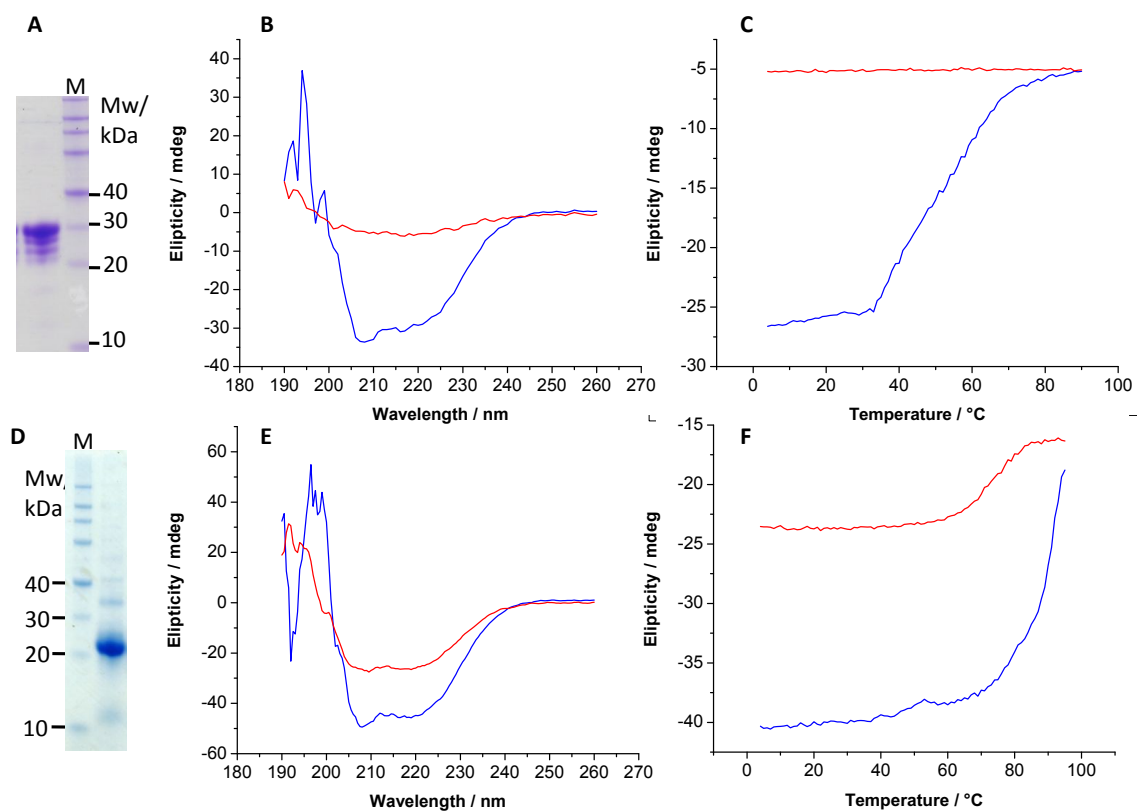


Figure 6 CD-spectroscopic characterization of wt YopP₁₋₂₈₈ (A, B, C) and self-degraded Z-YopP₁₋₂₈₈ (D, E, F). (A, B) respective SDS-PAGE (12%) from the samples used. (B, E) full Spectra were recorded at 5°C before temperature ramping (blue line) and afterwards (red line). (C, F) Temperature ramping

experiments (5-95°C) were performed at 223.5 nm (blue lines) and cooling (95-5°C) (red lines). (M: Marker: RotiMark 10-150)

The fl YopP-wt is drastically destabilized, compared to the degraded YopP-wt. Fl. YopP-wt was denatured and precipitated in the CD-cuvette after the temperature ramping experiment, whereas no precipitation was observed in the cuvette of the degraded Z-YopP. The melting curve of self-degraded YopP (Figure 6 F) shows a kink between 50 and 60°C. This kink could correspond to the longer Z-YopP species between 30 and 40 kDa (Figure 6 D) and could explain why the ellipticity drops only to 60% of its starting value upon cooling. This remarkable shift in melting temperature is probably not caused by formation of disulfide bonds, since YopP contains only two cysteine residues and the small fraction of aggregated protein, which elutes with the void volume during SEC runs was always independent of the addition of reducing agents such as TCEP, DTT and β -mercaptoethanol.

4.1.3.2 Investigation of Binding to Ligands

The acetyl-transferase activity of *Yersinia* YopP/YopJ is enhanced by binding to phytic acid, (inositolhexakisphosphate, IP6) [149], a hexaphosphorylated cyclohexane, which is present only in eukaryotic cells and not in bacteria. Mittal et al. were not able to produce sufficient amounts of *Yersinia* YopP/YopJ for interaction studies; but they could show an interaction of *Salmonella enterica* AvrA, a YopP homologue in a CD spectroscopy based assay. In order to transfer acetyl residues to serine and threonine residues of kinases, YopP has to bind to and react with acetyl-CoA. Hence it could be that it also binds CoA.

4.1.3.2.1 Binding of YopP with IP6

The ITC experiments revealed an enthalpy driven binding of YopP with IP6, dissociation constant K_D of $3.8 \pm 0.92 \mu\text{M}$ and a binding enthalpy of -5 kcal/mol. The integrated heat change for the first injections differs markedly from the fitted binding curve (Figure 7 lower panel). The stoichiometry factor n of the binding is 0.669 instead of the 1.0 for a presumed 1:1 binding of IP6 and YopP (Table 9).

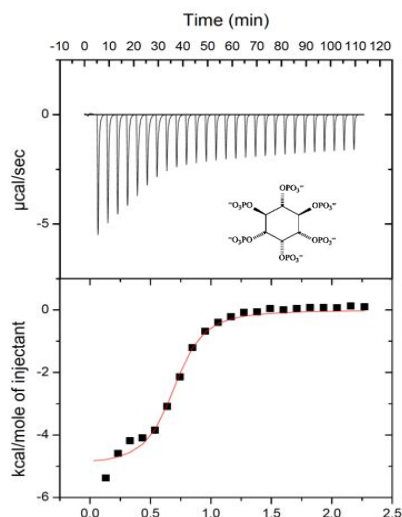


Figure 7 Calorimetric characterization of the YopP/IP6 interaction. IP6 (2.5 mM) was added to Z-YopP-wt 1-288 (0.173 mM). The upper panel shows the raw ITC and the lower panel shows the integrated heat change (squares) and the fitted binding curve (red).

4.1.3.2.2 Binding of YopP with CoA

The ITC experiment showed an enthalpy driven interaction for YopP and CoA with a dissociation constant K_D of $4.55 \pm 1.34 \mu\text{M}$ and a binding enthalpy of -4.3 kcal/mol . The stoichiometry parameter n is 0.485 instead of 1 (Table 9).

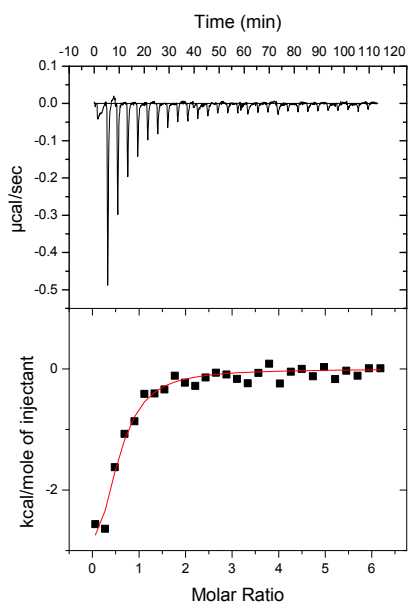


Figure 8 ITC characterization of the YopP/CoA interaction. CoA (0.54 mM) was added to Z-YopP-1-288 (0.018 mM). The upper panel shows the raw ITC and the lower panel shows the integrated heat change (squares) and the fitted binding curve (red).

4.1.3.2.3 Binding YopP/Co-A with IP6

To test if the binding of CoA bond YopP affects the interaction with IP6, CoA was added to YopP and then a titration with IP6 was performed. The affinity for the interaction of CoA bound YopP to IP6 is with a K_D of 3.18 μM increased by 16% compared to YopP alone. With -14.65 kcal/mol, the heat of interaction of the CoA bound YopP to IP6 exceeds the heat of interaction of the YopP binding to IP6 by almost by a factor of 3 and also the stoichiometry factor n reaches only 0.375 instead of 1 for a presumed 1:1 binding (Table 9).

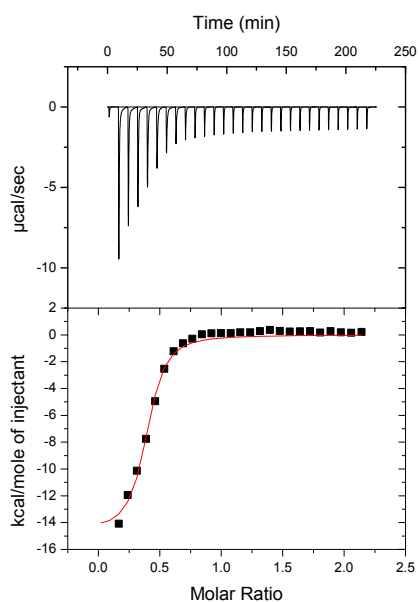


Figure 9 ITC titration of YopP-Z/CoA (0.204 mM/1.0 mM CoA) and IP6 (2.08 mM) The upper panel shows the raw ITC and the lower panel shows the integrated heat change (squares) and the fitted binding curve (red).

Table 9 Binding parameter of YopP with IP6 and coenzyme-A

	n	$K_D / \mu\text{M}$	ΔG kcal/mol	$\Delta H / \text{kcal/mol}$	$-T\Delta S / \text{kcal/mol}$
IP6	0.669	3.8±0.92	-2.58±0.157	-4.99±0.157	2.406
CoA	0.485	4.55±1.34	-1.27±0.7	-4.28±0.69	3.011
CoAIP6	0.375	3.18±0.62	-7.49±0.51	-14.65±0.52	7.156

4.1.3.3 Limited proteolysis

It was reported that binding to IP6 induces changes in secondary structure content in AvrA [149]. To investigate the effect of IP6 binding to YopP, a series of limited proteolysis experiments with Z-YopP-wt in presence and absence of TEV-protease, IP6 and chymotrypsin (CT), thermolysin (TL) and subtilisin (S) at ratios of 1/10, 1/100 and 1/1000 (w/w) were performed. At protease concentrations of 1/10 (w/w), Z-YopP is entirely degraded, regardless of presence of IP6 or TEV protease (Figure 10). At protease concentrations of 1/100 (w/w), CT has only a limited proteolytic effect on YopP, whereas S degrades YopP entirely. In presence of TL however, two distinct bands are visible, an intense band at 20 kDa and a weaker band just below 30 kDa (Figure 10). The upper band is only present when IP6 was added to YopP. This indicates that binding to IP6 protects YopP partially from degradation by the proteases. The same pattern of protection against proteolysis through IP6 occurs as well when TL and S are used at concentrations 1/1000 (w/w)(Figure 10). Interestingly, the upper band is just below 30 kDa, compared to fl-YopP, which appears slightly above 30 kDa on the SDS-PAGE (Figure 4 D), indicating that even IP6 bound YopP is partially degraded by the proteases. Moreover, the upper band which appears in presence of IP6 is always much thinner than the band lower band which appears also independently of IP6. The self-degraded YopP appears to be slightly smaller on the SDS-PAGE than the proteolysed YopP species at 20 kDa (Figure 10 Deg). Besides the bands at 20 and below 30 kDa, also shorter fragments of 10 kDa are visible on the SDS-PAGE.

Results

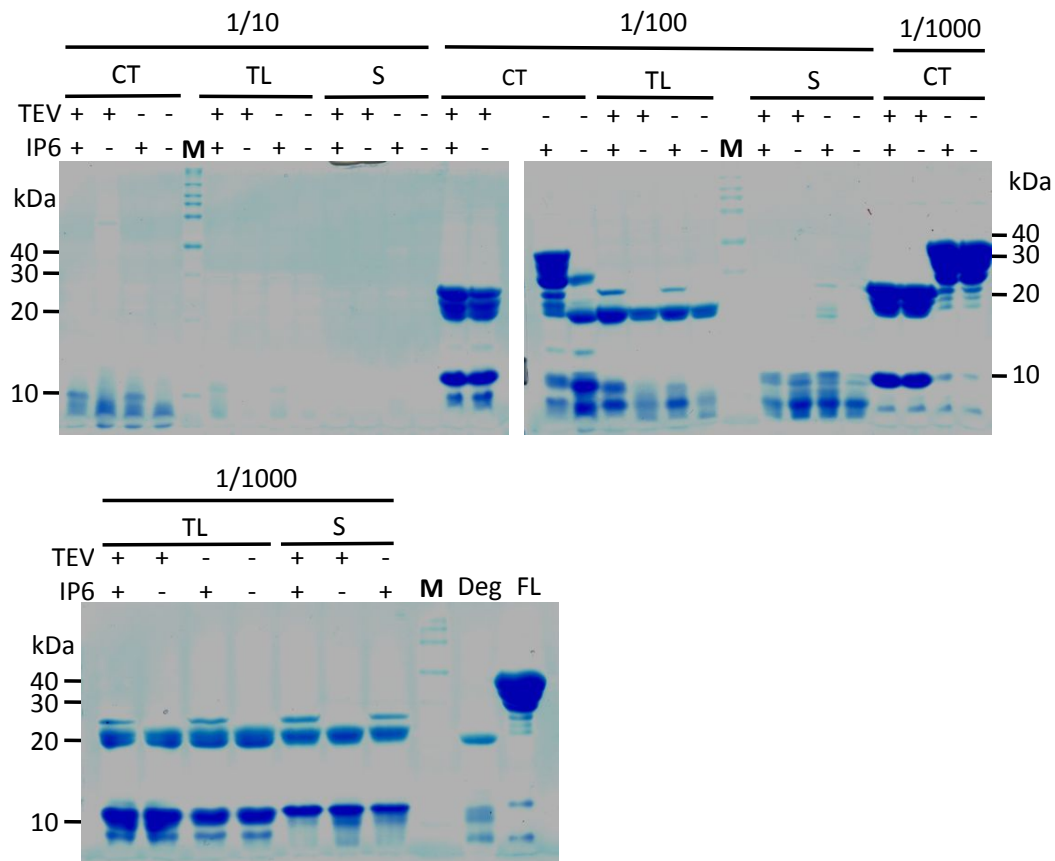


Figure 10 Limited proteolysis of wt Z-YopP₁₋₂₈₈ with chymotrypsin (CT), thermolysin (TL) and subtilisin (S) at (1/10), (1/100) and (1/1000) (w/w) in presence (+) and absence (-) of TEV-protease and IP6. Deg: self-degraded YopP. FL: fl-Z-YopP. (M: Marker RotiMark 10-150)

The IP6 binding site of YopP is not known. Even though, the atypical ITC data indicates that the binding could occur at the partially degraded C-terminus, a more precise analysis is needed.

4.1.3.4 N-terminal sequencing

To analyse the susceptibility of YopP toward limited proteolysis and the protective effect of IP6, as well as the self-degradation of YopP, samples from the two distinct bands at 20 and 30 kDa of the limited proteolysis experiments (Figure 10, 1/1000 subtilisin) and of the self-degraded YopP (Figure 5, Figure 10, Deg) were subjected to N-terminal sequencing. Three different N-termini were detected for the self-degraded YopP, starting from aa 10, aa 16 and aa 12. The signal starting from aa 10 was by far the most intense. The YopP samples, which were subjected to limited proteolysis start exclusively at aa 1, regardless of

presence of IP6. This indicates, that binding to IP6 has an exclusive effect on the C-terminus of YopP.

Table 10 N-terminal sequencing of YopP: The predominant species of the self-degraded YopP starts at aa 10. Only traces of species starting at aa 16 and aa 10 were found as well. YopP subjected to limited proteolysis starts exclusively at aa 1.

Sample	N-terminal sequence	Start
Self degraded	S P G G L S E K E T	aa 10
Self degraded	E K E T S S L I S N	aa 16
Self degraded	G G L S E K E T S S	aa 12
Limited proteolysis	M I G P I S	aa 1
Limited proteolysis + IP6	M I G P I S	aa 1

MALDI-TOF of the self-degraded Z-YopP-wt sample revealed a Mw of 24416 Da (Figure 11), however the shoulder to the left of the peak at 24416 Da indicates a certain degree of heterogeneity, which could reflect the shorter species starting at aa 12 and aa 16 as well as short truncations at the C-terminus. Therefore, it is most likely that the self-degraded YopP spans from aa 10 to aa 226.

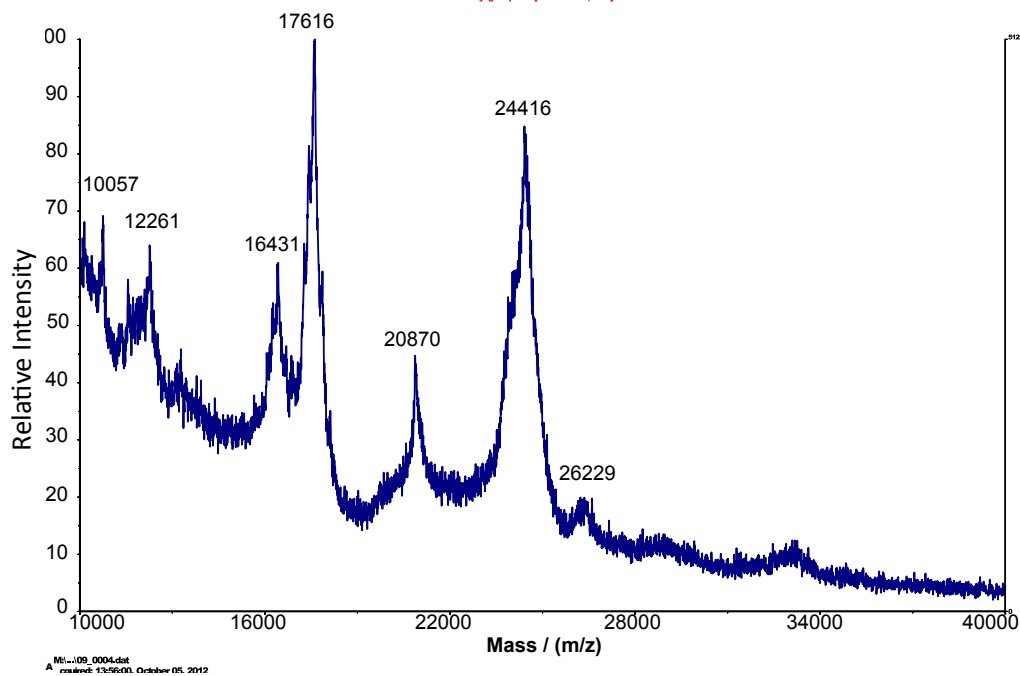


Figure 11 MALDI-TOF of self-degraded YopP. Masses in Da are indicated above the respective peaks.

Unfortunately, despite several attempts, it was not possible to get a meaningful MALDI-TOF measurement to determine the molecular weight and the precise C-terminal end of the two distinct bands of YopP, which was subjected to limited proteolysis in presence and absence of IP6. Therefore, it can only be concluded that binding to IP6 involves residues between aa 226 and aa 288.

4.1.4 Crystallization experiments with YopP

4.1.4.1 Bioinformatic analysis

According to PsiPred secondary structure prediction server [260], YopP is predicted to have a high α -helical content (Figure 12), which is also consistent with the CD-spectra of of fl and degraded YopP (Figure 6).

Results

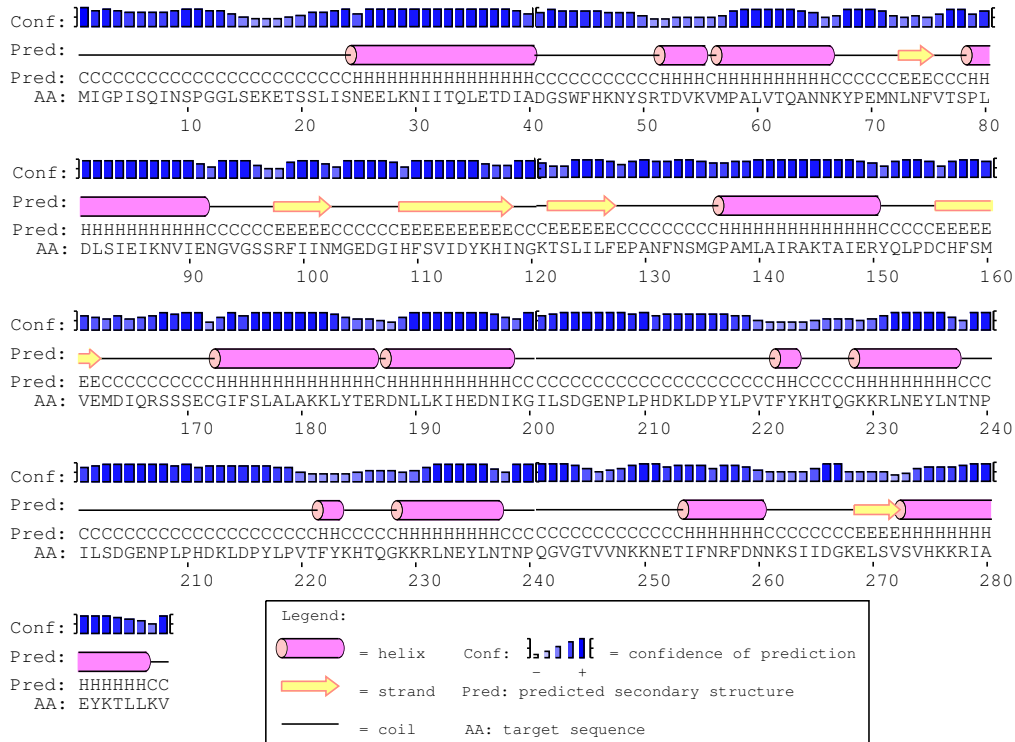


Figure 12 Prediction of secondary structure elements using Psipred [260]

The HHpred server takes the primary structure and the predicted secondary structure of a protein into account and compares it to PDB entries [261]. The PDB entry with the highest sequence identity to YopP is *Xanthomonas* outer protein D (XopD) [262](PDB: 2oix_A), a SUMO protease. A core domain of YopP, spanning from aa41 to 185 has a 14% sequence identity to XopD (Figure 13). The PDB entry with the second highest sequence identity to YopP is the *S. cerevisiae* SUMO protease Ulp1 [263] (PDB: 1euv_A) with a sequence identity of 11% to a YopP core domain spanning from aa39 to aa189 (Figure 13). The N- and C-terminus of YopP do not match any known protein structures. However, the 11 C-terminal aa of YopP have a 50% sequence identity to a CREB binding protein (CEB) which is particularly interesting, since inhibition of the transcription factor CREB is an important function of YopP [135], [264] (Figure 13). The C-terminus of YopP could hence be involved in the transient interaction with other factors besides MAP kinases.

Results

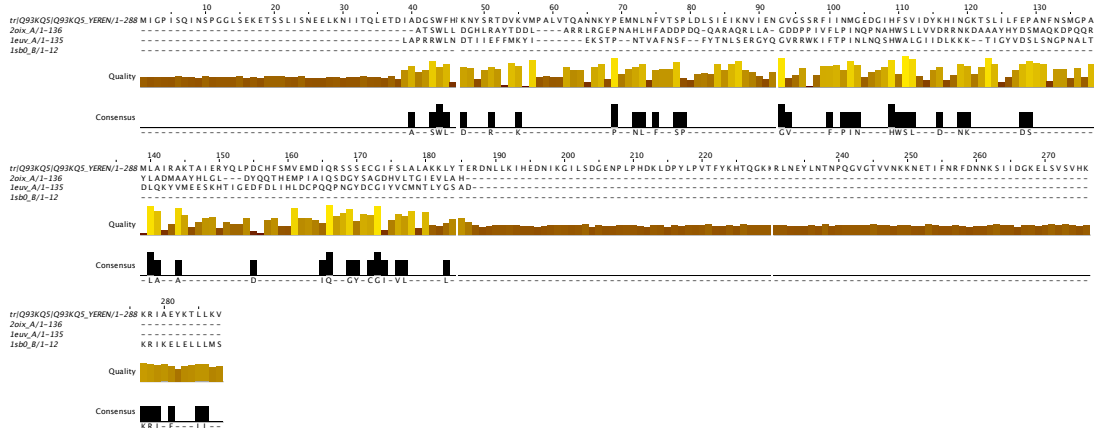


Figure 13 Sequence alignment of YopP with XopD, Ulp1 and CEB generated with HHpred [261].

The GlobPlot Server [265] predicts a globular domain of YopP spanning from aa 18 to aa 200. According to GlobPlot, the N- and C-termini of YopP are predicted to be intrinsically disordered.

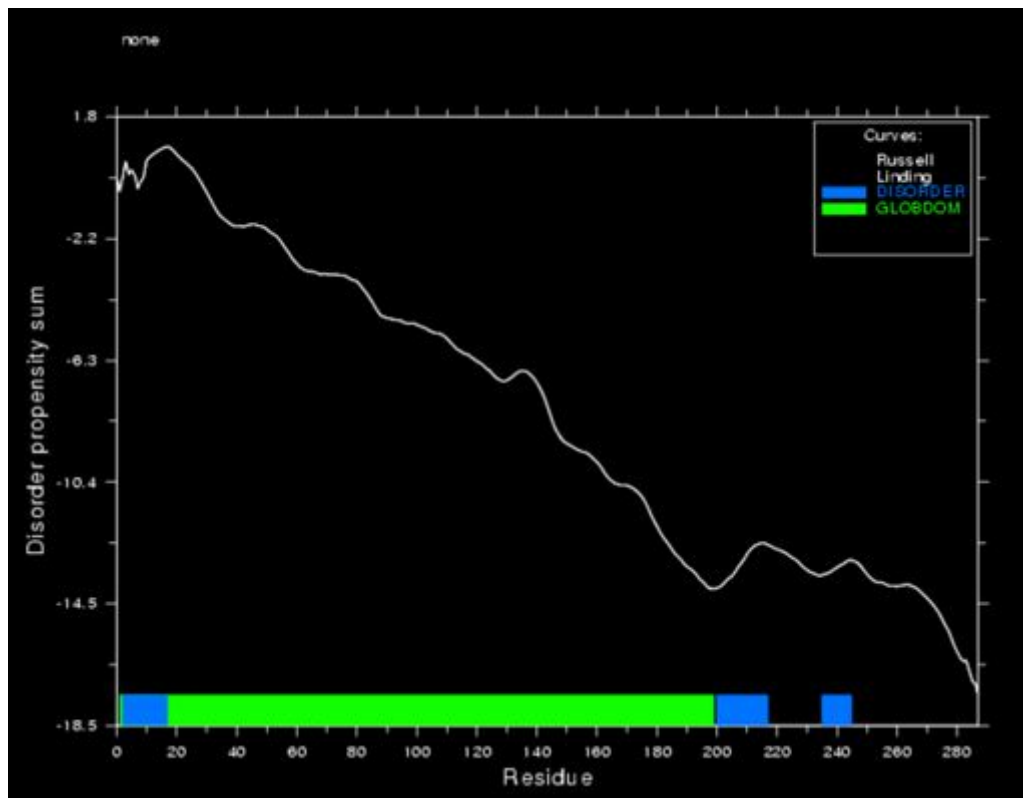


Figure 14 Prediction of a globular domain of YopP by GlobPlot [265].

XopD and Ulp1 share a five-stranded β -sheet, sandwiched by six alpha helices. YopP is predicted to have 6 β -sheets and 10 α -helices. A homology model, created with HHpred and Modeller [266], using YopP 41-185 and XopD as template, shows a four stranded β -sheet sandwiched by 5 α -helices. The catalytic triad H109 E128 and C172 are in close proximity to each other, suggesting that this part of the model is correct.

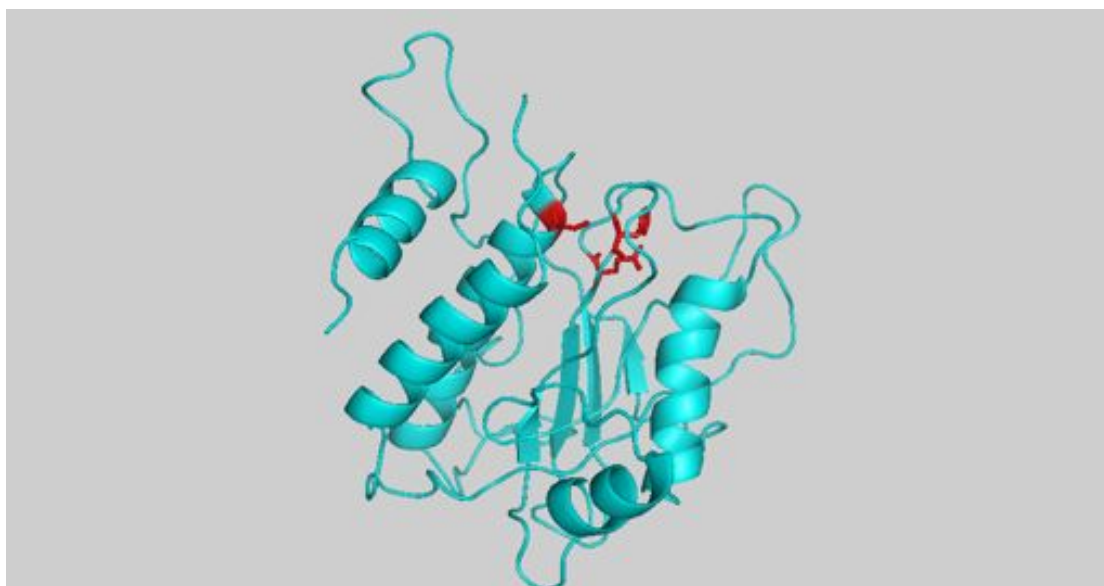


Figure 15 Homology model of YopP_41-185 based on XopD (PDB:2oix). The catalytical residues H109 E128 and C172 are highlighted in red.

The PDB contains several entries of proteins bound to IP6, among them are cysteine protease domains of the *Vibrio cholerae* RTX toxin (PDB 3eeb) and the *Clostridium difficile* toxin (PDB 3ppe). The toxins are secreted into host cells where they undergo auto-proteolysis, which results in the release of individual effector domains. The proteolytic activity of this domain is allosterically activated by IP6 [267]. However, due to low sequence identity, no homology model using the *V. cholerae* or the *C. difficile* toxins could be generated.

4.1.4.2 Crystallization trials with full length YopP

Initial crystallisation trials were performed with Z-YopP-wt at a protein concentration of 12 mg/mL. Around 1/3 of the drops remained clear after

setting up the plates. This situation changed dramatically, when the Z-tag was removed with TEV-protease. At concentrations of 12 mg/mL, YopP-wt showed heavy precipitation in 90 to 95 % of the conditions. The conditions without initial precipitation shared a high NaCl concentration, providing evidence that YopP is stabilized by high salt concentrations according to the salting in mechanism.

YopP is in particular sensitive against PEG as precipitant, in the Qiagen PEG and Qiagen PEGII screens, YopP did immediately precipitate in all 96 conditions. Decreasing the protein concentration up to 3 mg/mL reduced the initial precipitation rate, but still did not lead to the formation of protein crystals. In many cases, where conditions in vapour diffusion or batch crystallisation experiments remained clear, or only light precipitation was observed, or phase separation occurred, manual optimization of crystallisation conditions was performed, but still no protein crystals could be obtained for fl YopP. The inactive fl YopP C172A mutant did show the same unfavourable crystallisation properties.

4.1.4.3 Co-crystallisation of YopP and small molecule ligands

Binding to a ligand can have a positive effect on a proteins ability to crystallize and many proteins can be only crystallized in presence of small molecule ligands. Since it was shown that YopP binds IP6 and CoA (Section 4.1.3.2) and is partially protected from C-terminal degradation by IP6 (Section 4.1.3.3), it was assumed that a co-crystallisation of YopP with its ligands might stabilize it, reduce the initial rate of denatured protein and make it more prone to crystallise. IP6 and acetyl-CoA were either added alone or together to fl YopP wt and at a 2- to 5-fold excess after purification at various protein concentrations, but no change in the crystallisation properties was observed and the initial precipitation rate remained high. In another attempt all purification steps starting from cell lysis were performed in presence of 1 mM IP6, but also no effect on the crystallisation properties was observed. Co-crystallisation of YopP with acetyl-coenzyme-A alone and in combination with IP6, which results in acetylated YopP did also not change the crystallisation properties. YopP was also incubated with 1 mM iodoacetamide, which leads to an alkylation of cysteine 172 but no effect on the

crystallisation properties was observed. YopP-C172A was also incubated in a 1:1 stoichiometry with a synthetic peptide (GQLIDSMANSFVGTR), mimicking the activation loop of MEK2, but again no positive effect was observed.

4.1.4.4 Investigation of YopP aggregation by DLS

In order to get a better understanding, why YopP is reluctant to crystallize, YopP supplemented with IP6 was monitored by DLS in dialysis buffer. Immediately after setting up the DLS experiment, YopP-wt is monomeric and monodisperse with a hydrodynamic radius of approximately 6 nm (Figure 16). After 5 h the peak for monomeric YopP fades away and the light scattering is dominated by particles of a radius of 10 nm, which increases over the course of the experiment to and radius of 100 nm. This indicates the presence of particles in the large MDA range [268] instead of the presence of smaller assemblies of few proteins in the range of to 8 to 10 nm which could lead to the formation crystallisation nuclei.

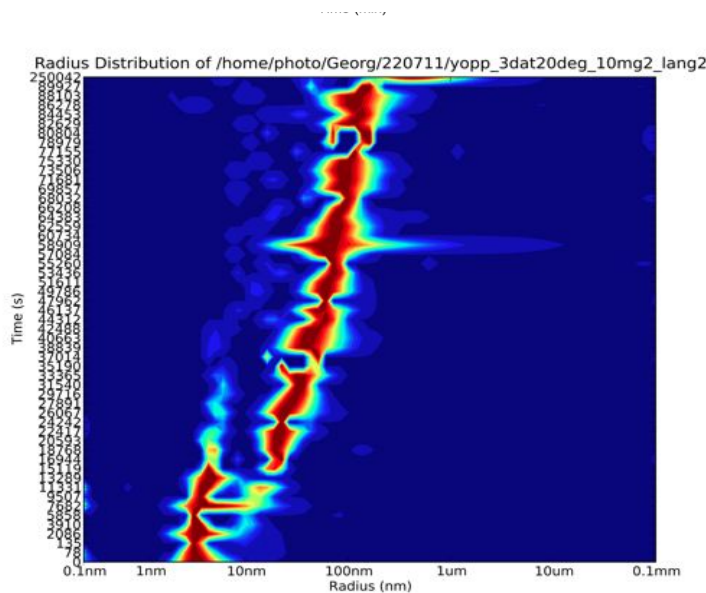


Figure 16 DLS heatmap of the radius distribution of YopP-wt (x-axis) supplemented with IP6 over time (y-axis). The heat map indicates the intensity of the particles with blue equals zero and dark red maximum.

After 12 h, the signal for the monomeric YopP disappeared entirely and after 69 h at the end of the experiment, the signal was dominated by particles of 100 nm radius.

4.1.4.5 Buffer optimization

Aggregation of YopP seems to contribute to the unfavourable crystallisation properties (Figure 16). Glycerol and poly-alcohols such as MPD can prevent protein aggregation and stabilize proteins in solution and are widely used as additives in buffers to stabilize proteins and enhance crystallisation [269], [270]. Accordingly, 5% (v/v) glycerol and MPD were added to YopP prior to setting up the plates, but did also not have a positive effect on the crystallisation properties and could not significantly reduce the rate of initial denaturation.

The Thermofluor assay allows to monitor effects of various factors such as salt concentrations, pH, buffer systems on the thermal denaturation of proteins and to optimize buffer systems for crystallisation purposes accordingly [271]. Consistent with the crystallisation experiments, YopP was only stabilized at high concentrations of NaCl. Other buffer systems had no significantly stabilizing effect compared to the usually used Tris/HCl buffer system. Only one buffer, consisting of succinic acid (14 mM), NaH₂-phosphate (49 mM) glycine (49 mM) pH 6.0, a common buffer from the PACT screen caused a shift in T_m of +5°C. Accordingly, YopP was dialyzed against this buffer and subjected to crystallisation trials, but still the protein precipitated in almost all conditions immediately. Despite no stabilizing effect was observed in the Thermfluor screen, YopP was also purified in HEPES and phosphate buffer and subjected to crystallisation trials, but no different behaviour was observed. Instead of the usual 200 mM NaCl, YopP was also purified with 400 mM NaCl, but still no improvement was observed.

Arginine and glutamate are known to prevent protein aggregation [272], [273]. YopP was dialyzed against a buffer containing 200 mM NaCl, 50 mM Tris/HCl pH 8.0, supplemented with 50 mM arginine and 50 mM glutamate according to a protocol by Golovanov [274]. However also this attempt could not increase the number of conditions in the crystallisation trials with clear drops.

Similarly to the arginine and glutamate addition, also other amino acids and amino acid derivates such as glycine-amide, proline-amide and glycine-ethyl-ester were reported to stabilize proteins, inhibit aggregation and increase the

number of crystal hits in screens significantly [275]. YopP was dialyzed against buffer 200 mM NaCl, 100 mM phosphate pH 6.5, supplemented with either 200 mM glycine-amide, proline-amide or glycine-ethyl ester but it had no effect on the crystallisation properties and did not lead to crystals.

Besides vapour diffusion crystallisation experiments, also microbatch and under oil crystallisation was tried out, but it eventually did not lead to protein crystals. All purification steps were usually performed at 4°C. However, the pipetting robot operates at 25°C. Performing the pipetting manually at 4°C did not change the crystallisation properties of YopP. Performing all purification steps at 25°C and storing the crystallisation plate at 25°C had no effect on the precipitation rate as well.

4.1.4.6 Reductive Methylation of YopP-1-288.

Many factors contribute to a protein's ability to crystallize. The statistical analysis of large scale structural genomics protein crystallisation experiments revealed that proteins with high content of well ordered surface epitopes such as glycine and alanine and hence a low surface entropy are more likely to crystallize than proteins with disordered epitopes such as lysine and glutamic acid and hence a high surface entropy [276]. YopP contains 25 lysines, of which 12 are located within the C-terminal 88 amino acids. The SERP server [277] predicts a high surface entropy for YopP and identifies three lysine clusters which potentially negatively affect the crystallization properties of YopP.

Results

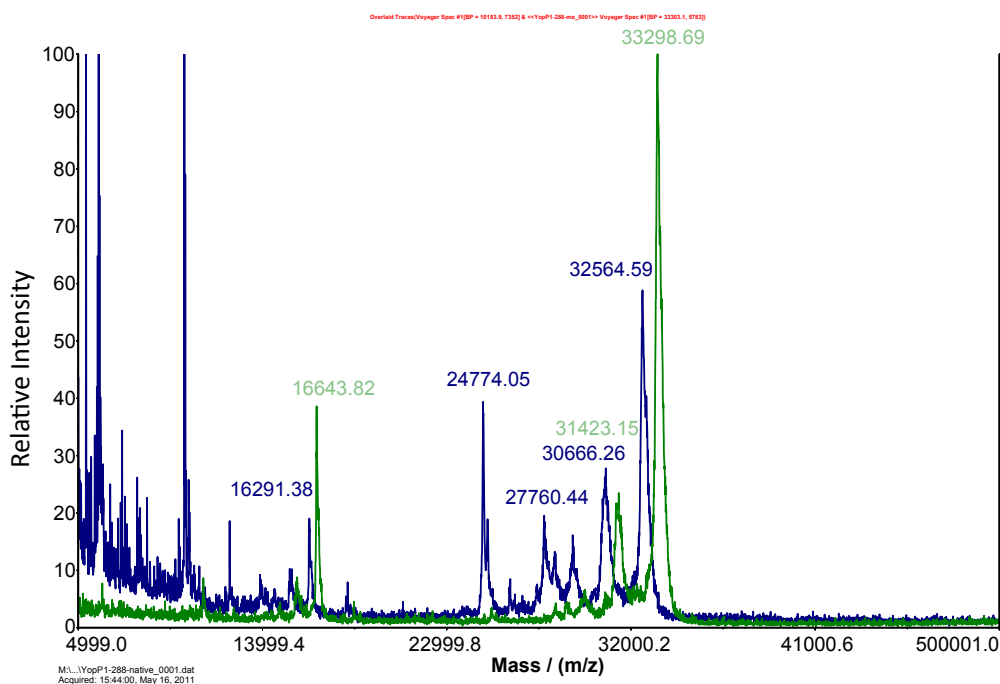


Figure 17 MALDI-TOF spectrum of native (blue) and reductively methylated wt YopP 1-288.

In order to reduce the high surface entropy of YopP, reductive methylation according to the protocol Walters [236] resulted in a mass shift of 734 Da (Figure 17), which indicates that all 25 lysine residues were methylated (Table 11).

Table 11 Analysis of reductive methylation of fl YopP wt

Native /Da	peaks	Methylated peaks / Da	ΔM /Da	n(H ₃ C)
32564.59		33298.69	734.1	48.94
30773.15		31423.15	650.0	43.33

Vapour diffusion crystallisation experiments of methylated YopP (YopP_{Me}) showed a small increase of conditions that remained clear compared to native YopP. Notably, in a number of PEG conditions, which showed 100% of initial precipitation for native YopP, YopP_{Me} was denatured immediately, but the denatured protein dissolved after 14 to 20 days and the drops remained clear, but afterwards no crystals formed.

4.1.4.7 Crystallization trials with truncated constructs of YopP

Full length YopP proved to have unfavourable crystallisation properties. A small fraction of YopP was already partially degraded immediately after purification. The Mw of the degraded core domain is most likely 24.4 kDa. The basic amino acid content of the C-terminus could cause a dipole moment, which might be responsible for the aggregation of YopP. Taking into account the secondary structure prediction of YopP, the N-terminal sequencing and LC-MS/MS of degraded YopP, a series of N- and C-terminally truncated constructs of YopP wt was designed, starting N-terminally at aa 18 and 88 and ending C-terminally at aa 200, 223 and 250.

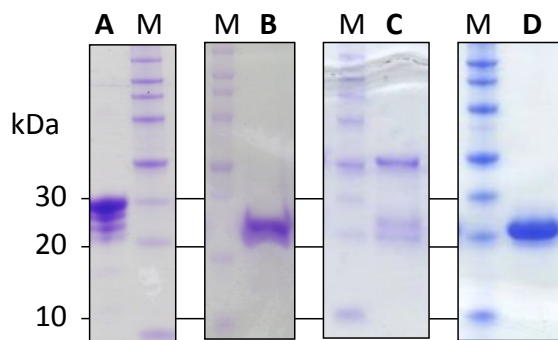


Figure 18 SDS-PAGE (12%) of YopP-wt **(A)** 1-288, **(B)** 1-223, **(C)** 88-250, **(D)** 18-200. (M: Marker RotiMark 10-150)

The truncated constructs were clones in the pETZ2-1a/Lic. Initial expression test were performed.

YopP 1-223, 88-250 and 18-200 showed the highest expression levels of the truncated constructs (Figure 18). Constructs 1-223 and 18-200 (Figure 18 B and D) did not exhibit the characteristic degradation pattern anymore. Construct 88-250 still showed a double band slightly above 20 kDa (Figure 18 C). Taken together, the truncated constructs of YopP clearly indicate that the degradation of YopP predominately, if not exclusively appears on the C-terminus of the protein, which is consistent with the limited proteolysis experiments and the N-terminal sequencing. Expressions for the constructs 1-223 and 18-200 were scaled up and were subsequently subjected to crystallisation trials.

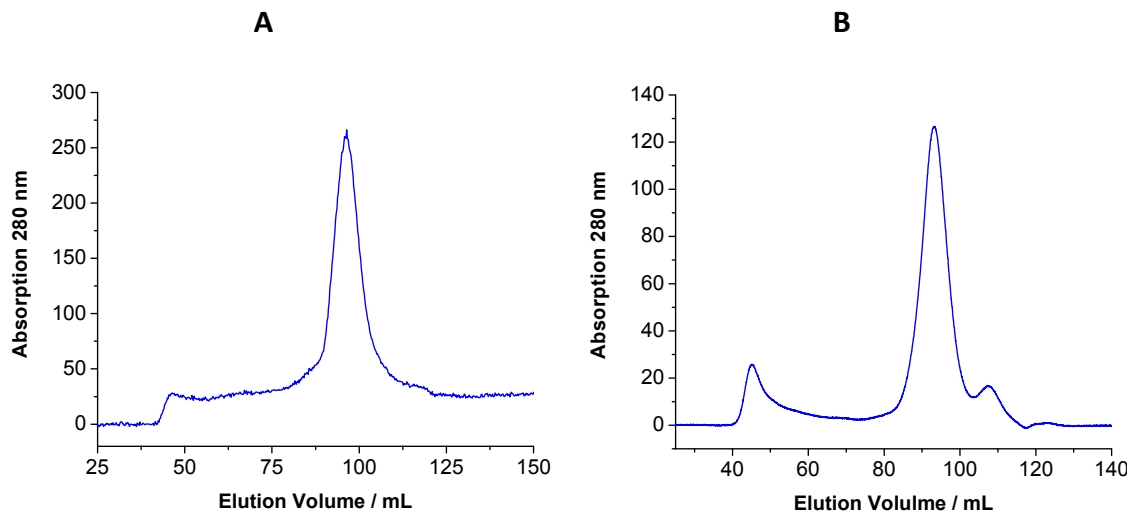


Figure 19 SEC elution profiles of truncated YopP-wt constructs. **(A)** YopP₁₈₋₂₀₀ and **(B)** YopP₁₋₂₂₃.

Even though the truncated constructs could be purified by SEC and did exhibit only a small degree of aggregation in the void volume (Figure 19), they immediately showed aggregation and precipitation upon concentrating. Hence, they could only be concentrated up to 4 mg/mL and were subjected to crystallisation trials. However, like for the fl YopP, there was immediate precipitation and/or denaturation in almost all conditions tested.

4.1.4.8 Crystallization of proteolysed YopP

The choice of the truncated construct can be crucial for the success of a crystallisation experiment. Even one additional or missing amino acid can prevent a protein from forming crystals. *In situ* proteolysis can lead to the crystallisation of proteins in cases where the choice of the truncated constructs was suboptimal [278], [279]. Subtilisin was added to full length Z-YopP-wt 1/1000 (w/w). Precipitation started immediately. After 1 h incubation at 4°C, The samples were spun down and the supernatant was sterile-filtered and further purified by SEC (Figure 20 A).

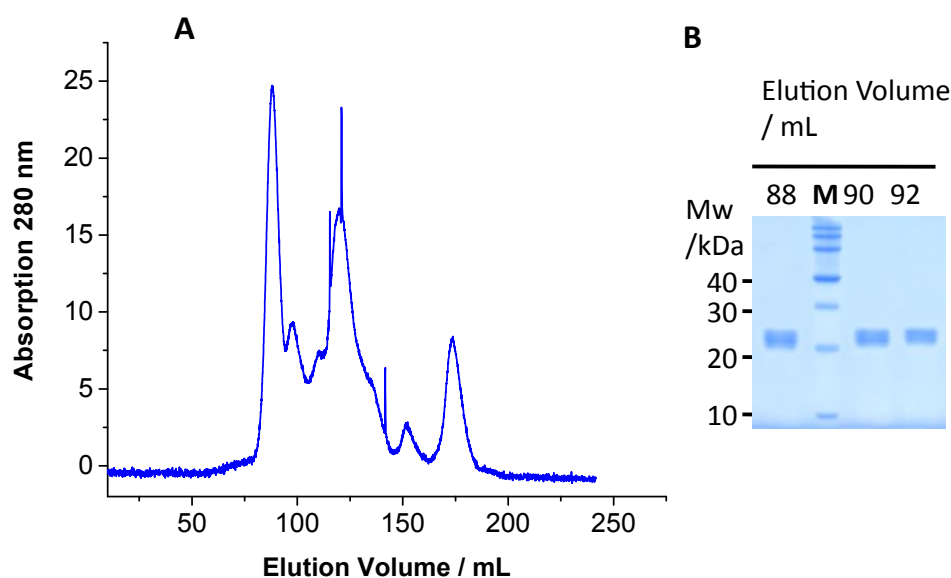


Figure 20 YopP 1-288 was incubated with Subtilisin (1/1000) for 30 min and then purified by SEC (Superdex S200). The SDS-PAGE (12%) indicates two or three truncated species of YopP. (M: Marker RotiMark 10-150).

Between 80 and 90% of the initial protein was lost by precipitation. The proteolysed sample also appeared to be not homogeneous on the SDS-PAGE, at least two truncated protein species slightly above 20 kDa could be distinguished (Figure 20 B). The proteolysed YopP was concentrated to 4 mg/mL and was subjected to crystallisation trials. Even though it did not lead to protein crystals and the usual high degree of precipitation was observed, the precipitate showed a more dynamic behaviour including formation of spherulites in a few cases.

4.1.4.9 *In situ* crystallisation

In a similar approach, subtilisin 1/10000 (w/w) was added to Z-YopP just before setting up crystallisation plates at 4°C. It was hypothesized that the Z-tag prevents YopP from initial precipitation and truncated YopP is released slowly, which could allow the formation of crystallisation nuclei. However, also this approach did not lead to the formation of protein crystals.

4.1.4.10 Crystallization trials with YopP homologue *AvrA*

Using homologues or orthologues of a given protein can increase the success rate of protein crystallography significantly [280]. Because of the unfavourable crystallisation properties of YopP, a homologue of YopP was also subjected to

Results

crystallisation trials. Since all the *Yersinia* homologues have a high sequence identity of around 95% and hence different crystallisation properties seem to be unlikely, AvrA (AY769766.1 GI:54397749), a YopP homologue of *Salmonella enterica* with a sequence identity of 57% was selected for crystallisation trials (Figure 21). Proteins of *Salmonella* have been studied extensively in regard to the TTSS and effector proteins. AvrA was shown to possess acetyltransferase activity [281] and to bind IP6 [149].

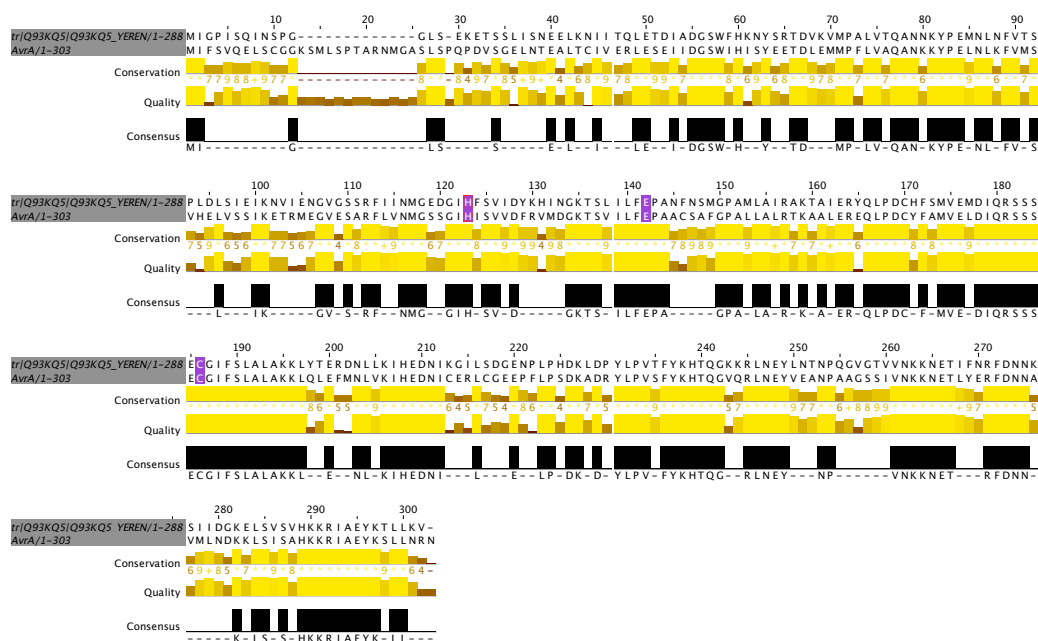


Figure 21 ClustalW Alignment of YE YopP and *S. enterica* AvrA. The catalytic residues HEC are highlighted in red [282].

A plasmid, pSV220 [283], harbouring AvrA was kindly provided by Prof. Sima Yaron (Haifa, Israel). AvrA was cloned into the pETZ2-1a/Lic, transformed into *E. coli* BL21(DE3), expressed and purified as described for YopP. Expression and purification was complicated by low yield, presence of aggregated protein and co-expression of *E. coli* chaperones bound to Z-AvrA (Figure 22 A). Z-AvrA (Figure 22 A) was cleaved with TEV-protease, however only a small fraction of AvrA was susceptible to TEV-protease cleavage (Figure 22 B). Nevertheless, AvrA could be separated from chaperone bound Z-AvrA and has an elution volume between 80 and 90 mL with Superdex 200 (16/60), which is comparable

to YopP for this column. After SEC the yield was about 1.5 mg/L TB medium, less than 1/10 of what was observed for YE YopP. Fortunately, full length AvrA did not show a degradation pattern, which was characteristic for YopP (Figure 22 A&C).

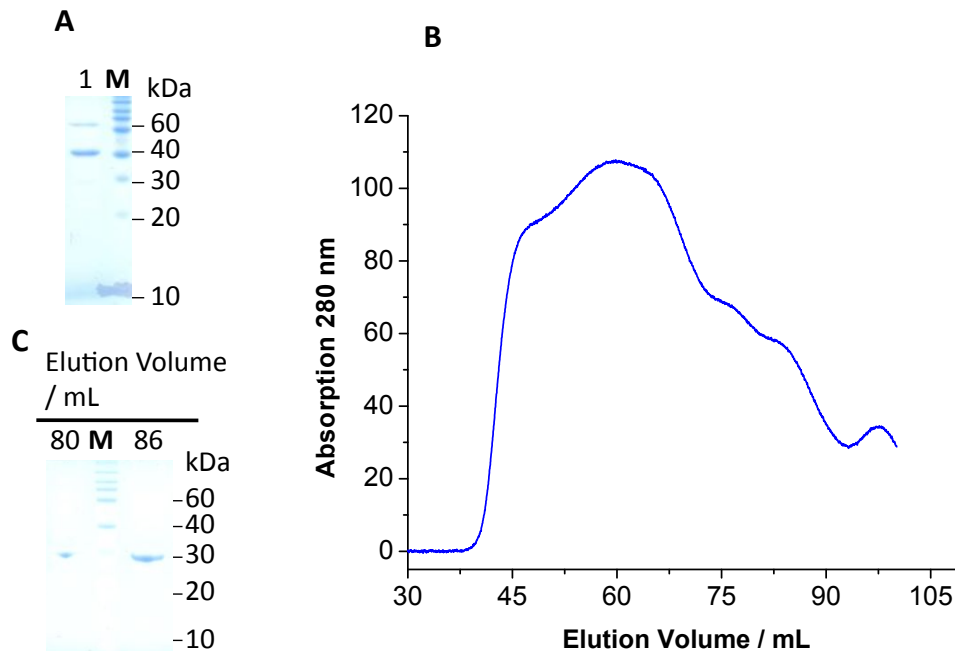


Figure 22 (A) SDS-PAGE of Z-AvrA after IMAC. (B) SEC (Superdex S200) chromatogram of Z-AvrA after incubation with TEV-protease over night. (C) SDS-PAGE of indicated fractions of the SEC in (B). (M Marker: RotiMark 10-150)

After the SEC, AvrA was concentrated to 8 mg/mL and subjected to crystallisation trials. However, AvrA was precipitated or denatured in 90% of the crystallisation conditions, similar to what was observed for YopP.

4.1.5 Interaction with Chaperones

The aforementioned properties of YopP led to the hypothesis that isolated YopP is too instable to form crystals.

As already been mentioned in the introduction, some of the TTSS effector proteins require a specific class Ia TTSS chaperones for their interaction with the TTSS and the translocation to the host cell.

The SycO/YopO/YopP-operon is highly conserved among the pathogenic *Yersinia* spp. [284]. SycO is a canonical class Ia TTSS chaperone with an acidic pI of 4.3, a propensity to form homodimers and it was shown to bind to [285] and influences the secretion of YopO [285], [286]. The secretion efficiency of YopP is decreased by deletion YopO. Over-expression of SycO negatively affects the secretion of both YopO and YopP [287]. However, no direct interaction between YopP and SycO nor YopO has been shown yet [287]. Moreover, YopP lacks the canonical chaperone-binding domain adjacent to the N-terminal signal peptide, which is also consistent with the limited proteolysis work (Figure 10, Table 10). However, the C-terminus is flexible and partially disordered and could hence allow an interaction with a TTSS chaperone or other bacterial factors.

In some of the human pathogenic *Yersinia* spp., orf91a is inserted between YopO and YopP. Orf91a is shorter than the canonical class Ia TTSS and has a higher pI value, however the insertion of orf91a in front of YopP could indicate a possible interaction of the gene product of orf91a with YopP.

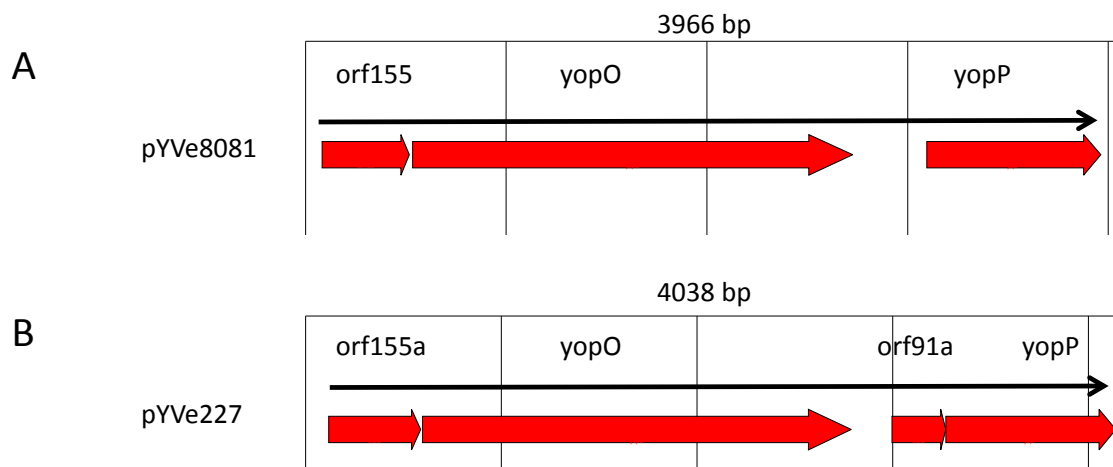


Figure 23 Organization of the SycO/YopO/YopP operon in the *Y. enterocolitica* virulence plasmids **(A)** pYVe8081 and **(B)** pYVe227.

4.1.5.1 Expression and purification of potential chaperones

4.1.5.1.1 Expression and purification of orf91a

The orf91a gene was amplified from YE pYVe227 DNA and cloned in the pET-Z2-1a/Lic vector and transformed into *E. coli* BL21(DE3). Induction of expression results in an intense band on the SDS-PAGE just below 20 kDa, which is the

expected size for the Z-orf91a fusion protein (Figure 24 A). The protein was purified by IMAC and further purified by SEC (Figure 24 B). The SEC elution profile reveals a double peak between 80 and 90 mL and the corresponding SDS PAGE shows that orf91a is still partially bound to a possible chaperone of around 50 kDa (Figure 24 C). In addition, the yield was too low to use orf91a for further interaction studies.

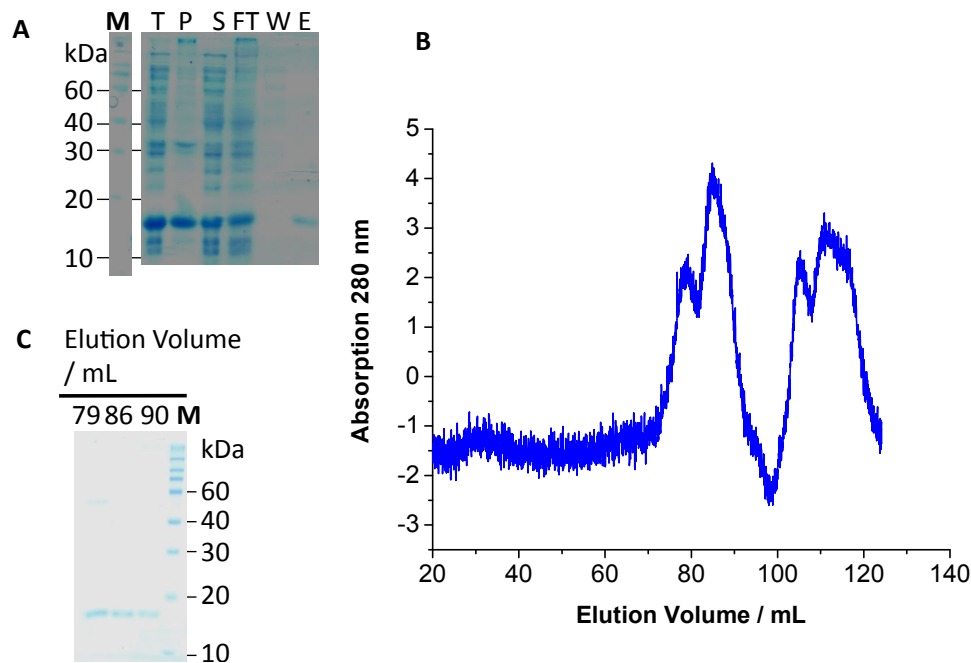


Figure 24 Expression and purification of Z-orf91a. **(A)** SDS-PAGE (12%) shows an intense band below 20 kDa. The band is present in the pellet (P) as well as in the supernatant (S) and can be eluted from the Ni-NTA-agarose (E). **(B)** SEC chromatogram of Z-orf91a (SuperdexS200) and a **(C)** SDS-PAGE(12%) of indicated elution volumes. (Due to detector malfunction of the FPLC system, the $A_{280\text{ nm}}$ values are only approx. 1% of their actual value). (M: Marker: RotiMark 10-150)

4.1.5.1.2 Expression and purification of orf155a (SycO)

SycO was amplified from YE pYVe8081 DNA, cloned in the pETZ2-1a/Lic vector and transformed into *E. coli* BL21(DE3). Z-SycO has an expected mass of 25 kDa, but no protein of this size was overexpressed in the cells (Figure 25 A). However, $A_{280\text{ nm}}$ of the IMAC elution indicated the presence of protein, even though nothing could be seen on the SDS-PAGE (Figure 25). Z-SycO is supposed to form

a dimer of 50 kDa, the SEC chromatogram shows aggregation protein eluting with the void volume at 40 mL and a second peak between 60 and 70 mL which could correspond to a Z-SycO dimer (Figure 25 B). However, SDS-PAGE of the corresponding fractions does not show any sign of a protein (Figure 25 C). Due to its acidic pI, SycO was reported to have a higher mobility on the SDS-PAGE [287] and the low pI could also negatively affect the Coomassie staining efficiency of SycO.

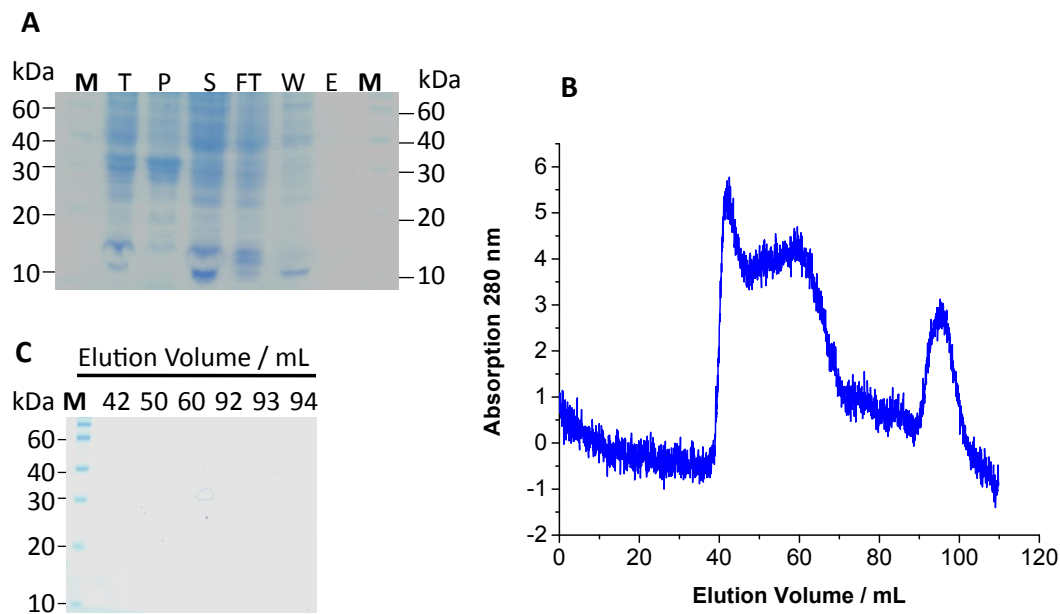


Figure 25 Expression and purification of SycO **(A)** lysed cells (T), the pellet after cell lysis (P), the supernatant (S), the IMAC flowthrough (FT), IMAC wash (W) and the imidazole elution (E) were separated on SDS-PAGE (12%). **(B)** SEC elution profile of the IMAC eluted protein. **(C)** SDS-PAGE (12%) of indicated fractions of (B)(Due to detector malfunction of the FPLC system, the $A_{280\text{ nm}}$ values are only approx. 1% of their actual value)

4.1.5.2 Co-expression of YopP and and potential chaperones

4.1.5.2.1 Co-expression of YopP with SycO

Due to the difficulty of expression with SycO alone, *E. coli* BL21(DE3) was co-transformed with pETZ2-YopP-wt and pCDF13-Z-SycO. The expressed proteins were purified with IMAC chromatography followed by SEC. Both proteins were tagged with an N-terminal 6xHis-Z-tag. After the Ni-NTA purification, SDS-PAGE

Results

showed an intense band for Z-YopP at 40 kDa and a weak band slightly above 20 kDa, which could correspond to Z-SycO (Figure 26 A1), which was not present when Z-YopP was expressed alone (Figure 26 A4). Due to its low pI, SycO has a marked higher mobility in SDS-PAGE than other proteins of the same size [287]. Upon TEV-protease cleavage of the 10 kDa Z-tag, a faint band is visible on the SDS-PAGE above the Z-tag, which could correspond to SycO (Figure 26 A2). After the 2nd Ni-NTA purification step to remove the Z-tag prior to SEC, the band disappears (Figure 26 A3). The elution volume of YopP co-expressed with SycO during SEC did not change in comparison to YopP expressed alone (Figure 26 B). SDS-PAGE analysis of selected fractions of the YopP SEC revealed the familiar pattern of full length YopP accompanied by bands of several smaller degradation products (Figure 26 C). No bands which could indicate presence of SycO are visible between 10 and 20 kDa.

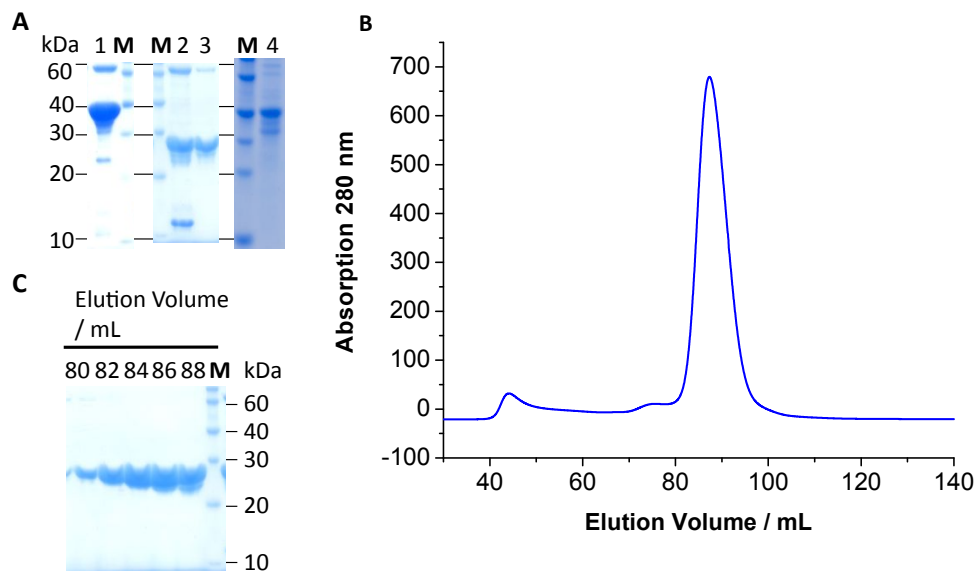


Figure 26 (A) SDS-PAGE (12%) of YopP/SycO-co-expression (1) IMAC elution (2) IMAC elution after 12 h incubation with TEV-protease. (3) 2nd IMAC step to remove the tag. (4) Z-YopP-Z alone. **(B)** SEC elution profile of A1 **(C)** SDS-PAGE (12%) of indicated fractions of B. (M: Marker RotiMark 10-150)

Even though, small amounts of SycO might have been co-expressed with YopP (Figure 26 A1), no complex formation was observed under the conditions tested. SycO as well as the other TTSS class Ia chaperones are known to form complexes with their secretion cargo in a 2:1 ratio. For SycO with a Mw of 15.9 kDa and

YopP with 32.4 kDa, hence a complex of 64.2 kDa with an significantly smaller elution volume than the 90 mL of YopP would be expected. This complex could be clearly distinguished from YopP, but no such complex was observed during SEC (Figure 26 B).

4.1.5.2.2 Co-expression of YopP orf91a

BL21(DE3) *E. coli* were co-transformed with pETZ2-YopP and pCDF13-Z-orf91a. Both proteins are tagged with an N-terminal Z-tag. Proteins were purified by IMAC followed by SEC. *E. coli* cells show a high expression of a protein slightly below 20 kDa as it was observed for orf91a alone, but no expression of YopP at 40 kDa (Figure 27 B). Moreover, orf91 appears to be aggregated and bound to several chaperone proteins during the imidazole elution. Only a small fraction of Z-orf91a appears to be susceptible for TEV-protease cleavage of the eluted protein, since only a small fraction of the corresponding band in the SDS-PAGE is shifted due to removal of the Z-tag. All this points to towards severe protein aggregation and in the subsequent SEC, all proteins elute with the void volume of the column (Figure 27 A), a behaviour, which was not observed, when orf91a was expressed alone (Figure 24).

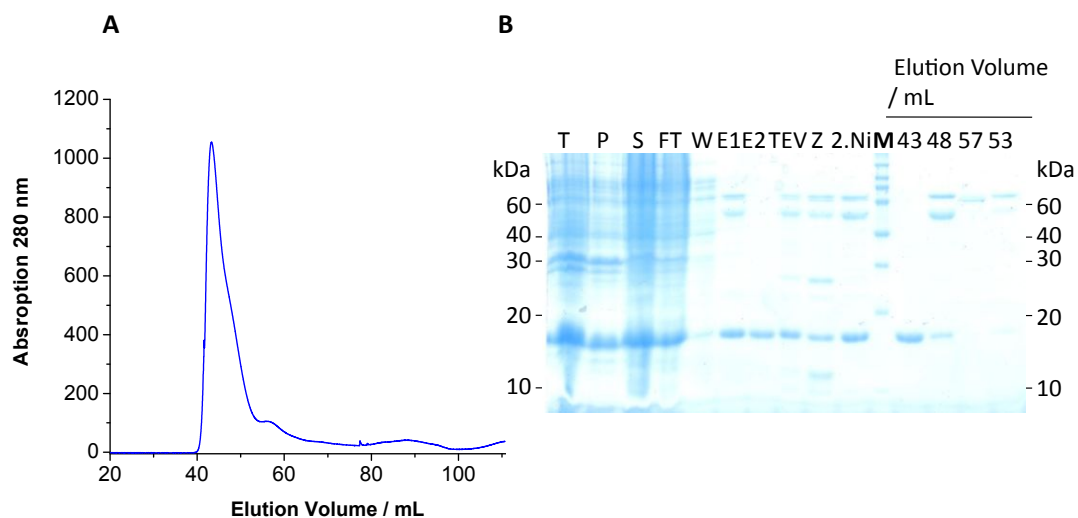


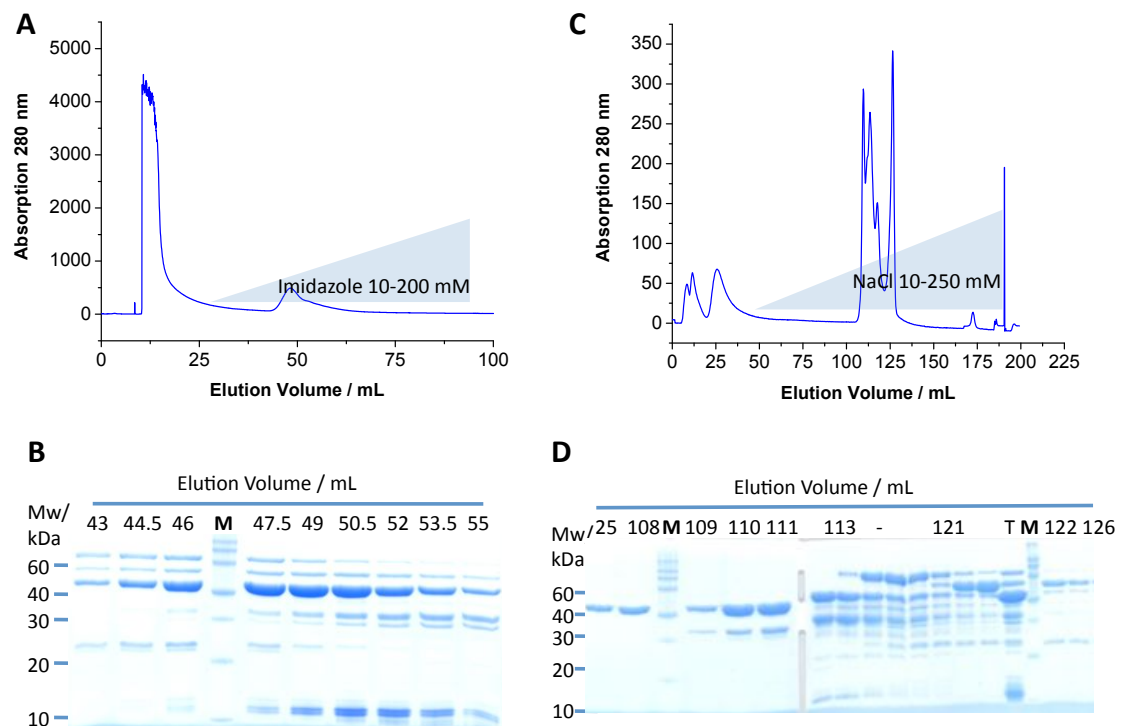
Figure 27 (A) SEC purification of YopP/orf91a co-expression product. **(B)** Total cell lysate (T), cell pellet (P), supernatant (S), IMAC flow through (FT), IMAC wash fraction (W), eluted protein (E1, E2), TEV-protease cleaved eluted protein and indicated fractions of the SEC A were separated by SDS-PAGE (12%). (M: Marker RotiMark 10-150)

4.1.6 Investigating the YopP/MEK2 interaction

MEK2 is the only member of the human MAPKK family, which has been structurally characterized [288]. MEK2 was also found to be acetylated by YopP during *in vivo* and *in vitro* assays [144] and to bind YopP in GST-pulldown assay [140]. Therefore it was decided to use MEK2 for interaction and co-crystallisation assays. MEK2 is a 400 aa serine kinase with an intrinsically disordered N-terminus. The N-terminal truncation was found to be an requirement for the successful crystallisation of MEK2 [288], [289], when an N-terminally truncated construct, spanning from aa 55 to 400 was crystallized in complex with a novel kinase-inhibitor.

4.1.6.1 Expression and Purification of MEK2

The described MEK2 55-400 fragment could be amplified by PCR from a human heart muscle cDNA library and was cloned in the pETZ2-1a/LIC expression vector. Z-MEK2 was heavily contaminated (Figure 28 A, B) after the first round of IMAC purification, but pure Z-MEK2 could be recovered from the flowthrough of a MonoQ ion exchange gradient at a concentration of 10 mM NaCl (Figure 28 D), after a combination of IMAC and SEC purification.



Results

Figure 28 Z-MEK2 55-400 purification. **(A)** IMAC imidazole gradient elution. **(B)** SDS-PAGE (12%) of indicated elution volumes of the imidazole gradient **(C)** MonoQ NaCl gradient elution. **(D)** SDS-PAGE (12%) of indicated fractions of the MonoQ elution. (M: Marker RotiMark 10-150).

The overall yield was between 1 to 3 mg/L of expression medium. The purity and identity of MEK2 was checked by MALDI-TOF.

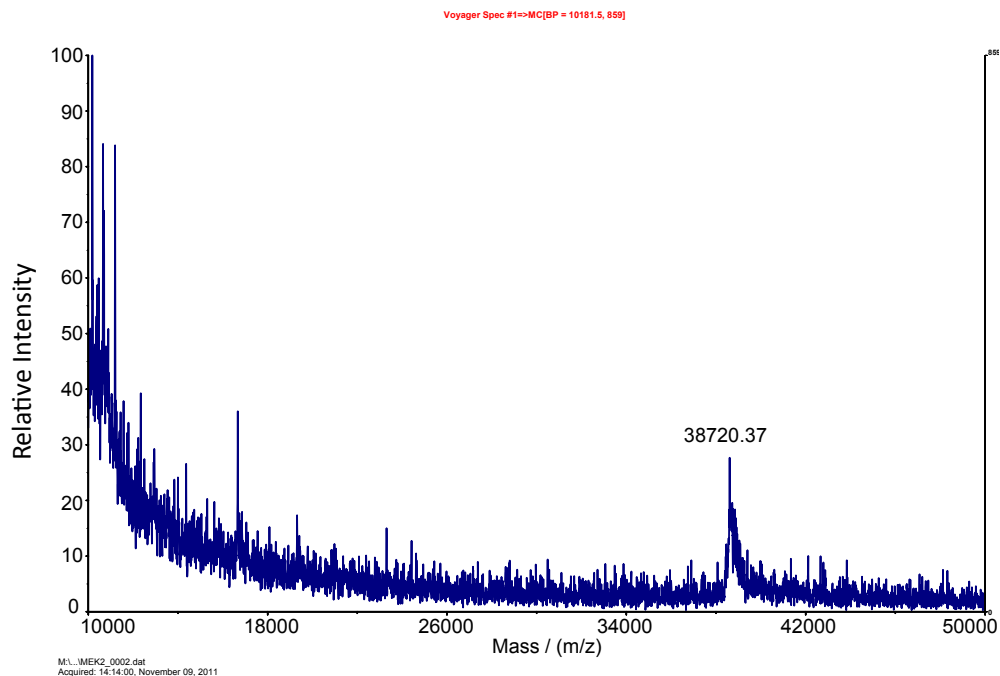


Figure 29 MALDI-TOF of MEK2 55-400. After removing the Z-tag, a single peak for MEK2 with a mass of 38.72 kDa.

4.1.6.2 YopP/MEK2 interaction

The biochemical and structural investigation of a host-pathogen protein-protein interaction is of great interest and could lead to a better understanding of the role of YopP *in vivo*. It could help to explain, why several YopP/J isoforms are translocated to the host cell with a higher affinity and show different abilities to inhibit the MAPK/NF- κ B signalling. Besides that, the poor performance isolated YopP during the crystallisation experiments could imply that YopP can only be crystallized in presence of an interacting host protein such as MEK2.

To perform the acetylation of MEK2 and other kinases, YopP has to - at least transiently - bind MEK2. Several studies describe GST-pulldown and Co-IP

experiments, which show that YopJ/YopP binds members of the MAPKK family including MEK2 and IKK- β [131], [140].

YopP and Z-tagged MEK2 55-400 were mixed in a 1/1 ratio to a final concentration of 4 mg /mL and analytical SEC was performed (Figure 30). The Z-tag was not cleaved off in order to have a better size separation between YopP and MEK2. Z-MEK2 alone elutes at 10.73 mL, this peak is shifted for Z-MEK2/YopP to 10.5 mL, whereas the YopP peak remains at 11.32 mL for both runs. Even though there is a small shift in the elution volume of Z-MEK2 in presence of YopP, the shoulder to the right of the Z-MEK2 peak is not changed, which indicates that no complex formation between Z-MEK2 and YopP has occurred during the SEC run.

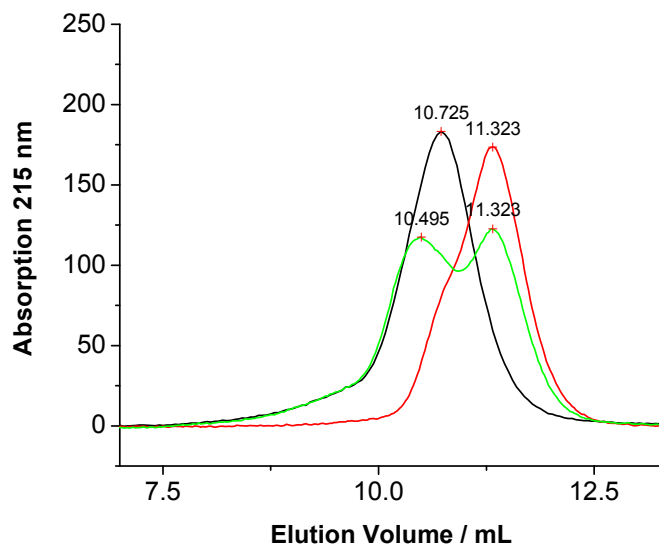


Figure 30 Analysis of complex formation between Z-MEK2 and wt YopP 1-288 by analytical SEC. Overlay of three runs Z-MEK2 (black line), wt YopP 1-288 (red line) and wt-YopP_1-288/Z-MEK2 (green line).

The fact, that YopP and MEK2 do not form a complex during the SEC run does not necessarily mean that they do not interact at all. The protein concentrations during such a run are necessarily relatively low and decrease during the course of the SEC run. A high affinity binding cannot be expected anyway, since YopP could not perform multiple acetylations if it would bind a kinase with a high affinity.

4.1.7 Co-crystallisation trials with YopP and MEK2

Co-crystallisation trials with 1:1 ratios of YopP/ MEK2 were set up with YopP-wt/MEK2-wt, YopP-wt/MEK2-S222/226A and YopP-C172A/MEK2-wt in presence and absence of IP6, acetyl-CoA, CoA, and the cysteine protease inhibitor iodoacetamide at final protein concentrations of 5 to 10 mg/mL and an 3 to 5 fold excess of the small molecules. In addition, crystallisation trials with YopP-C172A and a synthetic peptide (GQLIDSMANSFVGTR) mimicking the activation loop of MEK2 were set up. In most cases, the drops showed immediate precipitation as it has already been observed for isolated YopP. Occasionally, larger crystals were found, but they were either salt from the buffer or small molecule additives.

In one case, YopP was incubated with iodoacetamide, which inhibits all cysteine proteases by the formation of a covalent adduct with the cysteine. Then, MEK2 IP6, CoA were added. Within 30 to 40 days, small crystal grew within the precipitate in a number of PEG conditions (Figure 31). Even though they did not show fluorescence with the UV-imaging system, they appeared to be soft and of a gel-like consistence upon touching them with a acupuncture needle, unlike solid salt crystals. However, the drops were covered with a thick skin and the crystals were buried in precipitate. The biggest crystal in (Figure 31 B) could be mounted on a loop, but was destroyed through the freezing procedure and showed no diffraction in the x-ray beam. The tiny crystals were impossible to be harvested.

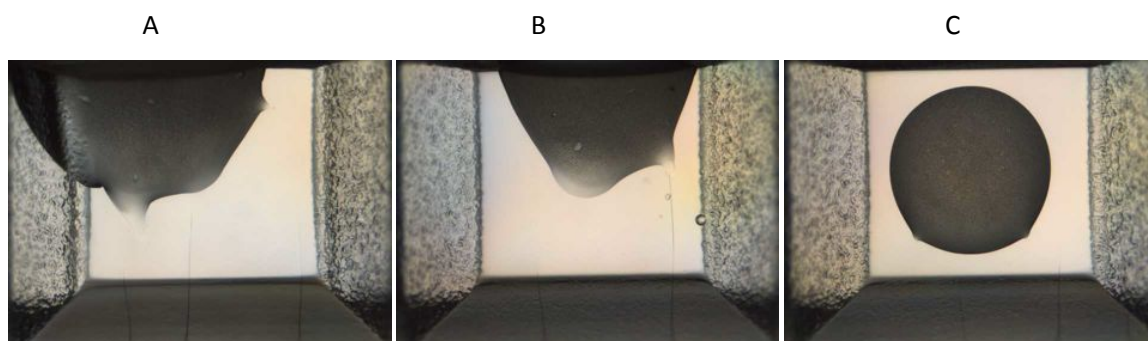


Figure 31 YopP/MEK2 10 mg/mL, 0.3 mM IP6, 0.3 mM CoA, 0.3 mM Iodoacetamide (A) 0.1 M HEPES pH 7.0, 10%(w/v) PEG 4000, 1%(v/v)

Isopropanol **(B)** 0.1 M bis-tris pH 6.5, 25% (w/v) PEG 3350 **(C)** 0.1 M HEPES pH 7.5, 25% (w/v) PEG 3350

The crystals were too small and the conditions still need further optimization before it can be determined if it was protein crystal or not. However, the use of covalent cysteine protease inhibitors such as idoacetamide or iodoacetic acid, which contain a carboxy-group is a promising approach since it resembles the acetyl group which is transferred by acetyl-CoA and could facilitate a recognition of the kinase substrate.

4.1.8 Co-expression of YopP and MEK2

In many cases, co-expression can lead to the formation of stable protein/protein complexes, which would not have been accessible by just mixing separately expressed proteins [290]. Active and inactive YopP and MEK2 were co-transformed to avoid MEK2 acetylation in the host cell (Table 12). MEK2 S222 and S226 and YopPC172 are the only residues of the two proteins, of which it is known with certainty that they are in close proximity to each other in order to transfer the acetyl residue. Therefore single and double cysteine mutants of MEK2 were generated to allow a possible cysteine bond formation between YopP wt and MEK2S222/226C in *E. coli* Origami(DE3) and hence cross-linking and the formation of a stable complex (Table 12).

Table 12 Co-expression constructs YopP MEK2

YopP	MEK2	Strain
C172A (pETZ2-1a/Lic)	wt (pCDF-13)	BL21(DE3)
wt (pETZ2-1a/Lic)	S222/226A (pCDF-13)	BL21(DE3)
wt (pGEX-4T-3)	S222C (pCDF-13)	Origami(DE3)
wt (pGEX-4T-3)	S226C (pCDF-13)	Origami(DE3)
wt (pGEX-4T-3)	S222/226C (pCDF-13)	Origami(DE3)

Test-co-expressions were performed, in case of Z-YopP-wt/Z-MEK2S222/226A and Z-YopP-172A/Z-MEK2-wt but only expression of Z-YopP at 40 kDa was

observed in the IMAC elution and no expression of Z-MEK2, which should be right above the Z-YopP band in the SDS-PAGE (Figure 32).

The Origami(DE3) co-expression showed bands for the GST-YopP below 60 kDa (Figure 32) for the IMAC purified proteins. MEK2S226C was the only Origami(DE3)-co-expression, where an additional faint band for MEK2 above 40 kDa was visible. However, the Origami cells did not grow well and IPTG induction lead to an immediate growth arrest at OD_{600 nm} 0.9. Also a new co-transformation of Origami(DE3) showed the same growth arrest. Improving the aeration of the culture by using a 2 L flask filled with only 200 mL culture did also not have a positive effect and led to the harvest of cells in the scale of 0.2 g/L of culture. All this points towards a toxic effect of YopP and MEK2 towards Origami(DE3).

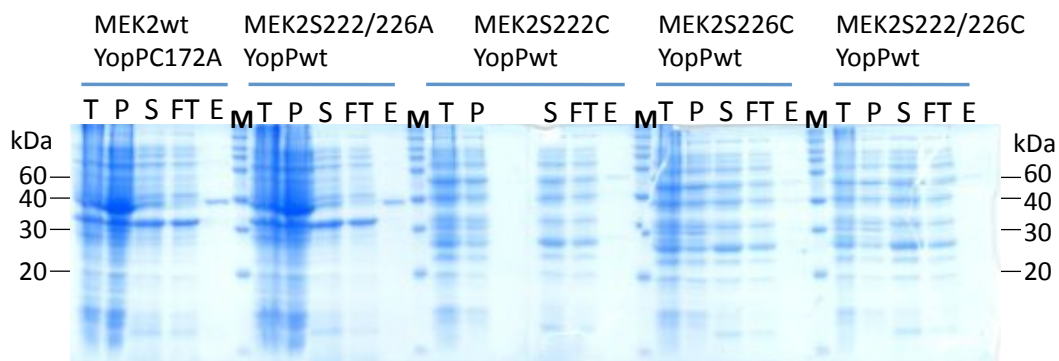


Figure 32 Test co-expression of YopP and MEK2. Total cell lysate (T), pellet (P), flow through after IMAC purification (FT) and eluted protein (E) of the co-expression constructs listed in **Table 12** were separated by SDS-PAGE (12%). (M: Marker RotiMark 10-150).

4.1.8.1 Up-scaling of Co-expression

Even though it seemed that predominantly YopP was expressed, the expression trials were scaled up since low expression can be difficult to monitor during test-expression.

4.1.8.1.1 YopP-wt/MEK2S222/226A

The co-expression of YopP-wt and MEK2S222/226A did only show expression of YopP and not of MEK2. The elution profile (Figure 33 A) of Z-YopP is not changed and the bulk of Z-YopP elutes at 80 mL.

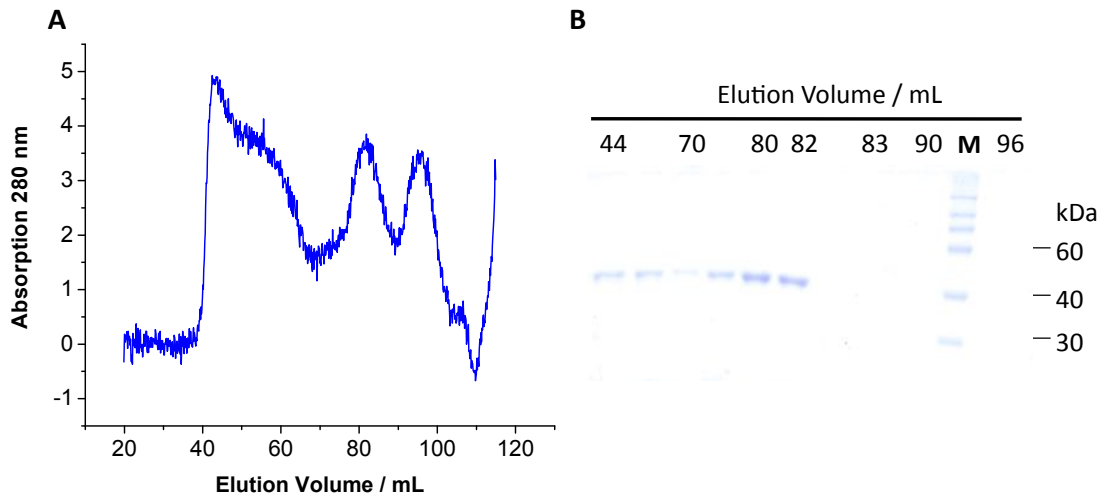


Figure 33 Co-expression of YopP-wt and MEK2 S222/226A. **(A)** SEC elution profile **(B)** SDS PAGE (12%) of selected fractions. Elution volumes are indicated. Due to detector malfunction of the FPLC system, the $A_{280\text{ nm}}$ values are only approx. 1% of their actual value. (M: Marker RotiMark 10-150).

The SEC shows an apparent increase in aggregation of YopP and an decrease in overall yield of purified protein compared to the expression of YopP alone (Figure 33 A), but the SDS-PAGE of the corresponding fractions shows only a single band for Z-YopP at 40 kDa and no other band which could correspond to Z-MEK2 (Figure 33 B).

4.1.8.1.2 YopP-C172A/MEK2-wt

The SEC profile shows a single peak with the elution of Z-YopP for the purification of the co-expressed YopP-C172A/MEK2-wt (Figure 34 A). The SDS-PAGE with the corresponding fractions reveals that only YopP has been expressed and purified (Figure 34 B).

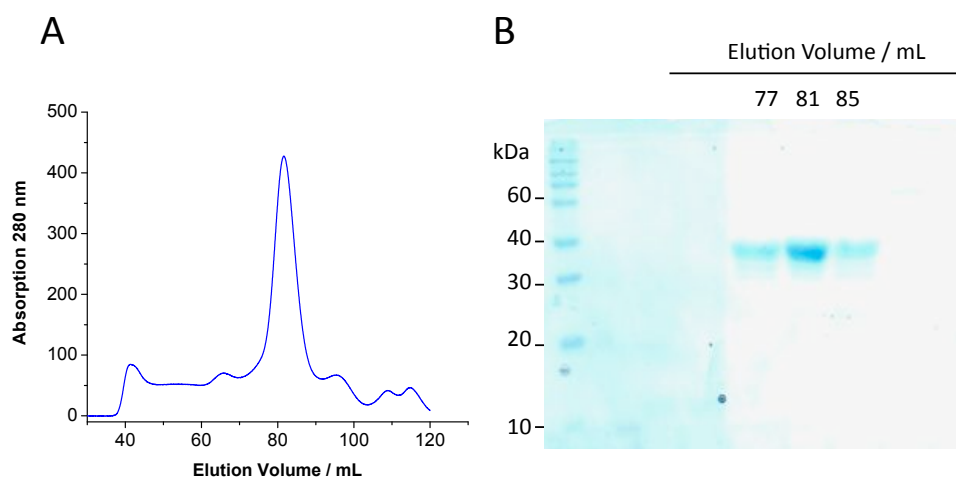
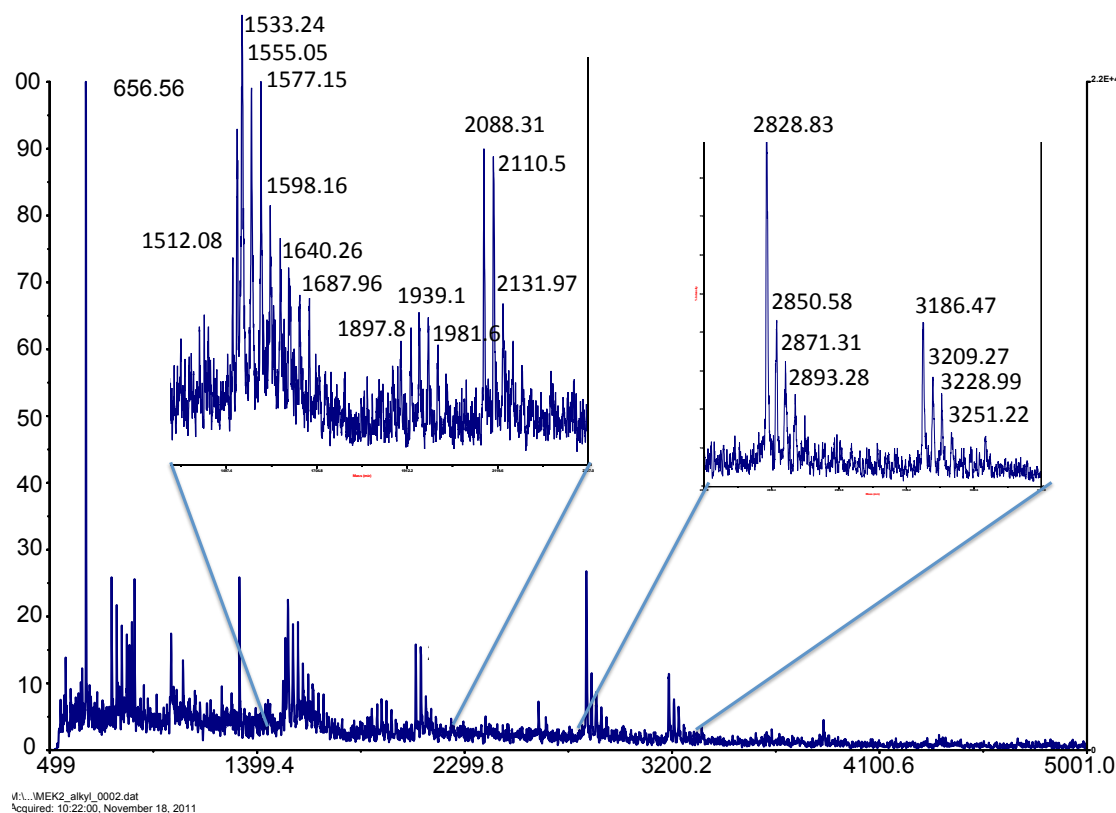


Figure 34 Co-expression of YopPC172A and MEK2-wt. **(A)** SEC elution profile **(B)** SDS PAGE (12%) of indicated fractions of A.

4.1.9 Mass spectrometric analysis of the acetylation of MEK2 by YopP

Z-YopP-wt and MEK2 were incubated in presence of acetyl-CoA for 1 h. Z-YopP was removed from the reaction by washing it over Ni-NTA resin. MEK2 was digested with trypsin and subjected to MALDI-TOF (Figure 35). Numerous peaks could be assigned to tryptic fragments of MEK2, a double acetylated peptide with a mass of 2828.83 Da comprising aa 206-231 (Table 13) was detected.



V:\...MEK2_alkyl_0002.dat
Acquired: 10:22:00, November 18, 2011

Figure 35 MALDI-TOF of tryptic digest MEK2 incubated with Z-YopP. YopP was removed from the reaction mixture prior to the tryptic digest.

This indicates, that the recombinantly expressed YopP is catalytically active. Moreover, the spectrum contains many peaks which are stepwise shifted by 42 Da, but could not be assigned to tryptic digests products of the activation loop of MEK2.

Table 13 Selected masses from the tryptic digest of (**Figure 35**) Masses were analyzed with the ExPASy web tool Peptide Mass [291], [292]. Table columns: User mass: Mass recorded during the experiment. DB mass: Database mass. Δ mass: user mass – DB mass. Presumed acetylated peptides are highlighted in bold.

User mass /Da	DB mass / Da	Δ mass (Da)	peptide	position	modifications
2828.833	2828.359	-0.473	(R)GEIKLCD FGVSGQLID <u>S</u> MAN <u>S</u> FVGTR(S)	206-231	ACET ACET

4.1.10 Kinetic analysis of the acetylation reaction

4.1.10.1 The effect of Elmann's reagent on YopP/MEK2/acetyl-CoA mixtures

DTNB reacts with free thiols groups and the absorption maximum shifts from 345 nm from DTNB to 412 nm. The change in the absorption at 412 nm is proportional to the change in concentrations of free thiol groups.

UV/Vis spectra of DTNB/acetyl-CoA show no absorption at 412 nm (Figure 36 A), and DTNB/YopP/MEK2/acetyl-CoA (Figure 36 B) shows increased absorption at 412 nm whereas MEK2/DTNB shows less absorption at 412 nm. These spectra suggest that the presence of YopP causes in a MEK2/acetyl-CoA/DTNB mixture a strong increase of free thiol groups, most likely due to release of CoA during the acetylation reaction. This means in return that the recombinantly expressed YopP is catalytically active and that the recombinantly expressed MEK2 can be acetylated by YopP.

Results

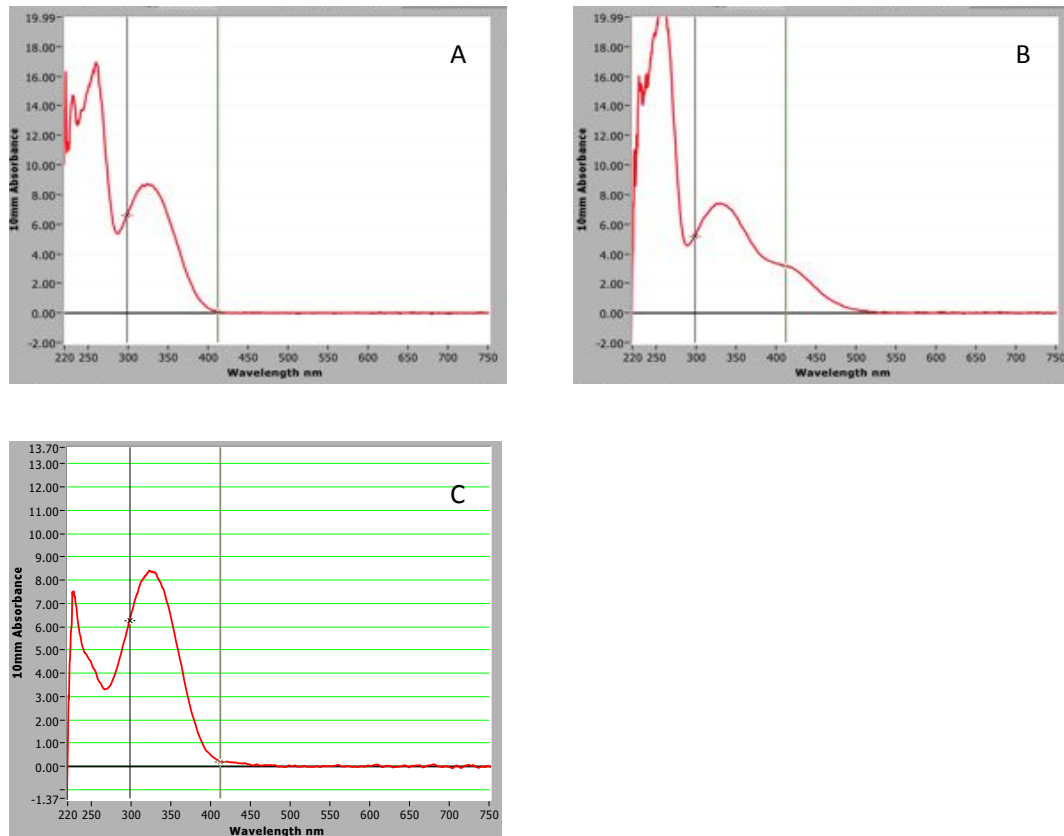


Figure 36 UV-Vis-Spectra **(A)** DTNB/AcCoA alone and **(B)** DTNB/YopP/AcCoA after 1h incubation and **(C)** DTNB/MEK2.

Moreover, the change in $A_{412 \text{ nm}}$ over time could allow the kinetic characterization of a serine/threonine acetyltransferase.

4.1.11 Steady state kinetic analysis of YopP/MEK2 acetylation

Despite of almost 180 publications on YopP/YopJ alone, no information is available on the reaction mechanism of YopP except the significance of the catalytic triad and activation through IP6. To investigate, if the reaction mechanism follows a simple Michaelis-Menten kinetics and to get an idea about the effect of IP6, YopP, MEK2, acetyl-CoA and IP6 were mixed with the indicated concentrations (Figure 37). The concentrations of all reactants were kept constant and only the concentration of the substrate MEK2 was varied. Even in absence of MEK2 (Figure 37 A), a basal absorption at 412 nm occurs but only a marginal increase over time and no effect of IP6 could be determined. YopP contains two cysteine residues, C156 and the catalytically active C172. This

Results

indicates that YopP itself either releases CoA or provides surface exposed cysteine residues, which can react with DTNB.

With increasing concentrations of MEK2 (Figure 37 B to F), the basal $A_{412\text{ nm}}$ increases linear with the total amount of protein in solution. The change in absorption can be divided into two phases, which become apparent at high kinase concentrations. Within the first 500 s, a rapid increase at the $A_{412\text{ nm}}$ occurs, followed by a lower progression of the increase in $A_{412\text{ nm}}$ (Figure 37 F). The first phase is independent of IP6, whereas the second phase shows a notable effect of IP6.

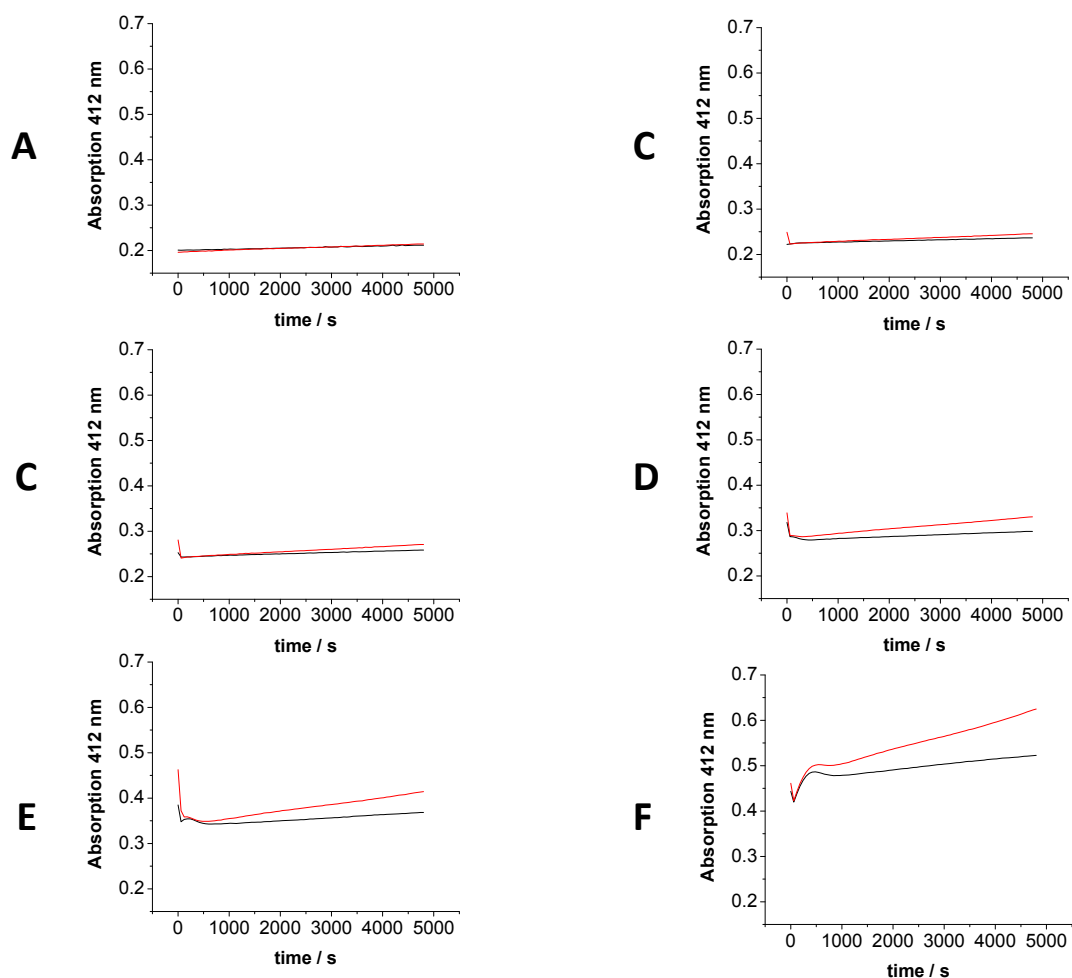


Figure 37 $A_{412\text{ nm}}$ of YopP(0.01 mM)/AcCoa(1.0 mM)/DTNB(1.0 mM) mixtures in presence (red lines) and absence (black lines) of IP6 (0.05 mM). Concentrations of MEK2: **(A)** 0 mM **(B)** 0.0055 mM **(C)** 0.011 mM **(D)** 0.022 mM **(E)** 0.044 mM **(F)** 0.088 mM.

The MEK2 construct 55-400 contains 5 cysteine residues. It can be assumed that the initial burst is caused by the reaction of DTNB with the cysteine residues of MEK2.

After 500-1000 s, $A_{412 \text{ nm}}$ increases much slower than during the initial burst phase. This progression is strongly dependent on IP6 and hence a result of YopPs acetyltransferase activity. Moreover $A_{412 \text{ nm}}$ of MEK2 in presence DTNB, acetyl-CoA, and IP6 remains constant over a long time (Figure 38). Therefore, the initial velocities of v_0 of the acetyltransferase activity of YopP have to be taken from an interval between e. g. 1000 and 2000 s in order to avoid the introduction of an error with the MEK2-cysteine-DTNB side reaction.

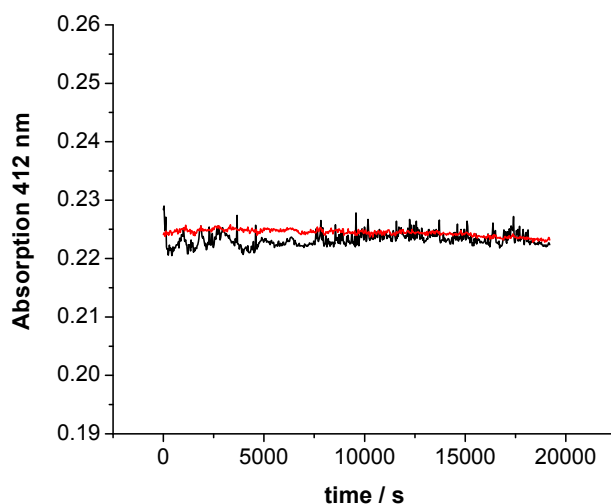


Figure 38 AcCoA (1.0 mM), DTNB (1.0 mM) and MEK2 (0.02 mM) in absence in presence (red) and absence (black) of IP6 (0.05 mM)

However, plotting the initial velocities against the substrate concentrations according to a nonlinear Michaelis-Menten curve-fit results in an almost linear dependency of v_0 values in absence of IP6, whereas in presence of IP6 the velocities grow in an exponential manner with the substrate concentration and do not reach a V_{\max} value in both cases (Figure 37). Since the substrate is a protein, substrate saturation seems impossible to achieve. Accordingly, the Michaelis-Menten plot (Figure 39) gives ambiguous results and the K_m and V_{\max} values are very high (Table 14), indicating that the reaction mechanism does not follow Michaelis-Menten kinetics.

An acetylation assay with a synthetic peptide, which allows higher substrate concentrations, did not give increasing A_{412nm} , indicating that the entire kinase domain is required for the acetylation reaction (Data not shown).

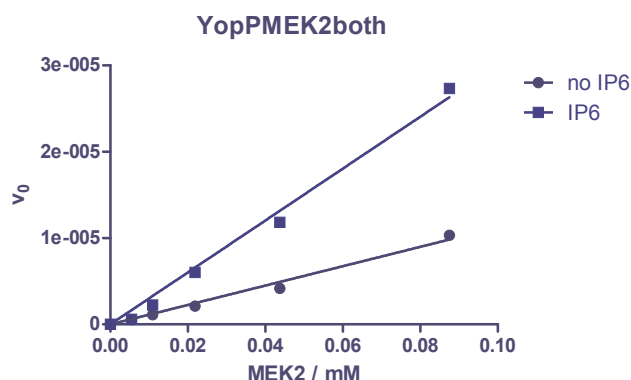


Figure 39 Non linear curve fitting according to Michaelis-Menten kinetics for the acetylation of MEK2 by YopP with slopes derived from (Figure 37) with GraphPad Prism.

Table 14 GraphPad Prism derived Michaelis Menten parameters of (Figure 39)

_Michaelis-Menten	Ambiguous 0 mM IP6	Ambiguous IP6
Best-fit values		
V _{MAX} /mM/s	2.09e+12	~ 1.104e+011
K _M / mM	~ 1.865e+016	~ 3.674e+014
Std. Error		
VMAX	8.98E+10	~ 1.537e+021
KM	~ 1.007e+007	~ 5.117e+024

4.1.12 Lineweaver-Burk plot.

The double reciprocal Lineweaver-Burk plot [293] of the initial velocities against the substrate concentration in presence of IP6 (Figure 40 A) describes an exponentially growing curve instead of a straight line which would be expected if the reaction follows Michaelis-Menten-kinetics. In absence of IP6 the plot

describes a straight line (Figure 40 B). However, the y-axis intercept and hence $1/V_{\max}$ is negative, which indicates that also in absence of IP6 the reaction does not follow a Michaelis-Menten kinetics.

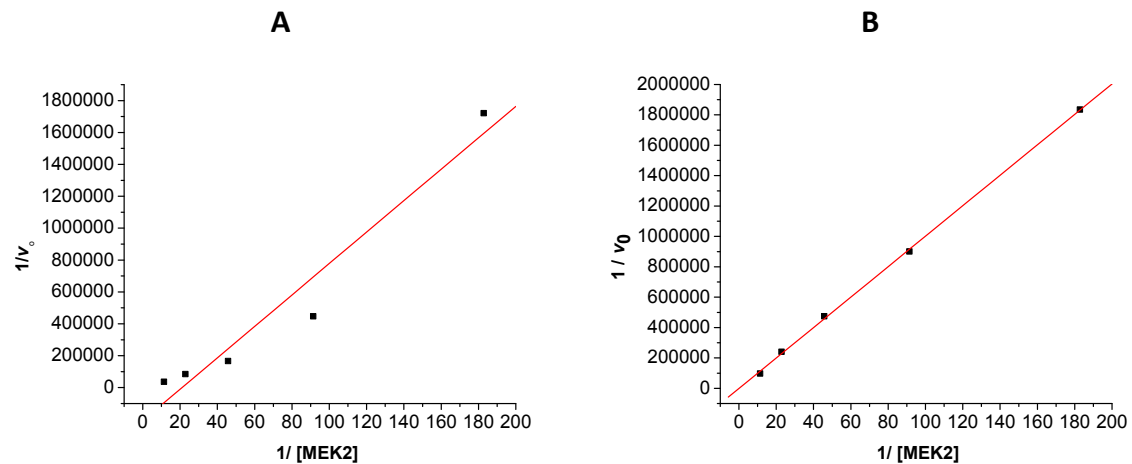


Figure 40 Lineweaver-Burk Plot of YopP/MEK2/acetyl-CoA in presence (A) and absence (B) of IP6 (v_0 values taken from (Figure 37))

4.1.13 Dissecting the reaction mechanism.

YopP catalysed serine/threonine acetylation is presumably multistep reaction: YopP has to bind (i) acetyl-CoA (ii) acetyl-group has to be transferred to C172 (iii) CoA has to be released (iv) YopP has to bind the kinase (v) acetyl has to be transferred to the kinase (vi) the kinase has to be released. It is not *a priori* obvious in which sequence the steps i-iv occur.

4.1.14 Reaction of YopP with acetyl-CoA

The auto-acetylation of YopP was probed in presence and absence of IP6 and increasing concentrations of acetyl-CoA as a substrate (Figure 41). In absence of acetyl-CoA, $A_{412\text{nm}}$ reaches 0.28 and 0.29 fast and remains constant after 750 s (Figure 41 A). This suggests that a thiol group, provided by YopP reacts with DTNB and causes an increase in $A_{412\text{ nm}}$. YopP C172 or C156 could react with DTNB and cause the increase in $A_{412\text{ nm}}$. This is similar to what was observed for MEK2 in presence of DTNB and absence of YopP (Figure 37, Figure 38), when presumably the five cysteine residues of MEK2 react with DTNB fast, causing a burst in $A_{412\text{ nm}}$ within the first 1000 s of the reaction and no further increase afterwards.

In absence of acetyl-Co (Figure 41 A), there is no significant effect of IP6 (red line) compared to absence of IP6 (black line). In presence of increasing concentrations of acetyl-CoA (Figure 41 B to F), $A_{412\text{ nm}}$ increases over time and the reaction is significantly accelerated in presence of IP6 (red lines) compared to absence of IP6 (black lines). In presence of IP6, $A_{412\text{ nm}}$ reaches maxima between 0.44 and 0.62, which is approximately 100% increase over $A_{412\text{ nm}}$ in absence of acetyl-CoA. IP6 has no effect on the stability of acetyl-CoA (Figure 38), which suggests that the increase in $A_{412\text{ nm}}$ is caused by the reaction of YopP with acetyl-CoA and the following release of CoA, which provides free thiol groups to react with DTNB. The t_0 values of $A_{412\text{ nm}}$ for the increasing concentrations of acetyl-CoA are between 0.25 and 0.35, which is in the same range as the final $A_{412\text{ nm}}$ values of YopP in absence of acetyl-CoA (Figure 38 A). The increase in $A_{412\text{ nm}}$ in presence of acetyl-CoA and IP6, hence the auto-acetylation occurs within the first 1500 s. This implies that the increase in $A_{412\text{ nm}}$ in presence of acetyl-CoA is caused by the release of CoA as well as a potential side reaction of C172 or C156 with DTNB. In absence of IP6, it can be clearly distinguished between the initial burst phase and the slow, linear progression in $A_{412\text{ nm}}$, hence the v_0 values can be derived from time intervals between 1000 and 2000 s and correlate the rate of the autoacetylation. In presence of IP6, the auto-acetylation is accelerated to such an amount that the initial velocities can only be derived from a time interval, where also the potential reaction of C172 or C156 contribute to the increase in $A_{412\text{ nm}}$.

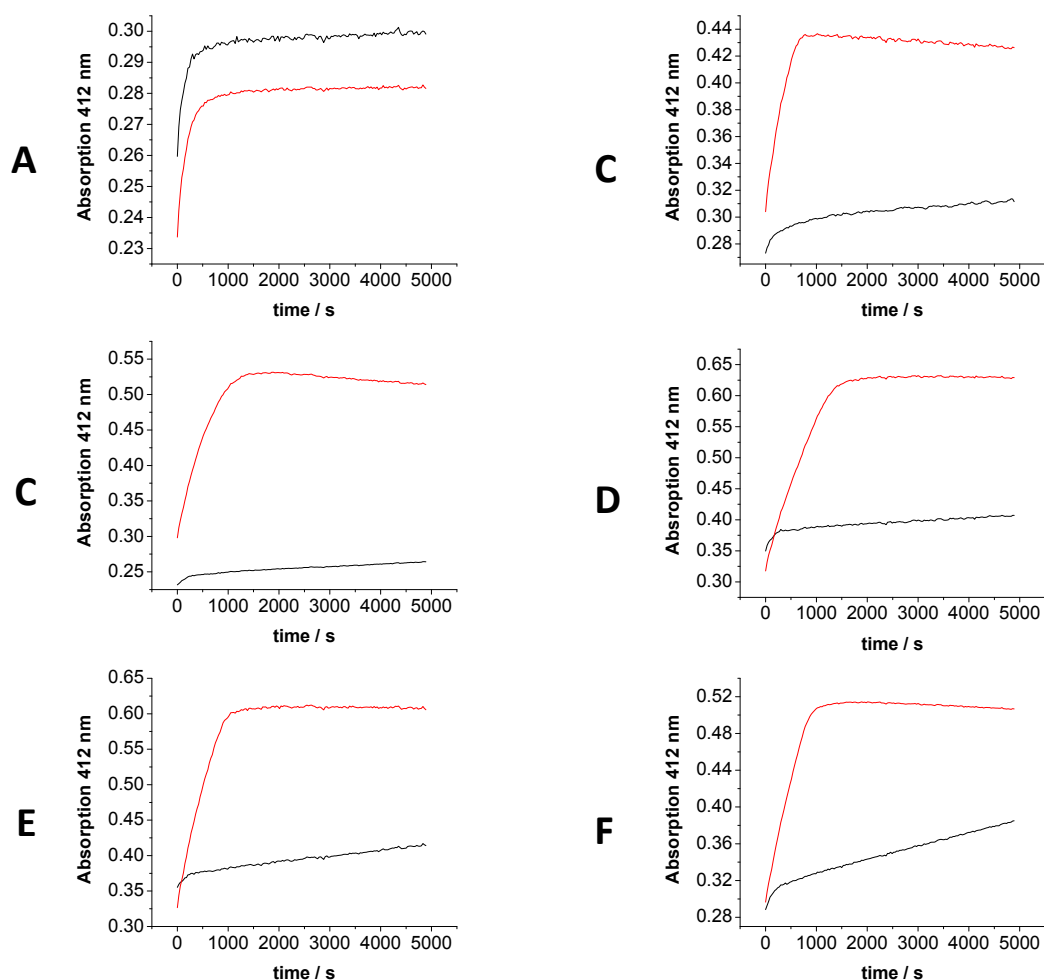


Figure 41 Auto-acetylation of YopP (0.03 mM) in presence DTNB (1.38 mM) in presence (red lines) and absence (black lines) of IP6 (0.5 mM). **(A)** 0mM acetyl-CoA , **(B)** 0.17 mM acetyl-CoA , **(C)** 0.34 mM acetyl-CoA , **(D)** 0.69 mM acetyl-CoA , **(E)** 1.38 mM acetyl-CoA , **(F)** 2.77 mM acetyl-CoA

Plotting of the initial velocities against increasing acetyl-CoA concentrations, shows that the initial velocities v_0 of the auto-acetylation in presence of IP6 do not decrease significantly at low substrate concentrations, even when there is only a fivefold excess of acetyl-CoA over YopP. The curve fit reveals Michaelis-Menten parameters (Table 15).

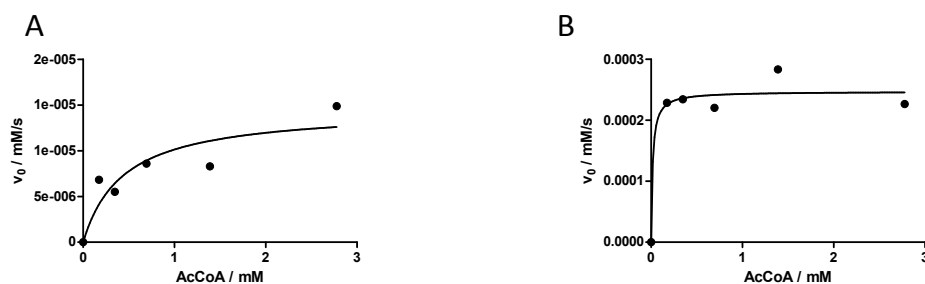


Figure 42 Auto-acetylation of YopP in absence **(A)** and presence **(B)** of IP6. Plotting the initial rates v_0 derived from **(Figure 41)** against the acetyl-CoA substrate concentrations.

V_{\max} increases by a factor of 16 and K_M decreases by a factor of 27 due to the addition of IP6 (Table 15).

Table 15 Michaelis-Menten parameters of the auto-acetylation of YopP in presence and absence of IP6 according to **Figure 42**

	0 mM IP6	0.1 mM IP6
–		
Michaelis-Menten		
Best-fit values		
V_{\max} / mM/s	1.46E-05	0.0002471
K_M / mM	0.4407	0.01626
Std. Error		
V_{\max}	3.30E-06	1.71E-05
K_M	0.3079	0.02616

The standard error in particular for K_M is too high for a quantitative analysis of the kinetics yet, the relative change in K_M and V_{\max} in absence and presence of IP6 is remarkable and shows clearly that the kinase is dispensable for the reaction of YopP with acetyl-CoA and for the release of CoA from YopP. Despite the technical difficulties due to the potential basal reaction of YopP with DTNB, the decrease in K_M and increase in V_{\max} shows that IP6 accelerates the auto-acetylation of YopP.

4.1.15 Time Course Analysis of MEK2 Acetylation

The shape of the product curves at high concentrations of MEK2 (Figure 37) suggested that the slope was increasing with the reaction time, which seems counterintuitive, since the amount of substrate decreases with the reaction time. Therefore the product formation was monitored over the entire reaction time. Both in presence and absence of IP6, the $A_{412\text{ nm}}$ t_0 start at approximately 0.45. In absence of IP6, (Figure 43 black line) product formation increases linear over time except for the approximately 1000 s and reaches 0.6 after 15000 s. In presence of IP6 (Figure 43 red line), the product formation increases linear as well, but with a higher slope than in absence of IP6. At $A_{412\text{ nm}}$ 0.65, which is at approximately 50% of the maximal product concentration, the slope suddenly increases and the product formation continues from there to grow linear until it reaches a maximum of 0.86 after 10000 s when no unacetylated MEK2 is left.

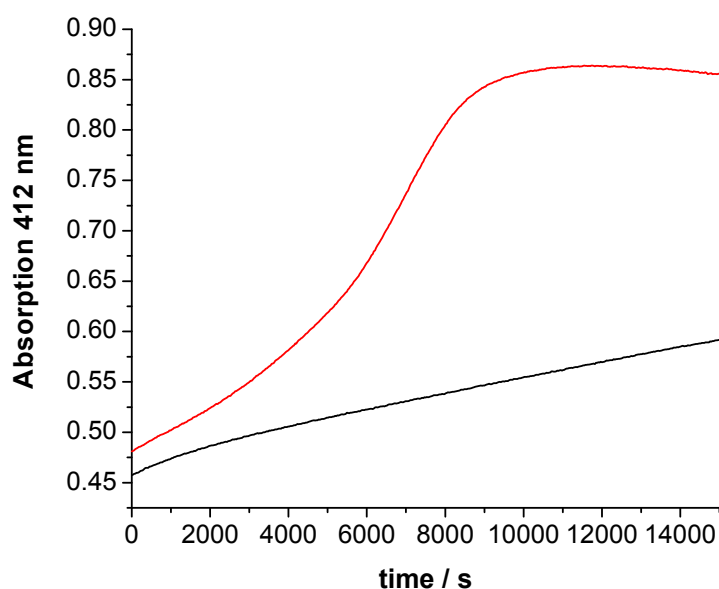


Figure 43 Product formation curve of YopP(0.01 mM)/MEK2 (0.08 mM)/DTNB (1.0 mM)/AcCoA (1.0 mM) in presence of IP6 (0.05 mM) (red line) and absence of IP6 (black line)

4.2 Rv2140c

4.2.1 Interaction of Rv2140c with PE analogues and Locostatin

Structural data and sequence homology indicate that Rv2140c is a PE binding protein [214]. To validate this hypothesis, ITC binding studies were performed with the short chain PE analogues dihexanoyl-phosphatidyl ethanolamine (DHPE), dihexanoyl phosphatidyl-glycerol (DHPG) dihexanoyl phosphatidylserine (DHPS) and dihexanoyl phosphatic acid (DHPA). Initial titrations were performed with DHPE at pH 8.0 (**Figure 44 A**). An interaction of Rv2140c with phospholipids was observed. However, at pH 8.0 the data was noisy and the K_d could only be estimated to be around 6 ± 2 mM. Recent data suggests that the interaction of *Rattus norvegicus* Rv2140c homologue PEBP1/RKIP with phospholipids is pH dependant [256]. Accordingly, titrations were repeated at pH 6.5 and precise fitting of the binding curve could be performed (**Figure 44 B**).

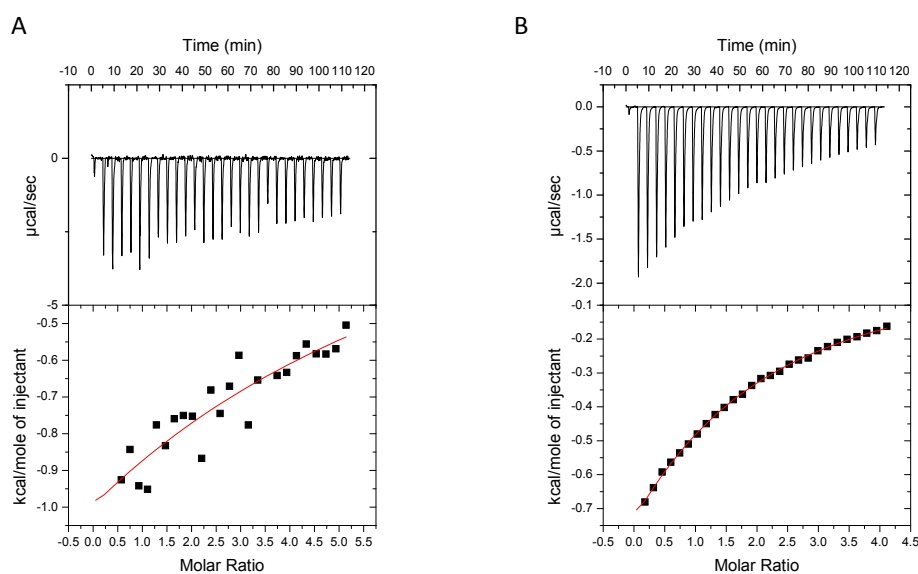


Figure 44 The binding of Rv2140c to DHPE was monitored at pH 8.0 (**A**) and at pH 6.5 (**B**) by ITC. The top panel shows the raw heat change and the bottom panel shows the integrated heat change per injection and the fitted binding curve.

Under low pH conditions, Rv2140c binds the phospholipids with K_d of 1 to 4 mM (Table 16, Figure 45). In case of DHPS and DHPG (Figure 45 A and B), the K_d is with 1.15 and 1.35 mM notably lower than for DHPE and DHPA with 2.31 and 3.99 mM. In case of DHPE, the heat of dilution and heat of interaction is significantly lower than for the other phospholipids (Figure 45 C). Due to poor solubility or impurity of DHPA (see section 3.4.1), the concentration of DHPE could actually be lower than calculated and therefore explain the apparent lower K_d and heats of dilution and interaction. However, the titrations show clearly that Rv2140c binds DHPE with a low mM affinity. DHPA has the lowest affinity towards Rv2140c of the phospholipids tested. This divergence might be due to the high heat of dilution of DHPA alone, which exceeds the respective values of the other phospholipids almost to a factor of 10. With 1.5 to 1 kcal/mol of injectant, it is in the same range as the heat of interaction of DHPA and Rv2140c with 2.75 to 1.5 kcal/mol of injectant. Subtraction of the background process prior to curve fitting hence introduces considerable error and results in less reliable ΔH and K_d values. Nevertheless, Rv2140c binds DHPA with a comparable low mM affinity. Attempts to characterize the binding of Rv2140c to locostatin were unsuccessful due to technical reasons (data not shown). The poor solubility of locostatin in aqueous solutions required addition of 5% DMSO (v/v) to Rv2140c and locostatin. Even then, locostatin was only soluble up to 2.45 mM compared to ~20 mM for the phospholipids. The poor solubility of locostatin hence prevented titrations with a high excess of locostatin over Rv2140c as it is required for the accurate characterization of low affinity binding systems [255]. The high dipole moment of DMSO also resulted in high heats of dilution, which overruled the possible effect of the locostatin binding and prevented determination of a binding curve. The same technical reasons prevented attempts to investigate the displacement of phospholipids by locostatin.

NMR based titrations were performed by a collaborator, in which HSQC peaks were used as site specific probes for locostatin binding. These experiments suggest that locostatin binds at the conserved sulfate-binding site, which was also found in the Rv2140c crystal structure. Moreover, NMR titrations with locostatin allowed the determination of a K_d of 1.0 ± 0.2 mM [214].

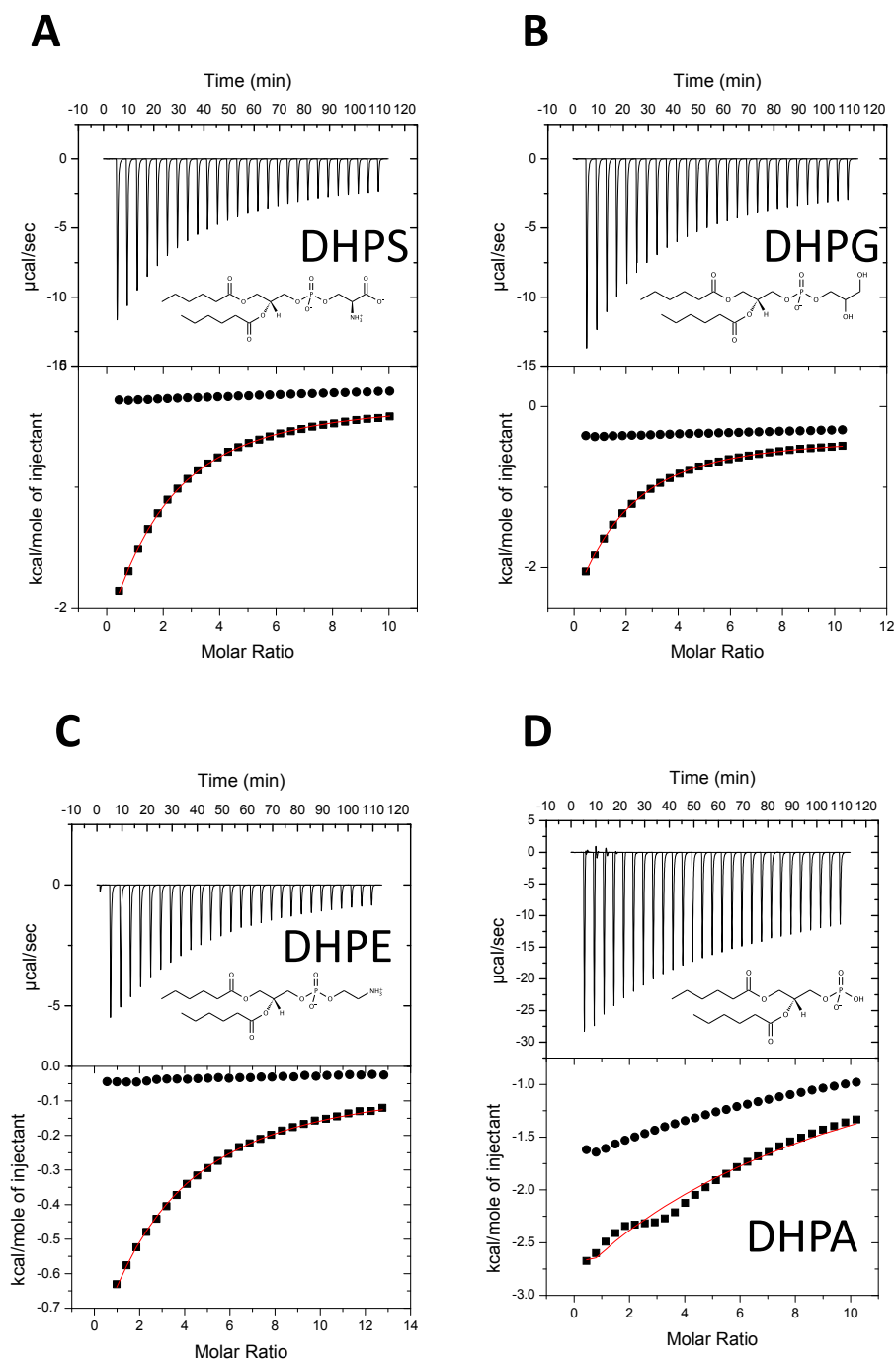


Figure 45 Binding studies of Rv2140c with DHPS (**A**), DHPG (**B**), DHEP (**C**) and DHPA (**D**). The top panel shows the raw binding data. The bottom panel shows the integrated heat change per injection for the interaction of Rv2140c with the phospholipids (square data points) and the respective heat of dilution, where phospholipid was injected into buffer (circles). The heat of dilution was subtracted from the heat of interaction prior to binding curve fitting (red).

Taken together, the ITC data clearly shows that Rv2140 binds the short chain PE analogues with a low mM affinity and can therefore be considered as a PE binding protein (Table 16).

Table 16 Binding parameters for the interaction of Rv2140c with DHPE, DHPS, DHPG and DHPA. Standard deviations are given from at least 3 repeated titrations each.

	n	K_d / mM	ΔG / kcal/mol	ΔH / kcal/mol	$-T\Delta S$ / kcal/mol
		1.35±0.07			
DHPS	1.0		-3.94±0.07	-7.62±0.55	3.68±0.62
		1.15±0.03			
DHPG	1.0		-4.01±0.02	-6.59±0.47	2.58±0.49
		2.31±0.05			
DHPE	1.0		-3.60±0.01	-4.99±0.24	1.40±0.15
		3.99 ±0.03			
DHPA	1.0		-3.28±kdjf	-8.31±1.75	5.03±1.77

4.2.2 Influence of locostatin and the Rv2140c homologues MSMEG_4199 on *M. smegmatis* growth.

4.2.2.1 Creation of a Δ MSMEG_4199 knock out mutant

The less pathogenic organism *Mycobacterium smegmatis* mimics many properties of Mtb and is often used as a model organism to study Mtb genetics and metabolism. The *M. smegmatis* gene MSMEG_4199 encodes a protein, which shares 76% sequence identity with Rv2140c (Figure 46). Moreover, the organization of the genome in this respective area is highly similar between *M. smegmatis*, *M. tuberculosis* and several other pathogenic mycobacteria, suggesting a similar conserved function for the Rv2140c and MSMEG_4199 (Figure 47).

Results

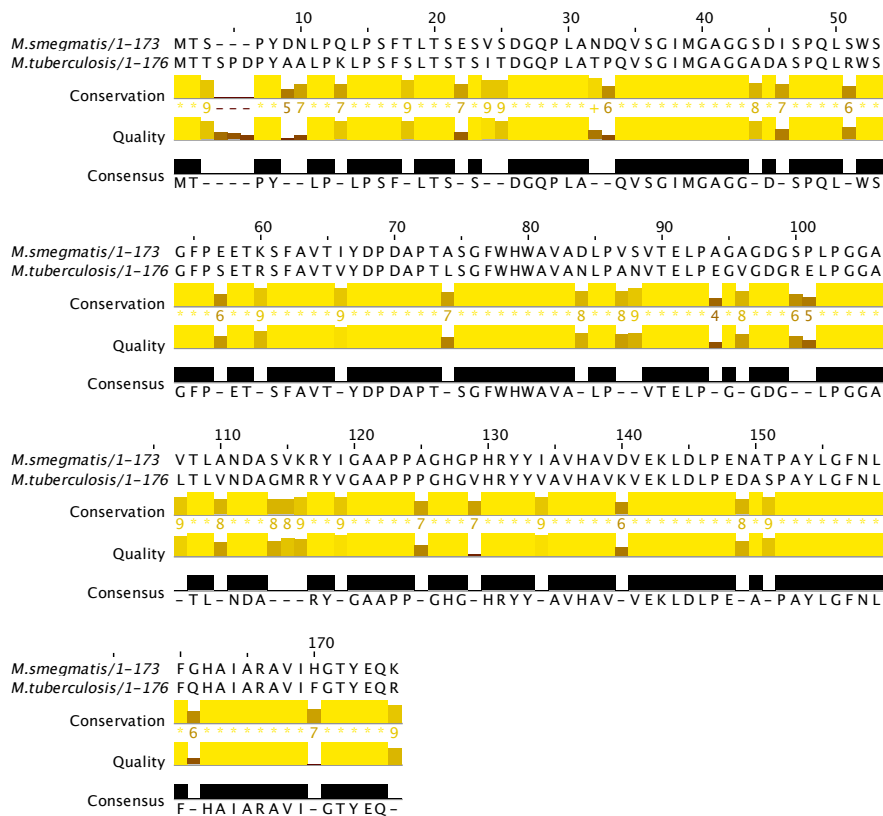


Figure 46 Alignment of *M. smegmatis* MSMEG_4199 and Mtb Rv2140c using ClustalW [294].

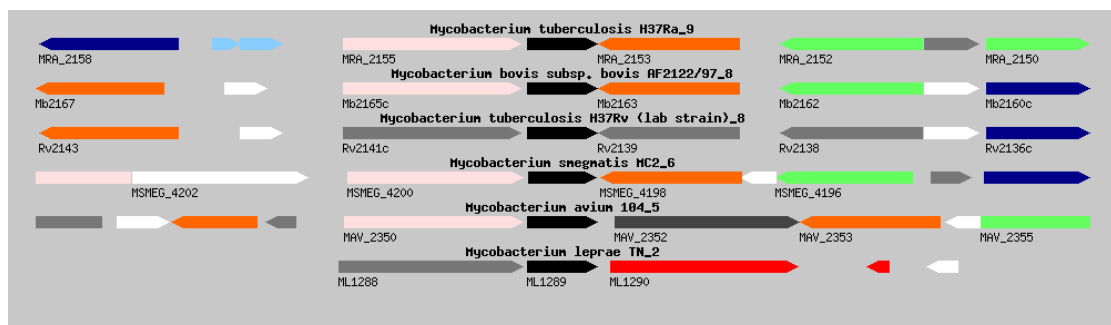


Figure 47 Genome organization of mycobacteria with respect to Rv2140. Rv2140c and homologues are shown in black. The figure was generated with the CMR server [295].

The high sequence identity of Rv2140c and MSMEG_4199 and the highly similar genome organization legitimises to investigate, if the effects of the binding of

Results

locostatin to Rv2140c translates to an *ex vivo* phenotype in *M. smegmatis* and to derive conclusions about the significance of this interaction. Accordingly, a knock out mutant of *M. smegmatis* mc¹⁵⁵ was engineered to further characterize the effect of MSMEG_4199 and locostatin on *M. smegmatis* growth. The knock out was generated using the recombineering method of van Kessel and Hatful [247], [248]. Transformation of wt *M. smegmatis* harbouring the recombination protein expression vector pJV53 with a specifically designed linear MSMEG_4199 knock out vector, containing a Hygromycin resistance cassette, gave rise to a Hyg insensitive *M. smegmatis* mutant. To verify the correct insertion of the HygR cassette into the MSMEG_4199 gene, genomic DNA of Hyg insensitive colonies was digested with various restriction enzymes and subjected to Southern Blot hybridization, in which DIG labelled HygR was used as a probe. The obtained fragmentation patterns (Figure 48 A) match the expected fragmentation patterns (Figure 48 B) for the correct insertion of the HygR in the MSMEG_4199 gene, thus proving the knock out of the MSMEG_4199 gene. None of the expected DNA fragmentation patterns which were observed for the knock out strains occur for the respective control with *M. smegmatis* wt genomic DNA (Figure 48 A).

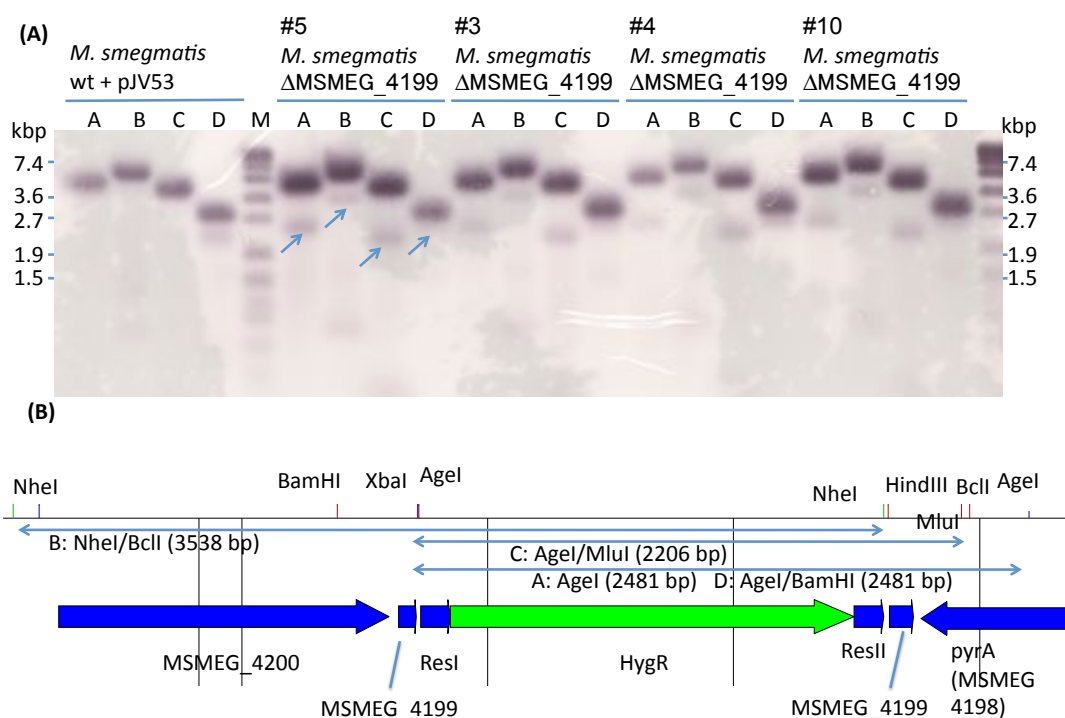


Figure 48 Confirmation of the creation of the $\Delta MSMEG_4199$ knock-out strains via southern blot hybridization of *M. smegmatis* wt + pJV53 and *M. smegmatis* $\Delta MSMEG_4199:res-HygR-res$. **(A)** Genomic DNA was digested with A (AgeI), B (NheI/BclI), C (AgeI/MluI), D (AgeI/BamHI), separated on a 0.9% agarose gel and transferred to a nylon membrane. DIG labeled HygR was used as a probe (MarkerType VII, DIG labeled (Roche)) For #5 *M. smegmatis* $\Delta MSMEG_4199$ arrows indicate the localization of the expected bands. **(B)** Expected fragmentation patterns for *M. smegmatis* $\Delta MSMEG_4199:res-HygR-res$ according to the localization of the HygR-cassette within the genome. Clone #5 was used for the following experiments.

Subsequent transformation of the recovered *M. smegmatis* $\Delta MSMEG_4199:res-HygR-res$ with a $\gamma\delta$ -resolvase expression pGH542 vector removed the HygR-cassette from the genome and resulted in a scar mutant, which is sensitive against Hyg, Kan and Strep. Genomic DNA of a Hyg/Kan/Strp sensitive clone was extracted and a PCR with oligonucleotide primers A and D was performed to verify the scar mutant (**Figure 49 A**). The length of the amplicon spanning from A to D for the of the Hyg/Kan/Strp sensitive clone matches the expected length of the amplicon for the scar mutant of 1230 bp (**Figure 49 B**), which can be clearly distinguished from wt *M. smegmatis* with an expected length of 1419 bp (**Figure 49 C**), thus proving the creation of an unmarked *M. smegmatis* $\Delta 4199$ scar mutant.

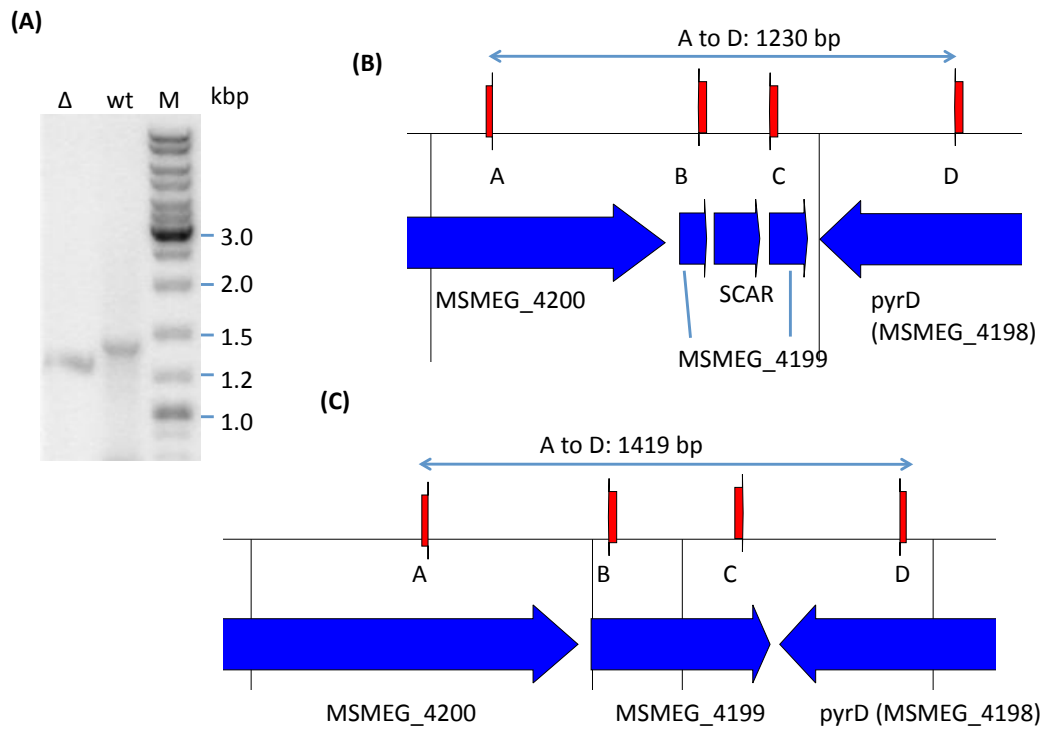


Figure 49 PCR verification of the Δ MSMEG_4199 scar mutant (A) Agarose gel of the PCR spanning from A to D of *M. smegmatis* wt genomic DNA and Δ MSMEG scar mutant (B) Expected length of a PCR product spanning from A to D for the scar mutant and (C) for the *M. smegmatis* wt. (M: Gene Ruler DNA Ladder Mix 1 kb+)

4.2.3 Growth curves of wt *M. smegmatis* and Δ MSMEG_4199 knock out in presence and absence of locostatin.

Growth curves were recorded for wt *M. smegmatis* the Δ MSMEG_4199 knock out strain both in presence and absence of 200 μ M locostatin (Figure 50). In absence of locostatin, *M. smegmatis* wt and Δ MSMEG_4199 grow at the same rate and reach maximal OD_{600 nm} of 0.3 after ~31 h. In presence of 200 μ M locostatin, both wt and Δ MSMEG_4199 grow at a slower rate and reach maximal OD_{600 nm} 0.275 after 32 respectively 33.5 h. The growth rate of Δ MSMEG_4199 is only insignificantly lower than the growth rate of wt *M. smegmatis* in presence of locostatin under the condition tested. Given the low affinity of locostatin to the MSMEG_4199 in low mM range and rich 7H9 medium, the potential effects of locostatin binding to MSMEG_4199 could be either overruled by other effects of

Results

locostatin or the rich medium is giving Δ MSMEG_4199 enough resources to compensate for the loss of MSMEG_4199.

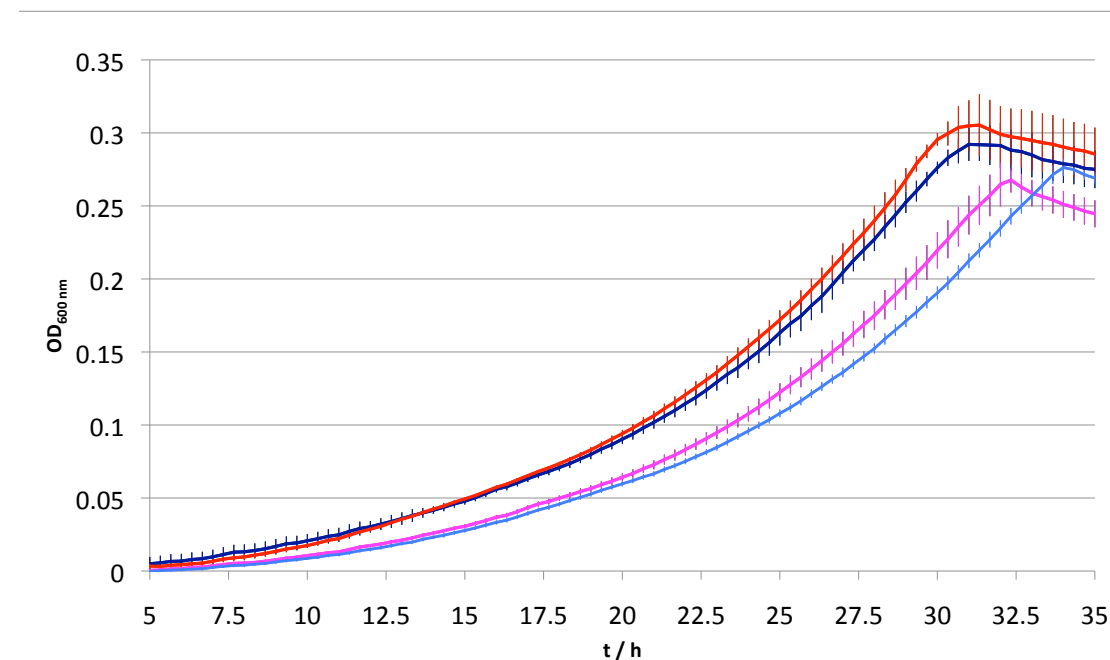


Figure 50 Growth curves of wt *M. smegmatis* and Δ MSMEG_4199 in absence and presence of 200 μ M locostatin. Wt *M. smegmatis* (blue), Δ MSMEG_4199 red, wt 200 μ M locostatin (magenta) and Δ MSMEG_4199 200 μ M locostatin light blue. Indicated error bars were derived from triplicate experiments.

5 Discussion

5.1 YopP

5.1.1 Binding to Ligands IP6 and CoA

The stoichiometric parameter n diverges from 1.0 for all three interactions (Table 9). As shown in (4.1.3.3), IP6 protects YopP partially from C-terminal proteolytic degradation, which indicates that the C-terminus plays an important role in the interaction of YopP with IP6 and that the respective shorter fragments have a lower affinity for IP6. This hypothesis is supported by the fact that 12 of YopP's 25 lysine residues are located within the last 77 amino acids. These basic amino acids are likely to be important ligands for the highly acidic IP6. Similarly also the interaction of YopP and CoA seems to be affected by the C-terminal degradation. The higher divergence of the stoichiometric parameter n from 1.0 indicates that the C-terminus of YopP could be even more important for the binding of CoA. The dissociation constants K_D for the interaction of YopP to IP6 and CoA are similar and the affinity to IP6 is not significantly changed, when CoA is already bound to YopP. However, the binding enthalpy is changed significantly. This indicates that binding of IP6 to YopP/CoA involves further interactions, which might also affect the binding state of CoA. Interestingly, activation through binding to IP6 was also reported for the *Vibrio cholerae* RTX cysteine protease domain [267], which binds IP6 with a similar K_D for 1.2 μM determined by Surface Plasmon Resonance (SPR). In this case, IP6 binds a conserved basic cleft, distant from the active site, which induces autoprocessing of the toxin and release of effector domains. IP6 binding does not change the affinity of the cysteine protease domain for its substrate. This suggests a role as an allosteric regulator for IP6, which might involve a change the exposure of the active site of the protease domain [267]. In case of YopP, binding to IP6 could induce structural rearrangements, which then promotes a more efficient transfer of the acetyl-CoA acutely group to YopP C172.

5.1.2 Self degradation and N-terminal sequencing

The N-terminus of the YopP samples, which were subjected to limited proteolysis starts at aa 1 both in presence and absence of IP6, proving that IP6 protects exclusively on the C-terminus of YopP (Figure 10, Table 10). Given the C-terminal degradation upon purification, the self-degradation that occurs predominantly at the C-terminus and the susceptibility of the C-terminus towards limited proteolysis, it can be concluded that the C-terminus beyond aa 226 is at least partially disordered. Moreover, the presuming rigid conformation of the N-terminus contradicts its predicted disorder as signal peptide (Figure 14). However, the rigidity is consistent with the predicted lack of a TTSS chaperone binding domain adjacent to the N-terminal signal sequence. In the case of YopE for example, binding to a secretion chaperones protects the chaperone binding domain adjacent to the N-terminal signal peptide from proteolytic degradation [296]. Only the C-terminus of YopP is affected by proteolytic degradation, which confirms that YopP does not have such a domain adjacent to its N-terminus. However, even though no secretion chaperone or interaction protein within *Yersinia* has been identified for YopP so far, the flexibility of the C-terminus indicates, that such an interaction could be mediated by the C-terminus.

5.1.3 Crystallization

YopP has very unfavourable crystallisation properties, which might be a reason, why no structure of YopP has been elucidated so far. Even at low concentrations of 3 mg/mL, fl YopP showed a high amount of initial precipitation and denaturation during crystallisation trials. Surprisingly, binding to its small molecule ligands IP6 and CoA did not stabilize YopP and could not reduce the high amount of initial precipitation. The use of additives such as polyalcohols, amino acids and amino acid derivatives also failed to reduce the high amount of initial precipitation and denaturation. A particular difficulty was that no pattern was recognizable what kind of conditions are required to stabilize YopP, no improvements or significant changes due to addition of ligands, additives buffer optimizations etc. could be made, which would indicate a direction for the optimization. The only obvious effect was observed after lysine methylation,

which resulted in the resolubilisation of denatured YopP in a number of PEG conditions, where previously no change was observed. The next steps towards a crystallisation of YopP could involve combinations of the above-mentioned methods like addition of ligands IP6, CoA, synthetic peptide, followed by reductive methylation and limited proteolysis in presence of additives, which prevent aggregation.

The C-terminus of YopP was found to be partially degraded upon purification of and YopP was found undergo self-degradation to a 24 kDa core domain with a remarkable thermostability (Figure 6). This is particularly enigmatic, since the degradation of YopP should also occur in the few remaining clear conditions in the crystallisation screen, as well as in the supernatants of the conditions where immediate precipitation and denaturation occurs.

The reason for this destabilization is not clear. The partially disordered C-terminus contains many lysine residues, which negatively affect the crystallisation properties as well as they could provide YopP with a dipole moment in solution, which could contribute to the observed aggregation. The hypothesis that truncated constructs, which lack the partially disordered C-terminus, might be more stable and exhibit better crystallisation properties proved to be wrong. All truncated constructs that could be expressed, were performing even worse than the fl YopP during the crystallisation experiments and precipitated already during purification process (Figure 19). Surprisingly, the YopP-18-223 construct, which matches almost the N- and C-termini of the highly stable self-degraded YopP proved to be very instable as well. It appears that the lysine residues in the C-terminus act as a kind of a solubility anchor for YopP, as the truncated constructs were more likely to precipitate and limited proteolysis which cleaves exclusively the C-terminus, also caused a high amount of precipitation (Figure 20).

The activation through IP6 in acetyltransferase assays indicates that YopP could be in a dynamic equilibrium between active and inactive states. Binding to IP6 could then shift the equilibrium towards an active conformer, as it was shown for the cysteine protease domain of the *C. difficile* toxin [297]. However, it

is difficult to draw conclusions regarding the crystallisation of YopP from the *C. difficile* or *V. cholerae* [267], [297] toxin cysteine protease domain, since these auto-processed domains – unlike YopP - crystallise easily in presence of IP6 and have only a 13% sequence identity. Besides binding to IP6 and acetyl-CoA, auto-acetylation of C172 and interaction with substrates in various acetylation states could also contribute to a conformational heterogeneity, which makes it more difficult to fix YopP in one conformation. This conformational heterogeneity is also reflected in the limited proteolysis experiments (Figure 10), where addition of a high excess of IP6 prevents only a fraction of YopP from limited proteolysis while the majority is still degraded to the small core domain. However, even this fraction is only partially protected against degradation, since the IP6 protected YopP is still shorter than full YopP. This indicates that even though the conformational heterogeneity has been reduced due to binding to IP6, YopP still retains a certain degree of flexibility, which probably contributes to the unfavourable crystallization properties. Using a synthetic peptide mimicking the activation loop of MEK2 did not influence the crystallisation properties of YopP-C172A and was not active in the acetylation assay with YopP-wt. In the case of *C. difficile* cysteine protease domain, only the use of a specifically designed peptide based inhibitor which covalently binds to the active site cysteine in combination with IP6 provided the cysteine protease domain with maximal protection against limited proteolysis and hence reduced its conformational heterogeneity to a minimum. [297], [298]. This effect could not be achieved by the use of simple alkylating agents.

The poor understanding and the limited control of the allosteric regulation of YopP could also explain why the widely used method of truncated protein constructs and optimized buffers failed to stabilize YopP during the crystallization experiments. A potential disruption of the allosteric circuit in truncated constructs could result in unregulated transitions between active and inactive states of YopP, which presumably negatively over-compensate for a potential beneficial effect of the removal of disordered terminal regions. The key for a successful crystallisation of YopP remains to stabilize it and to prevent the

initial aggregation and this can only be achieved by a better understanding of the allosteric dynamics of YopP in order to fix it in one conformation.

The unfavourable crystallisation properties are not limited to YopP alone, also the homologue AvrA was behaving in the same manner, indicating that the use of homologues of YopP for crystallization purposes without a proper understanding of the allosteric dynamics is ineffective.

5.1.4 Interaction with Chaperones

The available protein-protein interaction networks involving YopP feature surprisingly little interaction partners for YopP/J both for pathogen and host proteins [299], [300]. YopP secretion appears to be not strictly dependant on secretion chaperones encoded on the virulence plasmid [286], however this does not take into account, that type three secretion chaperones encoded in the genomic DNA could compensate for the loss of the plasmid encoded chaperones. Moreover, the poor performance of fl and truncated constructs of YopP both in presence and absence of small molecule ligands led to the hypothesis that binding to a bacterial chaperone could stabilize YopP in a protein complex which stabilizes YopP and allow crystallisation. The two most obvious choices, SycO and orf91a were found to be particularly difficult to express and purify in sufficient amounts both alone and in co-expression studies with YopP, hence no thorough interaction studies with YopP could be performed. For further interaction studies the use of monocistronic co-expression vectors would be advisable since the correct stoichiometry could not be matched. Even if SycO and orf91a would clearly not interact with YopP, it is still worth challenging the current paradigm that YopP does not have interaction partners/chaperones within *Yersinia*, since this hypothesis is partially based on the claim, that lack of IP6 in *Yersinia* is sufficient to keep YopP in a quiescent state, prevent depletion of acetyl-CoA and acetylation of bacterial proteins [147], [149]. However, the acetylation assays indicate, that even in absence of IP6, YopP still undergoes auto-acetylation (Figure 41) and is able to acetylate kinase substrate *in vitro* (Figure 37), supporting the hypothesis that YopP requires an interacting protein/chaperone to remain inactive in the bacteria as it is done with other effector proteins [285]. Moreover, even though the *E. coli* expression strains used

in this study are already deficient in some proteases, fl YopP could never be expressed without the degradation pattern. Binding to a chaperone could therefore prevent a potential degradation by *Yersinia* proteases. The paradigm of specific class Ia and unspecific class Ib secretion chaperones is questioned, since more class Ia chaperones show an interaction with more than one substrate [301]. Besides SycO and orf91a, promising candidates could predicted type three secretion chaperones which are encoded in the genomic DNA such as ysaK (Uniprot A1JQA4).

Another unexplored approach, which could not be addressed during this thesis, is the secretion of YopP in *Yersinia* culture supernatant under low Ca^{2+} concentrations. As already mentioned in the introduction, His-tagged YopE could be recovered from *Yersinia* culture supernatant in complex with the translocators YopB/YopD [97]. It has not been investigated yet, if YopP can form such a complex with translocators as well, but this could provide a unique opportunity to work with native YopP in complex with bacterial proteins.

5.1.5 YopP/MEK2 interaction

Despite reports that YopP and MAPKKs bind each other in pulldown assays [131], [140], analytical SEC of separately expressed YopP and MEK2 did not provide evidence for the formation of stable MEK2/YopP protein-protein-complex (Figure 30). Moreover, attempts to co-crystallise YopP/MEK2 did not change the high rate of precipitation, which was characteristic for YopP, indicating that no significant stabilisation occurred. The co-expression of YopP and MEK2 did not work with the pETZ2-1a/pCDF system. YopP expression effectively suppressed the expression of MEK2 (Figure 33), therefore no conclusion about a possible formation of a stable complex can be made. A change of the co-expression vector from two separate plasmids to a monocistronic co-expression vector which often allows a stoichiometric expression of the two proteins could be the method of choice [302]. Due to the high cytotoxicity of YopP, a co-expression system using mammalian cells does not seem to be advisable. The introduction of cysteines and co-expression in Origami(DE3) would have been an elegant way to form a YopP/MEK2 complex and to lock YopP in its active state by the introduction of a covalent bond to MEK2. However,

co-expression in Origami(DE3) cells led to a growth arrest. An alternative to introduce a cysteine bridge by co-expression, YopP-wt and the MEK2-cysteine mutants could be also expressed separately and mixed together and the atmospheric oxygen would facilitate the formation of a cysteine bond. Besides relying exclusively on the cysteines, cross-linking reagents or introduction of unnatural amino acids at YopP C172 or within the MEK2 activation loop at S222 or S226 could allow the formation of a covalent bond between YopP and MEK2. But instead of focusing only on the possible complex of YopP/MEK2, it has to be recapitulated that YopP/MEK2 is a highly artificial system. In macrophages, MAPK are organized in a scaffold, which is embedded in a dynamic multi-protein network localized at the cytosolic part of the TLRs [303]. YopP was found to be distributed evenly in host cells, but upon MAPK stimulation, YopP is rapidly recruited to the cell membrane [139]. YopP contains a motif of a eukaryotic SH2 domain, which is essential for its virulence [129]. The YopP homologue AvrRxv can bind the 14-3-3 scaffold with its C-terminus [176]. Even though several studies revealed binding of YopP to host kinases, it can not be excluded that YopP has other interaction partners such as scaffold proteins or could even interact with transcription factor binding partners such as CEB (Section 4.1.4.1). Binding to such partners could help to stabilize YopP in order to form a stable complex, which may help to stabilize YopP for crystallisation experiments.

5.1.6 Acetylation reaction

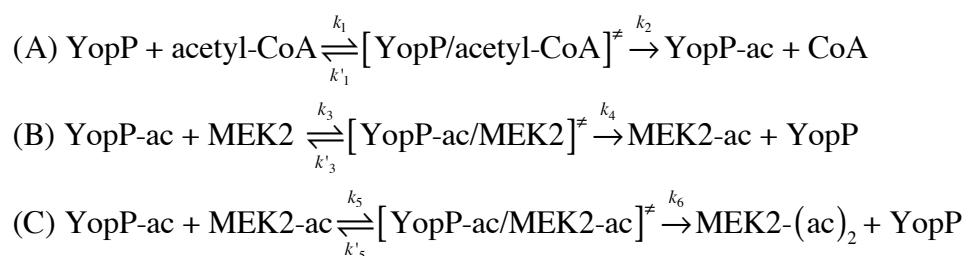
The DTNB assay, which was established in the course of this work, provides the first insight into the kinetics of a serine/threonine acetyltransferase. In case of YopP alone, an auto-acetylation step in presence of acetyl-CoA occurs independent of the presence of the kinase substrate and is significantly accelerated in presence of the regulator IP6 (Figure 42) (Equation 7 A). This also reflects that the parameters K_m and V_{max} are highly dependent on the presence of IP6 (Table 15), even though it could not be ruled out, if the high v_0 values of YopP in presence of IP6 are solely a result of the activation through IP6 and to what extent a side reaction of YopP with DTNB contributes to the high v_0 values. Moreover, the reaction could be also accelerated to such an extent that the steady state assumption is not fulfilled anymore. The activation through IP6 has

to be seen also in the context to the ITC binding data in chapter 4.1.3.2, where it was shown that binding of IP6 to YopP/CoA caused a threefold higher heat of interaction compared to the binding of IP6 to YopP alone. This could imply that binding to IP6 induces a conformational change, which shifts the dynamic equilibrium of YopP from inactive to active states and causes a different binding state for CoA and hence acetyl-CoA, which then accelerates the auto-acetylation of YopP. Even though technical difficulties of the DTNB assay do not allow a precise quantitative determination of the kinetic parameters of the auto-acetylation of YopP yet, the auto-acetylation of YopP in presence of acetyl-CoA and the effect of IP6 are obvious (Figure 41, Figure 42) and can hopefully contribute to a comprehensive kinetic characterization of this novel post-translational modification in the future.

The steady state kinetic analysis indicates that the acetylation of MEK2 by YopP does not follow a Michaelis-Menten mechanism in neither in presence nor absence of IP6 (Figure 40 A and B). Hence, a more complicated multi-substrate reaction has to be assumed, which can occur in various flavours. Binding of the co-factor acetyl-CoA and the acetyl transfer to C172 could either happen prior to substrate binding or could require binding of the kinase substrate [304].

The auto-acetylation of YopP and falsification of a Michaelis-Menten mechanism for the acetylation of MEK2 suggests a ping-pong-like mechanism rather than a random multi-substrate mechanism for the entire reaction cycle [304] (Equation 7). MEK2 has two acetylation sites, S222 and S226. The increase in the rate of product formation during the YopP/MEK2 time course analysis in presence of IP6 (Figure 43) could moreover indicate that YopP distinguishes between unacetylated (Equation 7 B) and monoacetylated kinase substrate (Equation 7 C). Apparently, the second acetylation of MEK2 is catalyzed with a higher rate than the first acetylation.

Equation 7 Presumed reactions during the acetylation of MEK2 by YopP



This could be accomplished by an inhibition mechanism, in which unacetylated MEK2 inhibits the second acetylation of MEK2. When no monoacetylated YopP is left, the faster second acetylation is not inhibited anymore. The change in slope is probably independent of CoA, since it should be abundant in the host cells.

However, no change in the slope of the product formation curve was observed in absence of IP6, even when the product curve approaches a level where the slope of the product curve in presence begins to increase (Figure 43). Therefore the change of the slope of the product formation curve could also be a result of IP6, which not only accelerates the auto-acetylation of YopP, but could also have an effect on YopP's the affinity towards the kinase. However, it is more likely that the acetylation of MEK2 in absence of YopP is under the regime of the slow auto-acetylation of YopP as rate limiting step. In presence of IP6, YopP undergoes auto-acetylation much faster (Figure 41) and hence the acetylation of MEK2 could be the rate-limiting step. Even though there is no data publicly available regarding the kinetics of phosphorylation of MEK2 S222 and S226 by Raf or any other MEK activating MAP-kinase, the phosphorylation of the corresponding residues S218 and S222 of the highly similar MEK1 by Raf seems to interestingly also involve a slow first – and a faster second phosphorylation step [305].

Even though DTNB provides a first insight into the kinetics of the reaction, the side-reactions of cysteine residues of MEK2 and YopP with DTNB cause a signal, which prevents investigation of the critical v_0 for steady state kinetic analysis yet. An alternative could be the protection of the MEK2 cysteines with iodoacetamide to prevent this interaction. It also has to be determined with YopP C156A and C172A mutants, if - and to what extent they contribute to $A_{412 \text{ nm}}$ in absence of acetyl-CoA. Further control experiments and a careful enzymological

investigation are also required regarding the acetylation of the kinase, since the ambiguous Michaelis-Menten parameters, the Lineweaver-Burk-plot and shape of the progress curve suggest a more complicated multi-substrate mechanism. The experiment has to be repeated with the MEK2-S222/226A, MEK2-S222A and MEK2S226A to validate that (i) no product formation occurs for MEK2-S222/226A, (ii) no change in slope occurs for the single mutants. Moreover, mass spectrometric analysis is required to validate that no or little double acetylation occurs during the first phase of the MEK2 acetylation and to determine if MEK2 has a preferred site for the first acetylation. Another important aspect, which could not be addressed in this work, is the effect of MEK2 phosphorylation on the acetylation by MEK2. MEK2 contains up to 17 experimentally validated phosphorylation sites [306], which are important for its activation, inhibition, association with scaffolding proteins and selective activation of downstream targets [307]. It is also not clear, at which stage of the assembly of the MAPK signalling complex the acetylation is performed. Prior to the activation of MAPK signalling, MEK1 forms a hetero-dimer with its scaffolding protein KSR2, in which the activation loops of the kinase domains of MEK1 and KSR2 are facing each other and are not susceptible for Raf phosphorylation [308]. Contact to a proposed regulatory Raf then leads to a rearrangement to a MEK1/KSR2/Raf complex, in which the activation loop of MEK1 can then be phosphorylated and activated by catalytic Raf [308]. At this stage, prior to phosphorylation, also the acetylation of the activation loop by YopP could take place. In this regard, the *in vitro* acetylation of MEK2 by YopP is an artificial system, which can not take possible interactions of YopP with other components of the presumed 1 MDa [303] MAPK signalling complex into account.

Interestingly the YopP homologue VopA [309] (36% sequence identity) is a lysine acetyltransferase. It acetylates lysine residues in the activation loop of kinases, which prevents binding of ATP. Therefore it inactivates phosphorylated kinases. Maybe YopP could also serve as a lysine acetyltransferase in MEK2 S222/226K mutant.

Even though the inactivation of the MAPK/NF- κ B signalling network by YopP through acetylation of serine and threonine residues provides an attractive

model to explain the effects caused by YopP, the physiological relevance of this finding is all but clear. Recent evidence suggests that YopP also has an inhibitory effect on the translation factor eIF2 α kinase through an unknown mechanism [310] (Figure 1 B). Intact eIF2 signalling is a prerequisite for NF- κ B activation and expression of pro-inflammatory cytokines following a bacterial infection [310]. Moreover, the presence of a CREB binding protein motif in the C-terminus of YopP could implicate that YopP has a potential effect on the CREB transcription factor and the regulation of transcription initiation [135], [264].

5.2 Discussion Rv2140c

ITC titrations proved that Rv2140c is a PEBP binding protein, which binds a range of phospholipids with a low mM affinity at slightly acidid pH. The Δ MSMEG_4199 knock out mutant grows at the same rate as *M. smegmatis* wt, which is consistent with the observation that Rv2140c is non-essential for Mtb *in vivo* and *in vitro* [311], [312]. Even in higher organisms such a mice, a PEBP/RKIP knockout has no apparent strong phonotype [313].

Under the conditions tested, locostatin has a negative effect on *M. smegmatis* growth for both wt and Δ MSMEG_4199, which indicates that the locostatin MSMEG_4199 interaction is not important in this *ex vivo* model. The significance of the Rv2140c/MSMEG_4199 and its interaction with locostatin remains to be further investigated. An interesting possibility could be to test the effect of locostatin on wt and Δ MSMEG_4199 under multiple stress conditions using the Biolog microassay [314].

The recent inhibitory effect of the Rv2140c homologue YBCL of pathogenic *E. coli* [227] on macrophages marks the first direct evidence for a host pathogen interaction mediated by a bacterial PEBP. It remains to be seen, if recombinant Rv2140c has a similar inhibitory effect on the migration of macrophages.

III. Literature

[315]

- [1] K. P. Williams, J. J. Gillespie, B. W. S. Sobral, E. K. Nordberg, E. E. Snyder, J. M. Shallom, and A. W. Dickerman, "Phylogeny of Gammaproteobacteria," *J. Bacteriol.*, vol. 192, no. 9, pp. 2305–2314, Jan. 2010.
- [2] A. M. Stenkova, M. P. Isaeva, E. P. Bystritskaya, K. V. Guzev, V. A. Rasskazov, and A. Rakin, "The Molecular Phylogeny of the *gyrB* Gene: A Molecular Marker for Systematic Characterization of the Genus *Yersinia*," in *Advances in Yersinia Research*, A. M. P. de Almeida and N. C. Leal, Eds. Springer New York, 2012, pp. 53–56.
- [3] P. Chen, C. Cook, A. Stewart, N. Nagarajan, D. Sommer, M. Pop, B. Thomason, M. Thomason, S. Lentz, N. Nolan, S. Sozhamannan, A. Sulakvelidze, A. Mateczun, L. Du, M. Zwick, and T. Read, "Genomic characterization of the *Yersinia* genus," *Genome Biology*, vol. 11, no. 1, p. R1, 2010.
- [4] M. Achtman, K. Zurth, G. Morelli, G. Torrea, A. Guiyoule, and E. Carniel, "Yersinia pestis, the cause of plague, is a recently emerged clone of *Yersinia pseudotuberculosis*," *Proceedings of the National Academy of Sciences of the United States of America*, vol. 96, no. 24, pp. 14043–14048, Nov. 1999.
- [5] G. Morelli, Y. Song, C. J. Mazzoni, M. Eppinger, P. Roumagnac, D. M. Wagner, M. Feldkamp, B. Kusecek, A. J. Vogler, Y. Li, Y. Cui, N. R. Thomson, T. Jombart, R. Leblois, P. Lichtner, L. Rahalison, J. M. Petersen, F. Balloux, P. Keim, T. Wirth, J. Ravel, R. Yang, E. Carniel, and M. Achtman, "Yersinia pestis genome sequencing identifies patterns of global phylogenetic diversity," *Nat Genet*, vol. advance online publication, Oct. 2010.
- [6] B. J. Hinnebusch, "The evolution of flea-borne transmission in *Yersinia pestis*," *Curr Issues Mol Biol*, vol. 7, no. 2, pp. 197–212, Jul. 2005.
- [7] B. L. Ligon, "Plague: A Review of its History and Potential as a Biological Weapon," *Seminars in Pediatric Infectious Diseases*, vol. 17, no. 3, pp. 161–170, Jul. 2006.
- [8] A. Yersin, "La peste bubonique à Hong Kong," *Ann Inst Pasteur (Paris)*, no. 8, pp. 662–667, 1894.
- [9] S. Kitasato, "THE BACILLUS OF BUBONIC PLAGUE.," *The Lancet*, vol. 144, no. 3704, pp. 428–430, Aug. 1894.
- [10] T. Butler, "Yersinia Infections: Centennial of the Discovery of the Plague Bacillus," *Clinical Infectious Diseases*, vol. 19, no. 4, pp. 655–661, Oct. 1994.
- [11] T. Butler, "Plague into the 21st century," *Clin. Infect. Dis.*, vol. 49, no. 5, pp. 736–742, Sep. 2009.
- [12] N. Drummond, B. P. Murphy, T. Ringwood, M. B. Prentice, J. F. Buckley, and S. Fanning, "Yersinia Enterocolitica: A Brief Review of the Issues Relating to the Zoonotic Pathogen, Public Health Challenges, and the Pork Production Chain," *Foodborne Pathogens and Disease*, vol. 9, no. 3, pp. 179–189, Mar. 2012.
- [13] H. Fukushima, M. Gomyoda, S. Ishikura, T. Nishio, S. Moriki, J. Endo, S. Kaneko, and M. Tsubokura, "Cat-contaminated environmental substances

- lead to *Yersinia pseudotuberculosis* infection in children.," *J. Clin. Microbiol.*, vol. 27, no. 12, pp. 2706–2709, Jan. 1989.
- [14] G. Wauters, K. Kandolo, and M. Janssens, "Revised biogrouping scheme of *Yersinia enterocolitica*," *Contrib. Microbiol. Immunol.*, vol. 9, pp. 14–21, 1987.
- [15] G. Wauters, S. Aleksić, J. Charlier, and G. Schulze, "Somatic and flagellar antigens of *Yersinia enterocolitica* and related species," *Contrib. Microbiol. Immunol.*, vol. 12, pp. 239–243, 1991.
- [16] E. Huovinen, L. Sihvonen, M. Virtanen, K. Haukka, A. Siitonen, and M. Kuusi, "Symptoms and sources of *Yersinia enterocolitica*-infection: a case-control study," *BMC Infectious Diseases*, vol. 10, no. 1, p. 122, 2010.
- [17] E. J. Bottone, "*Yersinia enterocolitica*: overview and epidemiologic correlates," *Microbes and Infection*, vol. 1, no. 4, pp. 323–333, Apr. 1999.
- [18] E. J. Bottone, "*Yersinia enterocolitica*: the charisma continues," *Clin. Microbiol. Rev.*, vol. 10, no. 2, pp. 257–276, Apr. 1997.
- [19] K. A. Heel, R. D. McCAULEY, J. M. Papadimitriou, and J. C. Hall, "REVIEW: Peyer's patches," *Journal of Gastroenterology and Hepatology*, vol. 12, no. 2, pp. 122–136, Feb. 1997.
- [20] C. Hanski, U. Kutschka, H. P. Schmoranzner, M. Naumann, A. Stallmach, H. Hahn, H. Menge, and E. O. Riecken, "Immunohistochemical and electron microscopic study of interaction of *Yersinia enterocolitica* serotype O8 with intestinal mucosa during experimental enteritis.," *Infect. Immun.*, vol. 57, no. 3, pp. 673–678, Jan. 1989.
- [21] P. D. Smith, L. E. Smythies, R. Shen, T. Greenwell-Wild, M. Gliozzi, and S. M. Wahl, "Intestinal macrophages and response to microbial encroachment," *Mucosal Immunol.*, vol. 4, no. 1, pp. 31–42, Jan. 2011.
- [22] J. L. Coombes and F. Powrie, "Dendritic cells in intestinal immune regulation," *Nat Rev Immunol.*, vol. 8, no. 6, pp. 435–446, Jun. 2008.
- [23] A. Aderem and D. M. Underhill, "Mechanisms of Phagocytosis in Macrophages," *Annual Review of Immunology*, vol. 17, no. 1, pp. 593–623, 1999.
- [24] M. Benoit, B. Desnues, and J.-L. Mege, "Macrophage Polarization in Bacterial Infections," *J Immunol.*, vol. 181, no. 6, pp. 3733–3739, Sep. 2008.
- [25] K. Newton and V. M. Dixit, "Signaling in innate immunity and inflammation," *Cold Spring Harb Perspect Biol.*, vol. 4, no. 3, Mar. 2012.
- [26] M. L. Schmitz, A. Weber, T. Roxlau, M. Gaestel, and M. Kracht, "Signal integration, crosstalk mechanisms and networks in the function of inflammatory cytokines," *Biochimica et Biophysica Acta (BBA) - Molecular Cell Research*, vol. 1813, no. 12, pp. 2165–2175, Dec. 2011.
- [27] T. J. Gibson, "Cell regulation: determined to signal discrete cooperation," *Trends in Biochemical Sciences*, vol. 34, no. 10, pp. 471–482, Oct. 2009.
- [28] T. Kawai and S. Akira, "The role of pattern-recognition receptors in innate immunity: update on Toll-like receptors," *Nat Immunol.*, vol. 11, no. 5, pp. 373–384, May 2010.
- [29] V. Auerbuch, D. T. Golenbock, and R. R. Isberg, "Innate Immune Recognition of *Yersinia pseudotuberculosis* Type III Secretion," *PLoS Pathog.*, vol. 5, no. 12, Dec. 2009.

- [30] M. H. Shaw, T. Reimer, Y.-G. Kim, and G. Nuñez, "NOD-like receptors (NLRs): bona fide intracellular microbial sensors," *Current Opinion in Immunology*, vol. 20, no. 4, pp. 377–382, Aug. 2008.
- [31] Y. Ben-Neriah and M. Karin, "Inflammation meets cancer, with NF- κ B as the matchmaker," *Nat Immunol*, vol. 12, no. 8, pp. 715–723, Aug. 2011.
- [32] A. Symons, S. Beinke, and S. C. Ley, "MAP kinase kinase kinases and innate immunity," *Trends in Immunology*, vol. 27, no. 1, pp. 40–48, Jan. 2006.
- [33] N. Mukaida, "Interleukin-8: an expanding universe beyond neutrophil chemotaxis and activation," *Int. J. Hematol.*, vol. 72, no. 4, pp. 391–398, Dec. 2000.
- [34] D. Chakravorty and M. Hensel, "Inducible nitric oxide synthase and control of intracellular bacterial pathogens," *Microbes Infect.*, vol. 5, no. 7, pp. 621–627, Jun. 2003.
- [35] A. L. Groeger, C. Cipollina, M. P. Cole, S. R. Woodcock, G. Bonacci, T. K. Rudolph, V. Rudolph, B. A. Freeman, and F. J. Schopfer, "Cyclooxygenase-2 generates anti-inflammatory mediators from omega-3 fatty acids," *Nat Chem Biol*, vol. 6, no. 6, pp. 433–441, Jun. 2010.
- [36] J.-M. Bruey, N. Bruey-Sedano, F. Luciano, D. Zhai, R. Balpai, C. Xu, C. L. Kress, B. Bailly-Maitre, X. Li, A. Osterman, S. Matsuzawa, A. V. Terskikh, B. Faustin, and J. C. Reed, "Bcl-2 and Bcl-XL Regulate Proinflammatory Caspase-1 Activation by Interaction with NALP1," *Cell*, vol. 129, no. 1, pp. 45–56, Apr. 2007.
- [37] A. Y. Wen, K. M. Sakamoto, and L. S. Miller, "The role of the transcription factor CREB in immune function," *J. Immunol.*, vol. 185, no. 11, pp. 6413–6419, Dec. 2010.
- [38] N. H. Philip and I. E. Brodsky, "Cell death programs in *Yersinia* immunity and pathogenesis," *Yersinia*, vol. 2, p. 149, 2012.
- [39] H. Kono and K. L. Rock, "How dying cells alert the immune system to danger," *Nat Rev Immunol*, vol. 8, no. 4, pp. 279–289, Apr. 2008.
- [40] F. Martinon, A. Mayor, and J. Tschopp, "The inflammasomes: guardians of the body," *Annu. Rev. Immunol.*, vol. 27, pp. 229–265, 2009.
- [41] P. Matzinger, "The danger model: a renewed sense of self," *Science*, vol. 296, no. 5566, pp. 301–305, Apr. 2002.
- [42] J. D. G. Jones and J. L. Dangl, "The plant immune system," *Nature*, vol. 444, no. 7117, pp. 323–329, Nov. 2006.
- [43] F. R. Greten, M. C. Arkan, J. Bollrath, L.-C. Hsu, J. Goode, C. Miething, S. I. Göktuna, M. Neuenhahn, J. Fierer, S. Paxian, N. Van Rooijen, Y. Xu, T. O. Cain, B. B. Jaffee, D. H. Busch, J. Duyster, R. M. Schmid, L. Eckmann, and M. Karin, "NF- κ B is a negative regulator of IL-1 β secretion as revealed by genetic and pharmacological inhibition of IKK β ," *Cell*, vol. 130, no. 5, pp. 918–931, Sep. 2007.
- [44] J. Banchereau and R. M. Steinman, "Dendritic cells and the control of immunity," *Nature*, vol. 392, no. 6673, pp. 245–252, Mar. 1998.
- [45] L. V. Hooper, D. R. Littman, and A. J. Macpherson, "Interactions Between the Microbiota and the Immune System," *Science*, vol. 336, no. 6086, pp. 1268–1273, Aug. 2012.
- [46] A. Iwasaki and R. Medzhitov, "Regulation of Adaptive Immunity by the Innate Immune System," *Science*, vol. 327, no. 5963, pp. 291–295, Jan. 2010.

- [47] K. M. Mikula, R. Kolodziejczyk, and A. Goldman, "Yersinia infection tools-characterization of structure and function of adhesins," *Front Cell Infect Microbiol*, vol. 2, p. 169, 2012.
- [48] R. Steinmann and P. Dersch, "Thermosensing to adjust bacterial virulence in a fluctuating environment," *Future Microbiol*, vol. 8, pp. 85–105, Jan. 2013.
- [49] K. Herbst, M. Bujara, A. K. Heroven, W. Opitz, M. Weichert, A. Zimmermann, and P. Dersch, "Intrinsic Thermal Sensing Controls Proteolysis of Yersinia Virulence Regulator RovA," *PLoS Pathog*, vol. 5, no. 5, p. e1000435, May 2009.
- [50] N. Quade, M. Dieckmann, M. Haffke, A. K. Heroven, P. Dersch, and D. W. Heinz, "Structure of the effector-binding domain of the LysR-type transcription factor RovM from Yersinia pseudotuberculosis," *Acta Crystallogr. D Biol. Crystallogr*, vol. 67, no. Pt 2, pp. 81–90, Feb. 2011.
- [51] R. R. Isberg and J. M. Leong, "Multiple β 1 chain integrins are receptors for invasin, a protein that promotes bacterial penetration into mammalian cells," *Cell*, vol. 60, no. 5, pp. 861–871, Mar. 1990.
- [52] K.-W. Wong and R. R. Isberg, "Emerging views on integrin signaling via Rac1 during invasin-promoted bacterial uptake," *Current Opinion in Microbiology*, vol. 8, no. 1, pp. 4–9, Feb. 2005.
- [53] A. Marra and R. R. Isberg, "Invasin-dependent and invasin-independent pathways for translocation of Yersinia pseudotuberculosis across the Peyer's patch intestinal epithelium," *Infect. Immun.*, vol. 65, no. 8, pp. 3412–3421, Jan. 1997.
- [54] M. Skurnik and P. Toivanen, "LcrF is the temperature-regulated activator of the yadA gene of Yersinia enterocolitica and Yersinia pseudotuberculosis," *J. Bacteriol.*, vol. 174, no. 6, pp. 2047–2051, Mar. 1992.
- [55] H. Schulze-Koops, H. Burkhardt, J. Heesemann, K. von der Mark, and F. Emmrich, "Plasmid-encoded outer membrane protein YadA mediates specific binding of enteropathogenic yersiniae to various types of collagen," *Infect. Immun.*, vol. 60, no. 6, pp. 2153–2159, Jun. 1992.
- [56] H. Nummelin, M. C. Merckel, J. C. Leo, H. Lankinen, M. Skurnik, and A. Goldman, "The Yersinia adhesin YadA collagen-binding domain structure is a novel left-handed parallel β -roll," *The EMBO Journal*, vol. 23, no. 4, pp. 701–711, Feb. 2004.
- [57] R. Terti, M. Skurnik, T. Vartio, and P. Kuusela, "Adhesion protein YadA of Yersinia species mediates binding of bacteria to fibronectin," *Infect. Immun.*, vol. 60, no. 7, pp. 3021–3024, Jul. 1992.
- [58] K. Ruckdeschel, A. Roggenkamp, S. Schubert, and J. Heesemann, "Differential contribution of Yersinia enterocolitica virulence factors to evasion of microbicidal action of neutrophils," *Infect. Immun.*, vol. 64, no. 3, pp. 724–733, Mar. 1996.
- [59] N. Grosdent, I. Maridonneau-Parini, M.-P. Sory, and G. R. Cornelis, "Role of Yops and Adhesins in Resistance of Yersinia enterocolitica to Phagocytosis," *Infect. Immun.*, vol. 70, no. 8, pp. 4165–4176, Jan. 2002.
- [60] D. L. Zink, J. C. Feeley, J. G. Wells, C. Vanderzant, J. C. Vickery, W. D. Roof, and G. A. O'Donovan, "Plasmid-mediated tissue invasiveness in Yersinia enterocolitica," *Nature*, vol. 283, no. 5743, pp. 224–226, Jan. 1980.

- [61] G. R. Cornelis, A. Boland, A. P. Boyd, C. Geuijen, M. Iriarte, C. Neyt, M.-P. Sory, and I. Stainier, "The Virulence Plasmid of *Yersinia*, an Antihost Genome," *Microbiol. Mol. Biol. Rev.*, vol. 62, no. 4, pp. 1315–1352, Jan. 1998.
- [62] G. P. Salmond and P. J. Reeves, "Membrane traffic wardens and protein secretion in gram-negative bacteria," *Trends Biochem. Sci.*, vol. 18, no. 1, pp. 7–12, Jan. 1993.
- [63] G. R. Cornelis, "The *Yersinia* Ysc-Yop 'Type III' weaponry," *Nat Rev Mol Cell Biol*, vol. 3, no. 10, pp. 742–754, 2002.
- [64] G. R. Cornelis, "The type III secretion injectisome," *Nature Reviews Microbiology*, vol. 4, no. 11, pp. 811–825, Jan. 2006.
- [65] H. Matsumoto and G. M. Young, "Translocated effectors of *Yersinia*," *Current Opinion in Microbiology*, vol. 12, no. 1, pp. 94–100, Feb. 2009.
- [66] B. M. Young and G. M. Young, "Evidence for targeting of Yop effectors by the chromosomally encoded Ysa type III secretion system of *Yersinia enterocolitica*," *J. Bacteriol.*, vol. 184, no. 20, pp. 5563–5571, Oct. 2002.
- [67] K. Böhme, R. Steinmann, J. Kortmann, S. Seekircher, A. K. Heroven, E. Berger, F. Pisano, T. Thiermann, H. Wolf-Watz, F. Narberhaus, and P. Dersch, "Concerted Actions of a Thermo-labile Regulator and a Unique Intergenic RNA Thermosensor Control *Yersinia* Virulence," *PLoS Pathog*, vol. 8, no. 2, p. e1002518, Feb. 2012.
- [68] C. K. Yip and N. C. J. Strynadka, "New structural insights into the bacterial type III secretion system," *Trends in Biochemical Sciences*, vol. 31, no. 4, pp. 223–230, Apr. 2006.
- [69] G. M. Preston, "Metropolitan Microbes: Type III Secretion in Multihost Symbionts," *Cell Host & Microbe*, vol. 2, no. 5, pp. 291–294, Nov. 2007.
- [70] E. Hoiczyk and G. Blobel, "Polymerization of a single protein of the pathogen *Yersinia enterocolitica* into needles punctures eukaryotic cells," *PNAS*, vol. 98, no. 8, pp. 4669–4674, Oct. 2001.
- [71] T. C. Marlovits, T. Kubori, A. Sukhan, D. R. Thomas, J. E. Galán, and V. M. Unger, "Structural Insights into the Assembly of the Type III Secretion Needle Complex," *Science*, vol. 306, no. 5698, pp. 1040–1042, Nov. 2004.
- [72] T. C. Marlovits and C. E. Stebbins, "Type III secretion systems shape up as they ship out," *Current Opinion in Microbiology*, vol. 13, no. 1, pp. 47–52, Feb. 2010.
- [73] O. Schraidt and T. C. Marlovits, "Three-Dimensional Model of *Salmonella*'s Needle Complex at Subnanometer Resolution," *Science*, vol. 331, no. 6021, pp. 1192–1195, Apr. 2011.
- [74] A. Kosarewicz, L. Königsmaier, and T. C. Marlovits, "The blueprint of the type-3 injectisome," *Phil. Trans. R. Soc. B*, vol. 367, no. 1592, pp. 1140–1154, Apr. 2012.
- [75] S.-I. Aizawa, "Bacterial flagella and type III secretion systems," *FEMS Microbiology Letters*, vol. 202, no. 2, pp. 157–164, 2001.
- [76] A. Block, G. Li, Z. Q. Fu, and J. R. Alfano, "Phytopathogen type III effector weaponry and their plant targets," *Curr. Opin. Plant Biol.*, vol. 11, no. 4, pp. 396–403, Aug. 2008.
- [77] S. S. Abby and E. P. C. Rocha, "The Non-Flagellar Type III Secretion System Evolved from the Bacterial Flagellum and Diversified into Host-Cell Adapted Systems," *PLoS Genet*, vol. 8, no. 9, p. e1002983, Sep. 2012.

- [78] P. Broz, C. A. Mueller, S. A. Müller, A. Philippsen, I. Sorg, A. Engel, and G. R. Cornelis, "Function and molecular architecture of the Yersinia injectisome tip complex," *Molecular Microbiology*, vol. 65, no. 5, pp. 1311–1320, 2007.
- [79] L. Journet, C. Agrain, P. Broz, and G. R. Cornelis, "The Needle Length of Bacterial Injectisomes Is Determined by a Molecular Ruler," *Science*, vol. 302, no. 5651, pp. 1757–1760, May 2003.
- [80] F. S. Cordes, K. Komoriya, E. Larquet, S. Yang, E. H. Egelman, A. Blocker, and S. M. Lea, "Helical structure of the needle of the type III secretion system of *Shigella flexneri*," *J. Biol. Chem.*, vol. 278, no. 19, pp. 17103–17107, May 2003.
- [81] A. Loquet, N. G. Sgourakis, R. Gupta, K. Giller, D. Riedel, C. Goosmann, C. Griesinger, M. Kolbe, D. Baker, S. Becker, and A. Lange, "Atomic model of the type III secretion system needle," *Nature*, vol. 486, no. 7402, pp. 276–279, Jun. 2012.
- [82] C. A. Mueller, P. Broz, S. A. Müller, P. Ringler, F. Erne-Brand, I. Sorg, M. Kuhn, A. Engel, and G. R. Cornelis, "The V-Antigen of Yersinia Forms a Distinct Structure at the Tip of Injectisome Needles," *Science*, vol. 310, no. 5748, pp. 674–676, Oct. 2005.
- [83] M. Lunelli, R. Hurwitz, J. Lambers, and M. Kolbe, "Crystal structure of PrgI-SipD: insight into a secretion competent state of the type three secretion system needle tip and its interaction with host ligands," *PLoS Pathog.*, vol. 7, no. 8, p. e1002163, Aug. 2011.
- [84] P. Dean, "Functional domains and motifs of bacterial type III effector proteins and their roles in infection," *FEMS Microbiol Rev*, Apr. 2011.
- [85] C. E. Stebbins and J. E. Galán, "Maintenance of an unfolded polypeptide by a cognate chaperone in bacterial type III secretion," *Nature*, vol. 414, no. 6859, pp. 77–81, Nov. 2001.
- [86] M. S. Francis, "Type III secretion chaperones: a molecular toolkit for all occasions," 2010.
- [87] M. Lara-Tejero, J. Kato, S. Wagner, X. Liu, and J. E. Galán, "A Sorting Platform Determines the Order of Protein Secretion in Bacterial Type III Systems," *Science*, vol. 331, no. 6021, pp. 1188–1191, Apr. 2011.
- [88] T. Edgren, Å. Forsberg, R. Rosqvist, and H. Wolf-Watz, "Type III Secretion in Yersinia: Injectisome or Not?," *PLoS Pathog.*, vol. 8, no. 5, p. e1002669, May 2012.
- [89] C. Montagner, C. Arquint, and G. R. Cornelis, "Translocators YopB and YopD from Yersinia enterocolitica Form a Multimeric Integral Membrane Complex in Eukaryotic Cell Membranes," *J. Bacteriol.*, vol. 193, no. 24, pp. 6923–6928, Dec. 2011.
- [90] L. J. Mota, "Type III secretion gets an LcrV tip," *Trends in Microbiology*, vol. 14, no. 5, pp. 197–200, May 2006.
- [91] A. J. Olive, R. Kenjale, M. Espina, D. S. Moore, W. L. Picking, and W. D. Picking, "Bile Salts Stimulate Recruitment of IpaB to the *Shigella flexneri* Surface, Where It Colocalizes with IpaD at the Tip of the Type III Secretion Needle," *Infect. Immun.*, vol. 75, no. 5, pp. 2626–2629, Jan. 2007.
- [92] K. F. Stensrud, P. R. Adam, C. D. L. Mar, A. J. Olive, G. H. Lushington, R. Sudharsan, N. L. Shelton, R. S. Givens, W. L. Picking, and W. D. Picking, "Deoxycholate Interacts with IpaD of *Shigella flexneri* in Inducing the

- Recruitment of IpaB to the Type III Secretion Apparatus Needle Tip," *J. Biol. Chem.*, vol. 283, no. 27, pp. 18646–18654, Apr. 2008.
- [93] T. R. D. Costa, P. J. Edqvist, J. E. Bröms, M. K. Åhlund, Å. Forsberg, and M. S. Francis, "YopD Self-assembly and Binding to LcrV Facilitate Type III Secretion Activity by *Yersinia pseudotuberculosis*," *J. Biol. Chem.*, vol. 285, no. 33, pp. 25269–25284, Aug. 2010.
- [94] K. G. Ligtenberg, N. C. Miller, A. Mitchell, G. V. Plano, and O. Schneewind, "LcrV Mutants That Abolish *Yersinia* Type III Injectisome Function," *J. Bacteriol.*, vol. 195, no. 4, pp. 777–787, Feb. 2013.
- [95] J. Heesemann, B. Algermissen, and R. Laufs, "Genetically manipulated virulence of *Yersinia enterocolitica*," *Infect. Immun.*, vol. 46, no. 1, pp. 105–110, Jan. 1984.
- [96] D. A. Portnoy, S. L. Moseley, and S. Falkow, "Characterization of plasmids and plasmid-associated determinants of *Yersinia enterocolitica* pathogenesis," *Infect. Immun.*, vol. 31, no. 2, pp. 775–782, Jan. 1981.
- [97] M. I. Ivanov, B. L. Noel, R. Rampersaud, P. Mena, J. L. Benach, and J. B. Bliska, "Vaccination of Mice with a Yop Translocon Complex Elicits Antibodies That Are Protective against Infection with F1- *Yersinia pestis*," *Infect. Immun.*, vol. 76, no. 11, pp. 5181–5190, Jan. 2008.
- [98] K. Akopyan, T. Edgren, H. Wang-Edgren, R. Rosqvist, A. Fahlgren, H. Wolf-Watz, and M. Fallman, "Translocation of surface-localized effectors in type III secretion," *PNAS*, vol. 108, no. 4, pp. 1639–1644, Jan. 2011.
- [99] M. Aepfelbacher, C. Trasak, and K. Ruckdeschel, "Effector functions of pathogenic *Yersinia* species," *Thromb. Haemost.*, vol. 98, no. 3, pp. 521–529, Sep. 2007.
- [100] J. E. Trosky, A. D. B. Liverman, and K. Orth, "Yersinia outer proteins: Yops," *Cell. Microbiol.*, vol. 10, no. 3, pp. 557–565, Mar. 2008.
- [101] F. Shao, "Biochemical functions of *Yersinia* type III effectors," *Current Opinion in Microbiology*, vol. 11, no. 1, pp. 21–29, Feb. 2008.
- [102] G. I. Viboud and J. B. Bliska, "Yersinia outer proteins: role in modulation of host cell signaling responses and pathogenesis," *Annu. Rev. Microbiol.*, vol. 59, pp. 69–89, 2005.
- [103] D. S. Black and J. B. Bliska, "Identification of p130Cas as a substrate of *Yersinia* YopH (Yop51), a bacterial protein tyrosine phosphatase that translocates into mammalian cells and targets focal adhesions," *The EMBO Journal*, vol. 16, no. 10, pp. 2730–2744, May 1997.
- [104] N. Hamid, A. Gustavsson, K. Andersson, K. McGee, C. Persson, C. E. Rudd, and M. Fällman, "YopH dephosphorylates Cas and Fyn-binding protein in macrophages," *Microb. Pathog.*, vol. 27, no. 4, pp. 231–242, Oct. 1999.
- [105] M. Fällman and A. Gustavsson, "Cellular Mechanisms of Bacterial Internalization Counteracted by *Yersinia*," in *International Review of Cytology*, vol. Volume 246, Kwang W. Jeon, Ed. Academic Press, 2005, pp. 135–188.
- [106] M. Aepfelbacher, B. Roppenser, M. Hentschke, and K. Ruckdeschel, "Activity modulation of the bacterial Rho GAP YopE: An inspiration for the investigation of mammalian Rho GAPs," *European Journal of Cell Biology*, vol. 90, no. 11, pp. 951–954, Nov. 2011.
- [107] K. Ruckdeschel, G. Pfaffinger, K. Trülzsch, G. Zenner, K. Richter, J. Heesemann, and M. Aepfelbacher, "The proteasome pathway destabilizes

- Yersinia outer protein E and represses its antihost cell activities," *J. Immunol.*, vol. 176, no. 10, pp. 6093–6102, May 2006.
- [108] F. Shao, P. O. Vacratsis, Z. Bao, K. E. Bowers, C. A. Fierke, and J. E. Dixon, "Biochemical characterization of the Yersinia YopT protease: Cleavage site and recognition elements in Rho GTPases," *PNAS*, vol. 100, no. 3, pp. 904–909, Apr. 2003.
- [109] A. G. Evdokimov, D. E. Anderson, K. M. Routzahn, and D. S. Waugh, "Unusual molecular architecture of the Yersinia pestis cytotoxin YopM: a leucine-rich repeat protein with the shortest repeating unit," *J. Mol. Biol.*, vol. 312, no. 4, pp. 807–821, Sep. 2001.
- [110] C. McDonald, P. O. Vacratsis, J. B. Bliska, and J. E. Dixon, "The yersinia virulence factor YopM forms a novel protein complex with two cellular kinases," *J. Biol. Chem.*, vol. 278, no. 20, pp. 18514–18523, May 2003.
- [111] M. Hentschke, L. Berneking, C. Belmar Campos, F. Buck, K. Ruckdeschel, and M. Aepfelbacher, "Yersinia virulence factor YopM induces sustained RSK activation by interfering with dephosphorylation," *PLoS ONE*, vol. 5, no. 10, 2010.
- [112] C. N. Larock and B. T. Cookson, "The Yersinia Virulence Effector YopM Binds Caspase-1 to Arrest Inflammasome Assembly and Processing," *Cell Host Microbe*, vol. 12, no. 6, pp. 799–805, Dec. 2012.
- [113] E. E. Galyov, S. Håkansson, A. Forsberg, and H. Wolf-Watz, "A secreted protein kinase of Yersinia pseudotuberculosis is an indispensable virulence determinant," *Nature*, vol. 361, no. 6414, pp. 730–732, Feb. 1993.
- [114] J.-M. Dukuzumuremyi, R. Rosqvist, B. Hallberg, B. Åkerström, H. Wolf-Watz, and K. Schesser, "The Yersinia Protein Kinase A Is a Host Factor Inducible RhoA/Rac-binding Virulence Factor," *J. Biol. Chem.*, vol. 275, no. 45, pp. 35281–35290, Oct. 2000.
- [115] S. J. Juris, A. E. Rudolph, D. Huddler, K. Orth, and J. E. Dixon, "A distinctive role for the Yersinia protein kinase: Actin binding, kinase activation, and cytoskeleton disruption," *PNAS*, vol. 97, no. 17, pp. 9431–9436, Aug. 2000.
- [116] S. E. Thorslund, T. Edgren, J. Pettersson, R. Nordfelth, M. E. Sellin, E. Ivanova, M. S. Francis, E. L. Isaksson, H. Wolf-Watz, and M. Fällman, "The RACK1 signaling scaffold protein selectively interacts with Yersinia pseudotuberculosis virulence function," *PLoS ONE*, vol. 6, no. 2, p. e16784, 2011.
- [117] K. N. Peters, M. O. Dhariwala, J. M. Hughes Hanks, C. R. Brown, and D. M. Anderson, "Early Apoptosis of Macrophages Modulated by Injection of Yersinia pestis YopK Promotes Progression of Primary Pneumonic Plague," *PLoS Pathog.*, vol. 9, no. 4, p. e1003324, Apr. 2013.
- [118] A. K. Sample, J. M. Fowler, and R. R. Brubaker, "Modulation of the low-calcium response in Yersinia pestis via plasmid-plasmid interaction," *Microb. Pathog.*, vol. 2, no. 6, pp. 443–453, Jun. 1987.
- [119] E. E. Galyov, S. Håkansson, and H. Wolf-Watz, "Characterization of the operon encoding the YpkA Ser/Thr protein kinase and the YopJ protein of Yersinia pseudotuberculosis," *J. Bacteriol.*, vol. 176, no. 15, pp. 4543–4548, Jan. 1994.
- [120] K. Ruckdeschel, A. Deuretzbacher, and R. Haase, "Crosstalk of signalling processes of innate immunity with Yersinia Yop effector functions," *Immunobiology*, vol. 213, no. 3–4, pp. 261–269, May 2008.

- [121] S. E. Erfurth, S. Gröbner, U. Kramer, D. S. J. Gunst, I. Soldanova, M. Schaller, I. B. Autenrieth, and S. Borgmann, "Yersinia enterocolitica induces apoptosis and inhibits surface molecule expression and cytokine production in murine dendritic cells," *Infect. Immun.*, vol. 72, no. 12, pp. 7045–7054, Dec. 2004.
- [122] U. Meinzer, F. Barreau, S. Esmiol-Welterlin, C. Jung, C. Villard, T. Léger, S. Ben-Mkaddem, D. Berrebi, M. Dussallant, Z. Alnabhani, M. Roy, S. Bonacorsi, H. Wolf-Watz, J. Perroy, V. Ollendorff, and J.-P. Hugot, "Yersinia pseudotuberculosis Effector YopJ Subverts the Nod2/RICK/TAK1 Pathway and Activates Caspase-1 to Induce Intestinal Barrier Dysfunction," *Cell Host & Microbe*, vol. 11, no. 4, pp. 337–351, Apr. 2012.
- [123] N. Paquette, J. Conlon, C. Sweet, F. Rus, L. Wilson, A. Pereira, C. V. Rosadini, N. Goutagny, A. N. R. Weber, W. S. Lane, S. A. Shaffer, S. Maniatis, K. A. Fitzgerald, L. Stuart, and N. Silverman, "Serine/threonine acetylation of TGF β -activated kinase (TAK1) by Yersinia pestis YopJ inhibits innate immune signaling," *Proc. Natl. Acad. Sci. U.S.A.*, vol. 109, no. 31, pp. 12710–12715, Jul. 2012.
- [124] R. Nakajima and R. R. Brubaker, "Association between virulence of Yersinia pestis and suppression of gamma interferon and tumor necrosis factor alpha," *Infect. Immun.*, vol. 61, no. 1, pp. 23–31, Jan. 1993.
- [125] H. U. Beuscher, F. Rödel, A. Forsberg, and M. Röllinghoff, "Bacterial evasion of host immune defense: Yersinia enterocolitica encodes a suppressor for tumor necrosis factor alpha expression," *Infect. Immun.*, vol. 63, no. 4, pp. 1270–1277, Apr. 1995.
- [126] L. E. Palmer, S. Hobbie, J. E. Galán, and J. B. Bliska, "YopJ of Yersinia pseudotuberculosis is required for the inhibition of macrophage TNF- α production and downregulation of the MAP kinases p38 and JNK," *Molecular Microbiology*, vol. 27, no. 5, pp. 953–965, 1998.
- [127] A. Boland and G. R. Cornelis, "Role of YopP in Suppression of Tumor Necrosis Factor Alpha Release by Macrophages during Yersinia Infection," *Infect. Immun.*, vol. 66, no. 5, pp. 1878–1884, Jan. 1998.
- [128] K. Ruckdeschel, S. Harb, A. Roggenkamp, M. Hornef, R. Zumbihl, S. Köhler, J. Heesemann, and B. Rouot, "Yersinia enterocolitica Impairs Activation of Transcription Factor NF- κ B: Involvement in the Induction of Programmed Cell Death and in the Suppression of the Macrophage Tumor Necrosis Factor α Production," *J Exp Med*, vol. 187, no. 7, pp. 1069–1079, Jun. 1998.
- [129] K. Schesser, A. Spiik, J. Dukuzumuremyi, M. F. Neurath, S. Pettersson, and H. Wolf-Watz, "The yopJ locus is required for Yersinia-mediated inhibition of NF- κ B activation and cytokine expression: YopJ contains a eukaryotic SH2-like domain that is essential for its repressive activity," *Molecular Microbiology*, vol. 28, no. 6, pp. 1067–1079, Jun. 1998.
- [130] R. Bose, J. Thinwa, P. Chaparro, Y. Zhong, S. Bose, G. Zhong, and P. H. Dube, "Mitogen-activated protein kinase-dependent interleukin-1 α intracrine signaling is modulated by YopP during Yersinia enterocolitica infection," *Infect. Immun.*, vol. 80, no. 1, pp. 289–297, Jan. 2012.
- [131] Y. Zheng, S. Lilo, I. E. Brodsky, Y. Zhang, R. Medzhitov, K. B. Marcu, and J. B. Bliska, "A Yersinia Effector with Enhanced Inhibitory Activity on the NF- κ B Pathway Activates the NLRP3/ASC/Caspase-1 Inflammasome in Macrophages," *PLoS Pathog*, vol. 7, no. 4, p. e1002026, Apr. 2011.

- [132] R. Hoffmann, K. Van Erp, K. Trülsch, and J. Heesemann, "Transcriptional responses of murine macrophages to infection with *Yersinia enterocolitica*," *Cellular Microbiology*, vol. 6, no. 4, pp. 377–390, 2004.
- [133] D. M. Rothwarf and M. Karin, "The NF- κ B Activation Pathway: A Paradigm in Information Transfer from Membrane to Nucleus," *Sci. STKE*, vol. 1999, no. 5, p. re1, Oct. 1999.
- [134] K. Ruckdeschel, J. Machold, A. Roggenkamp, S. Schubert, J. Pierre, R. Zumbihl, J.-P. Liautard, J. Heesemann, and B. Rouot, "Yersinia enterocolitica Promotes Deactivation of Macrophage Mitogen-activated Protein Kinases Extracellular Signal-regulated Kinase-1/2, p38, and c-Jun NH2-terminal Kinase CORRELATION WITH ITS INHIBITORY EFFECT ON TUMOR NECROSIS FACTOR- α PRODUCTION," *J. Biol. Chem.*, vol. 272, no. 25, pp. 15920–15927, Jun. 1997.
- [135] L. K. Meijer, K. Schesser, H. Wolf-Watz, P. Sassone-Corsi, and S. Pettersson, "The bacterial protein YopJ abrogates multiple signal transduction pathways that converge on the transcription factor CREB," *Cellular Microbiology*, vol. 2, no. 3, pp. 231–238, 2000.
- [136] R. Haase, K. Richter, G. Pfaffinger, G. Courtois, and K. Ruckdeschel, "Yersinia Outer Protein P Suppresses TGF- β -Activated Kinase-1 Activity to Impair Innate Immune Signaling in *Yersinia enterocolitica*-Infected Cells," *J Immunol*, vol. 175, no. 12, pp. 8209–8217, Dec. 2005.
- [137] A. Thiefes, A. Wolf, A. Doerrie, G. A. Grassl, K. Matsumoto, I. Autenrieth, E. Bohn, H. Sakurai, R. Niedenthal, K. Resch, and M. Kracht, "The *Yersinia enterocolitica* effector YopP inhibits host cell signalling by inactivating the protein kinase TAK1 in the IL-1 signalling pathway," *EMBO Rep.*, vol. 7, no. 8, pp. 838–844, Aug. 2006.
- [138] C. R. Sweet, J. Conlon, D. T. Golenbock, J. Goguen, and N. Silverman, "YopJ targets TRAF proteins to inhibit TLR-mediated NF- κ B, MAPK and IRF3 signal transduction," *Cell. Microbiol.*, vol. 9, no. 11, pp. 2700–2715, Nov. 2007.
- [139] L. E. Palmer, A. R. Pancetti, S. Greenberg, and J. B. Bliska, "YopJ of *Yersinia* spp. Is Sufficient To Cause Downregulation of Multiple Mitogen-Activated Protein Kinases in Eukaryotic Cells," *Infect. Immun.*, vol. 67, no. 2, pp. 708–716, Jan. 1999.
- [140] K. Orth, L. E. Palmer, Z. Q. Bao, S. Stewart, A. E. Rudolph, J. B. Bliska, and J. E. Dixon, "Inhibition of the Mitogen-Activated Protein Kinase Kinase Superfamily by a *Yersinia* Effector," *Science*, vol. 285, no. 5435, pp. 1920–1923, Sep. 1999.
- [141] K. Orth, Z. Xu, M. B. Mudgett, Z. Q. Bao, L. E. Palmer, J. B. Bliska, W. F. Mangel, B. Staskawicz, and J. E. Dixon, "Disruption of signaling by *Yersinia* effector YopJ, a ubiquitin-like protein protease," *Science*, vol. 290, no. 5496, pp. 1594–1597, Nov. 2000.
- [142] H. Zhou, D. M. Monack, N. Kayagaki, I. Wertz, J. Yin, B. Wolf, and V. M. Dixit, "Yersinia virulence factor YopJ acts as a deubiquitinase to inhibit NF- κ B activation," *J. Exp. Med.*, vol. 202, no. 10, pp. 1327–1332, Nov. 2005.
- [143] V. G. Bhoj and Z. J. Chen, "Ubiquitylation in innate and adaptive immunity," *Nature*, vol. 458, no. 7237, pp. 430–437, Mar. 2009.

- [144] S. Mukherjee, G. Keitany, Y. Li, Y. Wang, H. L. Ball, E. J. Goldsmith, and K. Orth, "Yersinia YopJ acetylates and inhibits kinase activation by blocking phosphorylation," *Science*, vol. 312, no. 5777, pp. 1211–1214, May 2006.
- [145] R. Mittal, S.-Y. Peak-Chew, and H. T. McMahon, "Acetylation of MEK2 and I kappa B kinase (IKK) activation loop residues by YopJ inhibits signaling," *Proc. Natl. Acad. Sci. U.S.A.*, vol. 103, no. 49, pp. 18574–18579, Dec. 2006.
- [146] S. Mukherjee and K. Orth, "In vitro signaling by MAPK and NFkappaB pathways inhibited by Yersinia YopJ," *Meth. Enzymol.*, vol. 438, pp. 343–353, 2008.
- [147] S. Mukherjee, Y.-H. Hao, and K. Orth, "A newly discovered post-translational modification--the acetylation of serine and threonine residues," *Trends Biochem. Sci.*, vol. 32, no. 5, pp. 210–216, May 2007.
- [148] Y.-H. Hao, Y. Wang, D. Burdette, S. Mukherjee, G. Keitany, E. Goldsmith, and K. Orth, "Structural requirements for Yersinia YopJ inhibition of MAP kinase pathways," *PLoS ONE*, vol. 3, no. 1, p. e1375, 2008.
- [149] R. Mittal, S. Y. Peak-Chew, R. S. Sade, Y. Vallis, and H. T. McMahon, "The Acetyltransferase Activity of the Bacterial Toxin YopJ of Yersinia Is Activated by Eukaryotic Host Cell Inositol Hexakisphosphate," *Journal of Biological Chemistry*, vol. 285, no. 26, pp. 19927–19934, Jun. 2010.
- [150] K. Ruckdeschel, A. Roggenkamp, V. Lafont, P. Mangeat, J. Heesemann, and B. Rouot, "Interaction of Yersinia enterocolitica with macrophages leads to macrophage cell death through apoptosis," *Infect. Immun.*, vol. 65, no. 11, pp. 4813–4821, Jan. 1997.
- [151] D. M. Monack, J. Meccas, N. Ghori, and S. Falkow, "Yersinia signals macrophages to undergo apoptosis and YopJ is necessary for this cell death," *Proceedings of the National Academy of Sciences of the United States of America*, vol. 94, no. 19, pp. 10385–10390, 1997.
- [152] S. D. Mills, A. Boland, M.-P. Sory, P. van der Smissen, C. Kerbouch, B. B. Finlay, and G. R. Cornelis, "Yersinia enterocolitica induces apoptosis in macrophages by a process requiring functional type III secretion and translocation mechanisms and involving YopP, presumably acting as an effector protein," *PNAS*, vol. 94, no. 23, pp. 12638–12643, Nov. 1997.
- [153] K. Ruckdeschel, O. Mannel, K. Richter, C. A. Jacobi, K. Trülsch, B. Rouot, and J. Heesemann, "Yersinia Outer Protein P of Yersinia enterocolitica Simultaneously Blocks the Nuclear Factor- κ B Pathway and Exploits Lipopolysaccharide Signaling to Trigger Apoptosis in Macrophages," *J Immunol*, vol. 166, no. 3, pp. 1823–1831, Jan. 2001.
- [154] K. Ruckdeschel and K. Richter, "Lipopolysaccharide Desensitization of Macrophages Provides Protection against Yersinia enterocolitica-Induced Apoptosis," *Infect. Immun.*, vol. 70, no. 9, pp. 5259–5264, Jan. 2002.
- [155] R. Haase, C. J. Kirschning, A. Sing, P. Schrottner, K. Fukase, S. Kusumoto, H. Wagner, J. Heesemann, and K. Ruckdeschel, "A Dominant Role of Toll-Like Receptor 4 in the Signaling of Apoptosis in Bacteria-Faced Macrophages," *J Immunol*, vol. 171, no. 8, pp. 4294–4303, Oct. 2003.
- [156] G. Denecker, W. Declercq, C. A. W. Geuijen, A. Boland, R. Benabdillah, M. van Gurp, M.-P. Sory, P. Vandenabeele, and G. R. Cornelis, "Yersinia enterocolitica YopP-induced Apoptosis of Macrophages Involves the Apoptotic Signaling Cascade Upstream of Bid," *Journal of Biological Chemistry*, vol. 276, no. 23, pp. 19706–19714, Jun. 2001.

- [157] Y. Zhang and J. B. Bliska, "Role of Toll-Like Receptor Signaling in the Apoptotic Response of Macrophages to *Yersinia* Infection," *Infect. Immun.*, vol. 71, no. 3, pp. 1513–1519, Jan. 2003.
- [158] K. Ruckdeschel, G. Pfaffinger, R. Haase, A. Sing, H. Weighardt, G. Häcker, B. Holzmann, and J. Heesemann, "Signaling of apoptosis through TLRs critically involves toll/IL-1 receptor domain-containing adapter inducing IFN-beta, but not MyD88, in bacteria-infected murine macrophages," *J. Immunol.*, vol. 173, no. 5, pp. 3320–3328, Sep. 2004.
- [159] C. Kantari and H. Walczak, "Caspase-8 and Bid: Caught in the act between death receptors and mitochondria," *Biochimica et Biophysica Acta (BBA) - Molecular Cell Research*, vol. 1813, no. 4, pp. 558–563, Apr. 2011.
- [160] S. L. Fink and B. T. Cookson, "Apoptosis, Pyroptosis, and Necrosis: Mechanistic Description of Dead and Dying Eukaryotic Cells," *Infect. Immun.*, vol. 73, no. 4, pp. 1907–1916, Apr. 2005.
- [161] T. Bergsbaken and B. T. Cookson, "Innate immune response during *Yersinia* infection: critical modulation of cell death mechanisms through phagocyte activation," *J. Leukoc. Biol.*, vol. 86, no. 5, pp. 1153–1158, Nov. 2009.
- [162] D. M. Monack, J. Meccas, D. Bouley, and S. Falkow, "Yersinia-induced apoptosis in vivo aids in the establishment of a systemic infection of mice," *J. Exp. Med.*, vol. 188, no. 11, pp. 2127–2137, Dec. 1998.
- [163] T. Bergsbaken and B. T. Cookson, "Macrophage Activation Redirects *Yersinia*-Infected Host Cell Death from Apoptosis to Caspase-1-Dependent Pyroptosis," *PLoS Pathog.*, vol. 3, no. 11, p. e161, Nov. 2007.
- [164] A. Zauberman, S. Cohen, E. Mamroud, Y. Flashner, A. Tidhar, R. Ber, E. Elhanany, A. Shafferman, and B. Velan, "Interaction of *Yersinia pestis* with macrophages: limitations in YopJ-dependent apoptosis," *Infect. Immun.*, vol. 74, no. 6, pp. 3239–3250, Jun. 2006.
- [165] I. E. Brodsky and R. Medzhitov, "Reduced Secretion of YopJ by *Yersinia* Limits In Vivo Cell Death but Enhances Bacterial Virulence," *PLoS Pathog.*, vol. 4, no. 5, p. e1000067, May 2008.
- [166] S. Lilo, Y. Zheng, and J. B. Bliska, "Caspase-1 activation in macrophages infected with *Yersinia pestis* KIM requires the type III secretion system effector YopJ," *Infect. Immun.*, vol. 76, no. 9, pp. 3911–3923, Sep. 2008.
- [167] I. E. Brodsky, N. W. Palm, S. Sadanand, M. B. Ryndak, F. S. Sutterwala, R. A. Flavell, J. B. Bliska, and R. Medzhitov, "A *Yersinia* effector protein promotes virulence by preventing inflammasome recognition of the type III secretion system," *Cell Host Microbe*, vol. 7, no. 5, pp. 376–387, May 2010.
- [168] A. Zauberman, A. Tidhar, Y. Levy, E. Bar-Haim, G. Halperin, Y. Flashner, S. Cohen, A. Shafferman, and E. Mamroud, "Yersinia pestis Endowed with Increased Cytotoxicity Is Avirulent in a Bubonic Plague Model and Induces Rapid Protection against Pneumonic Plague," *PLoS ONE*, vol. 4, no. 6, p. e5938, Jun. 2009.
- [169] E. Appel and D. Wallach, "Chimeric proteins comprising yersinia yop, their preparation and pharmaceutical compositions containing them," EP1871880 B812-Sep-2012.
- [170] S. Mukherjee and K. Orth, "O-acetyltransferases," US7291476 B106-Nov-2007.

- [171] Y.-W. Zhang, "Inhibition of tumor angiogenesis by combination of thrombospondin-1 and inhibitors of vascular endothelial growth factor," EP1648493 B109-Dec-2009.
- [172] U. Meinzer, S. Esmiol-Welterlin, F. Barreau, D. Berrebi, M. Dussailant, S. Bonacorsi, F. Chareyre, M. Niwa-Kawakita, C. Alberti, G. Sterkers, C. Villard, T. Lesuffleur, M. Peuchmaur, M. Karin, L. Eckmann, M. Giovannini, V. Ollendorff, H. Wolf-Watz, and J.-P. Hugot, "Nod2 mediates susceptibility to *Yersinia pseudotuberculosis* in mice," *PLoS ONE*, vol. 3, no. 7, p. e2769, 2008.
- [173] S. E. Autenrieth, I. Soldanova, R. Rösemann, D. Gunst, N. Zahir, M. Kracht, K. Ruckdeschel, H. Wagner, S. Borgmann, and I. B. Autenrieth, "*Yersinia enterocolitica* YopP inhibits MAP kinase-mediated antigen uptake in dendritic cells," *Cellular Microbiology*, vol. 9, no. 2, pp. 425–437, 2007.
- [174] I. Adkins, M. Köberle, S. Gröbner, S. E. Autenrieth, E. Bohn, S. Borgmann, and I. B. Autenrieth, "*Y. enterocolitica* inhibits antigen degradation in dendritic cells," *Microbes Infect.*, vol. 10, no. 7, pp. 798–806, Jun. 2008.
- [175] A. S. Shaw and E. L. Filbert, "Scaffold proteins and immune-cell signalling," *Nat. Rev. Immunol.*, vol. 9, no. 1, pp. 47–56, Jan. 2009.
- [176] M. Whalen, T. Richter, K. Zakharevich, M. Yoshikawa, D. Al-Azzeh, A. Adefioye, G. Spicer, L. L. Mendoza, C. Q. Morales, V. Klassen, G. Perez-Baron, C. S. Toebe, A. Tzovolous, E. Gerstman, E. Evans, C. Thompson, M. Lopez, and P. C. Ronald, "Identification of a host 14-3-3 Protein that Interacts with *Xanthomonas* effector AvrRxx," *Physiol Mol Plant Pathol*, vol. 72, no. 1–3, pp. 46–55, 2008.
- [177] C. Choudhary, C. Kumar, F. Gnad, M. L. Nielsen, M. Rehman, T. C. Walther, J. V. Olsen, and M. Mann, "Lysine Acetylation Targets Protein Complexes and Co-Regulates Major Cellular Functions," *Science*, vol. 325, no. 5942, pp. 834–840, Aug. 2009.
- [178] N. L. Reynaert, K. Ckless, S. H. Korn, N. Vos, A. S. Guala, E. F. M. Wouters, A. van der Vliet, and Y. M. W. Janssen-Heininger, "Nitric oxide represses inhibitory kappaB kinase through S-nitrosylation," *Proc. Natl. Acad. Sci. U.S.A.*, vol. 101, no. 24, pp. 8945–8950, Jun. 2004.
- [179] H. Rohde, J. Qin, Y. Cui, D. Li, N. J. Loman, M. Hentschke, W. Chen, F. Pu, Y. Peng, J. Li, F. Xi, S. Li, Y. Li, Z. Zhang, X. Yang, M. Zhao, P. Wang, Y. Guan, Z. Cen, X. Zhao, M. Christner, R. Kobbe, S. Loos, J. Oh, L. Yang, A. Danchin, G. F. Gao, Y. Song, Y. Li, H. Yang, J. Wang, J. Xu, M. J. Pallen, J. Wang, M. Aepfelbacher, and R. Yang, "Open-source genomic analysis of Shiga-toxin-producing *E. coli* O104:H4," *N. Engl. J. Med.*, vol. 365, no. 8, pp. 718–724, Aug. 2011.
- [180] A. P. Bhavsar, J. A. Guttman, and B. B. Finlay, "Manipulation of host-cell pathways by bacterial pathogens," *Nature*, vol. 449, no. 7164, pp. 827–834, Oct. 2007.
- [181] "WHO | Global tuberculosis report 2012," WHO. [Online]. Available: http://www.who.int/tb/publications/global_report/en/. [Accessed: 21-Mar-2013].
- [182] P. Sudre, G. ten Dam, and A. Kochi, "Tuberculosis: a global overview of the situation today.," *Bull World Health Organ*, vol. 70, no. 2, pp. 149–159, 1992.

- [183] I. Hershkovitz, H. D. Donoghue, D. E. Minnikin, G. S. Besra, O. Y.-C. Lee, A. M. Gernaey, E. Galili, V. Eshed, C. L. Greenblatt, E. Lemma, G. K. Bar-Gal, and M. Spigelman, "Detection and Molecular Characterization of 9000-Year-Old Mycobacterium tuberculosis from a Neolithic Settlement in the Eastern Mediterranean," *PLoS ONE*, vol. 3, no. 10, p. e3426, Oct. 2008.
- [184] S. Gagneux, "Host-pathogen coevolution in human tuberculosis," *Philos. Trans. R. Soc. Lond., B, Biol. Sci.*, vol. 367, no. 1590, pp. 850–859, Mar. 2012.
- [185] I. Smith, "Mycobacterium tuberculosis pathogenesis and molecular determinants of virulence," *Clin. Microbiol. Rev.*, vol. 16, no. 3, pp. 463–496, Jul. 2003.
- [186] A. WALLGREN, "The time-table of tuberculosis," *Tubercle*, vol. 29, no. 11, pp. 245–251, Nov. 1948.
- [187] R. van Crevel, T. H. M. Ottenhoff, and J. W. M. van der Meer, "Innate immunity to Mycobacterium tuberculosis," *Clin. Microbiol. Rev.*, vol. 15, no. 2, pp. 294–309, Apr. 2002.
- [188] J. Chan, Y. Xing, R. S. Magliozzo, and B. R. Bloom, "Killing of virulent Mycobacterium tuberculosis by reactive nitrogen intermediates produced by activated murine macrophages," *J. Exp. Med.*, vol. 175, no. 4, pp. 1111–1122, Apr. 1992.
- [189] Z. A. Malik, C. R. Thompson, S. Hashimi, B. Porter, S. S. Iyer, and D. J. Kusner, "Cutting edge: Mycobacterium tuberculosis blocks Ca²⁺ signaling and phagosome maturation in human macrophages via specific inhibition of sphingosine kinase," *J. Immunol.*, vol. 170, no. 6, pp. 2811–2815, Mar. 2003.
- [190] A. J. Crowle, R. Dahl, E. Ross, and M. H. May, "Evidence that vesicles containing living, virulent Mycobacterium tuberculosis or Mycobacterium avium in cultured human macrophages are not acidic," *Infect. Immun.*, vol. 59, no. 5, pp. 1823–1831, May 1991.
- [191] G. Gago, L. Diacovich, A. Arabolaza, S. Tsai, and H. Gramajo, "Fatty acid biosynthesis in actinomycetes," *FEMS Microbiology Reviews*, vol. 35, no. 3, pp. 475–497, May 2011.
- [192] V. Jarlier and H. Nikaido, "Mycobacterial cell wall: structure and role in natural resistance to antibiotics," *FEMS Microbiol. Lett.*, vol. 123, no. 1–2, pp. 11–18, Oct. 1994.
- [193] P. Draper, "The outer parts of the mycobacterial envelope as permeability barriers," *Front. Biosci.*, vol. 3, pp. D1253–1261, Dec. 1998.
- [194] R. Simeone, D. Bottai, and R. Brosch, "ESX/type VII secretion systems and their role in host-pathogen interaction," *Curr. Opin. Microbiol.*, vol. 12, no. 1, pp. 4–10, Feb. 2009.
- [195] Y. Akhter, M. T. Ehebauer, S. Mukhopadhyay, and S. E. Hasnain, "The PE/PPE multigene family codes for virulence factors and is a possible source of mycobacterial antigenic variation: perhaps more?," *Biochimie*, vol. 94, no. 1, pp. 110–116, Jan. 2012.
- [196] N. van der Wel, D. Hava, D. Houben, D. Fluitsma, M. van Zon, J. Pierson, M. Brenner, and P. J. Peters, "M. tuberculosis and M. leprae translocate from the phagolysosome to the cytosol in myeloid cells," *Cell*, vol. 129, no. 7, pp. 1287–1298, Jun. 2007.
- [197] D. G. Russell, P.-J. Cardona, M.-J. Kim, S. Allain, and F. Altare, "Foamy macrophages and the progression of the human tuberculosis granuloma," *Nat. Immunol.*, vol. 10, no. 9, pp. 943–948, Sep. 2009.

- [198] L. E. Connolly, P. H. Edelstein, and L. Ramakrishnan, "Why Is Long-Term Therapy Required to Cure Tuberculosis?," *PLoS Med*, vol. 4, no. 3, p. e120, Mar. 2007.
- [199] C. E. Barry 3rd, H. I. Boshoff, V. Dartois, T. Dick, S. Ehrt, J. Flynn, D. Schnappinger, R. J. Wilkinson, and D. Young, "The spectrum of latent tuberculosis: rethinking the biology and intervention strategies," *Nat. Rev. Microbiol.*, vol. 7, no. 12, pp. 845–855, Dec. 2009.
- [200] "Drugs for tuberculosis," *Treat Guidel Med Lett*, vol. 10, no. 116, pp. 29–36; quiz 37–38, Mar. 2012.
- [201] M. Døssing, J. T. R. Wilcke, D. S. Askgaard, and B. Nybo, "Liver injury during antituberculosis treatment: An 11-year study," *Tubercle and Lung Disease*, vol. 77, no. 4, pp. 335–340, Aug. 1996.
- [202] J. S. Kass and W. X. Shandera, "Nervous system effects of antituberculosis therapy," *CNS Drugs*, vol. 24, no. 8, pp. 655–667, Aug. 2010.
- [203] C. Nathan, B. Gold, G. Lin, M. Stegman, L. P. S. de Carvalho, O. Vandal, A. Venugopal, and R. Bryk, "A philosophy of anti-infectives as a guide in the search for new drugs for tuberculosis," *Tuberculosis (Edinb)*, vol. 88 Suppl 1, pp. S25–33, Aug. 2008.
- [204] S. H. E. Kaufmann, "Tuberculosis vaccines: Time to think about the next generation," *Seminars in Immunology*.
- [205] T. Doerks, V. van Noort, P. Minguez, and P. Bork, "Annotation of the M. tuberculosis Hypothetical Orfeome: Adding Functional Information to More than Half of the Uncharacterized Proteins," *PLoS ONE*, vol. 7, no. 4, p. e34302, Apr. 2012.
- [206] M. T. Ehebauer and M. Wilmanns, "The progress made in determining the Mycobacterium tuberculosis structural proteome," *PROTEOMICS*.
- [207] J.-C. Camus, M. J. Pryor, C. Médigue, and S. T. Cole, "Re-annotation of the genome sequence of Mycobacterium tuberculosis H37Rv," *Microbiology*, vol. 148, no. 10, pp. 2967–2973, Jan. 2002.
- [208] G. Lamichhane, S. Tyagi, and W. R. Bishai, "Designer arrays for defined mutant analysis to detect genes essential for survival of Mycobacterium tuberculosis in mouse lungs," *Infect. Immun.*, vol. 73, no. 4, pp. 2533–2540, Apr. 2005.
- [209] A. Deenadayalan, J. C. Sundaramurthi, and A. Raja, "Immunological and proteomic analysis of preparative isoelectric focusing separated culture filtrate antigens of Mycobacterium tuberculosis," *Exp. Mol. Pathol.*, vol. 88, no. 1, pp. 156–162, Feb. 2010.
- [210] H. Målen, F. S. Berven, K. E. Fladmark, and H. G. Wiker, "Comprehensive analysis of exported proteins from Mycobacterium tuberculosis H37Rv," *PROTEOMICS*, vol. 7, no. 10, pp. 1702–1718, 2007.
- [211] Weldingh, Hansen, Jacobsen, and Andersen, "High Resolution Electroelution of Polyacrylamide Gels for the Purification of Single Proteins from Mycobacterium tuberculosis Culture Filtrate," *Scandinavian Journal of Immunology*, vol. 51, no. 1, pp. 79–86, 2000.
- [212] A. Shafferman, A. Zvi, N. Ariel, J. Fulkerson, R. Sun, R. Chang, and J. C. Sadoff, "Recombinant BCG tuberculosis vaccine designed to elicit immune responses to ...," 767060902-Mar-2010.
- [213] A. S. Pym, P. Brodin, L. Majlessi, R. Brosch, C. Demangel, A. Williams, K. E. Griffiths, G. Marchal, C. Leclerc, and S. T. Cole, "Recombinant BCG exporting

- ESAT-6 confers enhanced protection against tuberculosis," *Nat Med*, vol. 9, no. 5, pp. 533–539, May 2003.
- [214] G. Eulenburg, V. A. Higman, A. Diehl, M. Wilmanns, and S. J. Holton, "Structural and biochemical characterization of Rv2140c, a phosphatidylethanolamine-binding protein from *Mycobacterium tuberculosis*," *FEBS Lett.*, vol. 587, no. 18, pp. 2936–2942, Sep. 2013.
- [215] F. Bollengier and A. Mahler, "Isolation and partial biochemical characterization of an unknown polypeptide from white and grey brain material," *Neuropeptides*, vol. 1, no. 2, pp. 119–135, Sep. 1980.
- [216] I. Bernier and P. Jollès, "Purification and characterization of a basic 23 kDa cytosolic protein from bovine brain," *Biochimica et Biophysica Acta (BBA) - Protein Structure and Molecular Enzymology*, vol. 790, no. 2, pp. 174–181, Oct. 1984.
- [217] I. Bernier, J.-P. Tresca, and P. Jollès, "Ligand-binding studies with a 23 kDa protein purified from bovine brain cytosol," *Biochimica et Biophysica Acta (BBA) - Protein Structure and Molecular Enzymology*, vol. 871, no. 1, pp. 19–23, May 1986.
- [218] J. Mima, M. Hayashida, T. Fujii, Y. Narita, R. Hayashi, M. Ueda, and Y. Hata, "Structure of the Carboxypeptidase Y Inhibitor IC in Complex with the Cognate Proteinase Reveals a Novel Mode of the Proteinase–Protein Inhibitor Interaction," *Journal of Molecular Biology*, vol. 346, no. 5, pp. 1323–1334, Mar. 2005.
- [219] Y. Otsuka and K. Ojika, "Demonstration and characterization of hippocampal cholinergic neurostimulating peptide (HCNP) processing enzyme activity in rat hippocampus," *Neurochem. Res.*, vol. 21, no. 3, pp. 369–376, Mar. 1996.
- [220] C. Atmanene, A. Laux, E. Glattard, A. Muller, F. Schoentgen, M.-H. Metz-Boutigue, D. Aunis, A. Van Dorsselaer, G. B. Stefano, S. Sanglier-Cianférani, and Y. Goumon, "Characterization of human and bovine phosphatidylethanolamine-binding protein (PEBP/RKIP) interactions with morphine and morphine-glucuronides determined by noncovalent mass spectrometry," *Med. Sci. Monit.*, vol. 15, no. 7, pp. BR178–187, Jul. 2009.
- [221] E. T. Keller, Z. Fu, and M. Brennan, "The role of Raf kinase inhibitor protein (RKIP) in health and disease," *Biochem. Pharmacol.*, vol. 68, no. 6, pp. 1049–1053, Sep. 2004.
- [222] J. M. Sedivy, "Phosphatidylethanolamine Binding Protein aka Raf Kinase Inhibitor Protein: A Brief History of Its Discovery and the Remarkable Diversity of Biological Functions," *Forum on Immunopathological Diseases and Therapeutics*, vol. 2, no. 1, pp. 1–12, 2011.
- [223] Z. Fu, P. C. Smith, L. Zhang, M. A. Rubin, R. L. Dunn, Z. Yao, and E. T. Keller, "Effects of raf kinase inhibitor protein expression on suppression of prostate cancer metastasis," *J. Natl. Cancer Inst.*, vol. 95, no. 12, pp. 878–889, Jun. 2003.
- [224] K. T. Mc Henry, S. V. Ankala, A. K. Ghosh, and G. Fenteany, "A Non-Antibacterial Oxazolidinone Derivative that Inhibits Epithelial Cell Sheet Migration," *ChemBioChem*, vol. 3, no. 11, pp. 1105–1111, 2002.
- [225] S. Zhu, K. T. Mc Henry, W. S. Lane, and G. Fenteany, "A chemical inhibitor reveals the role of Raf kinase inhibitor protein in cell migration," *Chem. Biol.*, vol. 12, no. 9, pp. 981–991, Sep. 2005.

- [226] A. N. Shemon, E. M. Eves, M. C. Clark, G. Heil, A. Granovsky, L. Zeng, A. Imamoto, S. Koide, and M. R. Rosner, "Raf Kinase Inhibitory Protein Protects Cells against Locostatin-Mediated Inhibition of Migration," *PLoS ONE*, vol. 4, no. 6, p. e6028, Jun. 2009.
- [227] M. E. Lau, J. A. Loughman, and D. A. Hunstad, "YbcL of Uropathogenic *Escherichia coli* Suppresses Transepithelial Neutrophil Migration," *Infect. Immun.*, Sep. 2012.
- [228] G. Palmieri, E. Langella, M. Gogliettino, M. Saviano, G. Pocsfalvi, and M. Rossi, "A novel class of protease targets of phosphatidylethanolamine-binding proteins (PEBP): a study of the acylpeptide hydrolase and the PEBP inhibitor from the archaeon *Sulfolobus solfataricus*," *Mol. BioSyst.*, vol. 6, no. 12, pp. 2498–2507, Nov. 2010.
- [229] G. Palmieri, G. Catara, M. Saviano, E. Langella, M. Gogliettino, and M. Rossi, "First Archaeal PEPB-Serine Protease Inhibitor from *Sulfolobus solfataricus* with Noncanonical Amino Acid Sequence in the Reactive-Site Loop," *J. Proteome Res.*, vol. 8, no. 1, pp. 327–334, Jan. 2009.
- [230] K. B. Mullis and F. A. Faloona, "[21] Specific synthesis of DNA in vitro via a polymerase-catalyzed chain reaction," in *Methods in Enzymology*, vol. Volume 155, Ray Wu, Ed. Academic Press, 1987, pp. 335–350.
- [231] K. J. Breslauer, R. Frank, H. Blöcker, and L. A. Marky, "Predicting DNA duplex stability from the base sequence," *PNAS*, vol. 83, no. 11, pp. 3746–3750, Jan. 1986.
- [232] "Oligo Property Scan (MOPS)." [Online]. Available: <https://ecom.mwgdna.com/services/webgist/mops.tcl>. [Accessed: 10-Dec-2012].
- [233] C. Aslanidis and P. J. de Jong, "Ligation-independent cloning of PCR products (LIC-PCR)," *Nucleic Acids Res.*, vol. 18, no. 20, pp. 6069–6074, Oct. 1990.
- [234] R. S. Haun, I. M. Serventi, and J. Moss, "Rapid, reliable ligation-independent cloning of PCR products using modified plasmid vectors," *BioTechniques*, vol. 13, no. 4, pp. 515–518, Oct. 1992.
- [235] G. J. Chen, N. Qiu, C. Karrer, P. Caspers, and M. G. P. Page, "Restriction site-free insertion of PCR products directionally into vectors," *BioTechniques*, vol. 28, no. 3, pp. 498–505.
- [236] T. S. Walter, C. Meier, R. Assenberg, K.-F. Au, J. Ren, A. Verma, J. E. Nettleship, R. J. Owens, D. I. Stuart, and J. M. Grimes, "Lysine Methylation as a Routine Rescue Strategy for Protein Crystallization," *Structure*, vol. 14, no. 11, pp. 1617–1622, Nov. 2006.
- [237] S. C. Gill and P. H. von Hippel, "Calculation of protein extinction coefficients from amino acid sequence data," *Anal. Biochem.*, vol. 182, no. 2, pp. 319–326, Nov. 1989.
- [238] H. Edelhoch, "Spectroscopic determination of tryptophan and tyrosine in proteins," *Biochemistry*, vol. 6, no. 7, pp. 1948–1954, Jul. 1967.
- [239] C. N. Pace, F. Vajdos, L. Fee, G. Grimsley, and T. Gray, "How to measure and predict the molar absorption coefficient of a protein," *Protein Science*, vol. 4, no. 11, pp. 2411–2423, Nov. 1995.
- [240] U. K. Laemmli, "Cleavage of structural proteins during the assembly of the head of bacteriophage T4," *Nature*, vol. 227, no. 5259, pp. 680–685, Aug. 1970.

- [241] J. A. Reynolds and C. Tanford, "Binding of Dodecyl Sulfate to Proteins at High Binding Ratios. Possible Implications for the State of Proteins in Biological Membranes," *PNAS*, vol. 66, no. 3, pp. 1002–1007, Jan. 1970.
- [242] P. Edman, E. Högfeldt, L. G. Sillén, and P.-O. Kinell, "Method for Determination of the Amino Acid Sequence in Peptides," *Acta Chemica Scandinavica*, vol. 4, pp. 283–293, 1950.
- [243] J. Mueller-Dieckmann, "The open-access high-throughput crystallization facility at EMBL Hamburg," *Acta Crystallogr. D Biol. Crystallogr.*, vol. 62, no. Pt 12, pp. 1446–1452, Dec. 2006.
- [244] N. E. Chayen, "Comparative Studies of Protein Crystallization by Vapour-Diffusion and Microbatch Techniques," *Acta Crystallographica Section D Biological Crystallography*, vol. 54, no. 1, pp. 8–15, Jan. 1998.
- [245] N. E. Chayen, P. D. Shaw Stewart, D. L. Maeder, and D. M. Blow, "An automated system for micro-batch protein crystallization and screening," *Journal of Applied Crystallography*, vol. 23, no. 4, pp. 297–302, Aug. 1990.
- [246] N. E. Chayen, "The role of oil in macromolecular crystallization," *Structure*, vol. 5, no. 10, pp. 1269–1274, Oct. 1997.
- [247] J. C. van Kessel and G. F. Hatfull, "Recombineering in *Mycobacterium tuberculosis*," *Nat. Methods*, vol. 4, no. 2, pp. 147–152, Feb. 2007.
- [248] J. C. van Kessel and G. F. Hatfull, "Mycobacterial recombineering," *Methods Mol. Biol.*, vol. 435, pp. 203–215, 2008.
- [249] E. M. Southern, "Detection of specific sequences among DNA fragments separated by gel electrophoresis," *Journal of Molecular Biology*, vol. 98, no. 3, pp. 503–517, Nov. 1975.
- [250] H. J. Hölte, W. Ankenbauer, K. Mühlegger, R. Rein, G. Sagner, R. Seibl, and T. Walter, "The digoxigenin (DIG) system for non-radioactive labelling and detection of nucleic acids--an overview," *Cell. Mol. Biol. (Noisy-le-grand)*, vol. 41, no. 7, pp. 883–905, Nov. 1995.
- [251] T. Maniatis, E. F. Fritsch, J. Sambrook, C. Bachmann-Waldmann, S. Jentsch, H. Tobler, F. Müller, T. R. Bachvaroff, M. P. Blanc, D. Humair, D. Hernández Felipe, J.-M. Neuhaus, N. Paris, B. A. Bühler, J. E. Stanek, A. Toulmay, R. Schneiter, F. Mauch, B. Mauch-Mani, C. Gaille, B. Kull, D. Haas, and C. Reimann, "Molecular cloning : a laboratory manual / J. Sambrook, E.F. Fritsch, T. Maniatis," 1989.
- [252] T. Wiseman, S. Williston, J. F. Brandts, and L.-N. Lin, "Rapid measurement of binding constants and heats of binding using a new titration calorimeter," *Analytical Biochemistry*, vol. 179, no. 1, pp. 131–137, May 1989.
- [253] J. Gibbs, "On the equilibrium of heterogeneous substances," *Trans. Connect. Acad. Sci.*, vol. 3, pp. 108–248, 1876.
- [254] H. Helmholtz, "Die thermodynamik chemischer vorgänge," *Sitzungsber. Preussische Akad. Wissensch. Berlin*, pp. 22–39, 1882.
- [255] W. B. Turnbull and A. H. Daranas, "On the Value of c: Can Low Affinity Systems Be Studied by Isothermal Titration Calorimetry?," *Journal of the American Chemical Society*, vol. 125, no. 48, pp. 14859–14866, Dec. 2003.
- [256] A. E. Granovsky, M. C. Clark, D. McElheny, G. Heil, J. Hong, X. Liu, Y. Kim, G. Joachimiak, A. Joachimiak, S. Koide, and M. R. Rosner, "Raf Kinase Inhibitory Protein Function Is Regulated via a Flexible Pocket and Novel

- Phosphorylation-Dependent Mechanism," *Mol. Cell. Biol.*, vol. 29, no. 5, pp. 1306–1320, Mar. 2009.
- [257] Y.-H. Chen, J. T. Yang, and K. H. Chau, "Determination of the helix and β form of proteins in aqueous solution by circular dichroism," *Biochemistry*, vol. 13, no. 16, pp. 3350–3359, Jul. 1974.
- [258] G. L. Ellman, "Tissue sulfhydryl groups," *Archives of Biochemistry and Biophysics*, vol. 82, no. 1, pp. 70–77, May 1959.
- [259] L. Michaelis and M. M. L. Menten, "The kinetics of invertin action: Translated by T.R.C. Boyde Submitted 4 February 1913," *FEBS Lett.*, vol. 587, no. 17, pp. 2712–2720, Sep. 2013.
- [260] L. J. McGuffin, K. Bryson, and D. T. Jones, "The PSIPRED protein structure prediction server," *Bioinformatics*, vol. 16, no. 4, pp. 404–405, Apr. 2000.
- [261] J. Söding, A. Biegert, and A. N. Lupas, "The HHpred interactive server for protein homology detection and structure prediction," *Nucleic Acids Res.*, vol. 33, no. Web Server issue, pp. W244–W248, Jul. 2005.
- [262] R. Chosed, D. R. Tomchick, C. A. Brautigam, S. Mukherjee, V. S. Negi, M. Machius, and K. Orth, "Structural Analysis of Xanthomonas XopD Provides Insights into Substrate Specificity of Ubiquitin-like Protein Proteases," *Journal of Biological Chemistry*, vol. 282, no. 9, pp. 6773–6782, Mar. 2007.
- [263] E. Mossesso and C. D. Lima, "Ulp1-SUMO crystal structure and genetic analysis reveal conserved interactions and a regulatory element essential for cell growth in yeast," *Mol. Cell*, vol. 5, no. 5, pp. 865–876, May 2000.
- [264] T. Zor, R. N. De Guzman, H. J. Dyson, and P. E. Wright, "Solution structure of the KIX domain of CBP bound to the transactivation domain of c-Myb," *J. Mol. Biol.*, vol. 337, no. 3, pp. 521–534, Mar. 2004.
- [265] R. Linding, R. B. Russell, V. Neduva, and T. J. Gibson, "GlobPlot: Exploring protein sequences for globularity and disorder," *Nucleic Acids Res.*, vol. 31, no. 13, pp. 3701–3708, Jul. 2003.
- [266] N. Eswar, B. Webb, M. A. Marti-Renom, M. S. Madhusudhan, D. Eramian, M.-Y. Shen, U. Pieper, and A. Sali, "Comparative protein structure modeling using MODELLER," *Curr Protoc Protein Sci*, vol. Chapter 2, p. Unit 2.9, Nov. 2007.
- [267] P. J. Lupardus, A. Shen, M. Bogyo, and K. C. Garcia, "Small Molecule-Induced Allosteric Activation of the Vibrio cholerae RTX Cysteine Protease Domain," *Science*, vol. 322, no. 5899, pp. 265–268, Oct. 2008.
- [268] H. P. Erickson, "Size and Shape of Protein Molecules at the Nanometer Level Determined by Sedimentation, Gel Filtration, and Electron Microscopy," *Biol Proced Online*, vol. 11, pp. 32–51, May 2009.
- [269] R. Sousa, "Use of glycerol, polyols and other protein structure stabilizing agents in protein crystallization," *Acta Crystallographica Section D Biological Crystallography*, vol. 51, no. 3, pp. 271–277, May 1995.
- [270] V. Vagenende, M. G. S. Yap, and B. L. Trout, "Mechanisms of protein stabilization and prevention of protein aggregation by glycerol," *Biochemistry*, vol. 48, no. 46, pp. 11084–11096, Nov. 2009.
- [271] L. Reinhard, H. Mayerhofer, A. Geerlof, J. Mueller-Dieckmann, and M. S. Weiss, "Optimization of protein buffer cocktails using Thermofluor," *Acta Crystallogr. Sect. F Struct. Biol. Cryst. Commun.*, vol. 69, no. Pt 2, pp. 209–214, Feb. 2013.

- [272] K. Tsumoto, M. Umetsu, I. Kumagai, D. Ejima, J. S. Philo, and T. Arakawa, "Role of Arginine in Protein Refolding, Solubilization, and Purification," *Biotechnology Progress*, vol. 20, no. 5, pp. 1301–1308, Jan. 2004.
- [273] U. Das, G. Hariprasad, A. S. Ethayathulla, P. Manral, T. K. Das, S. Pasha, A. Mann, M. Ganguli, A. K. Verma, R. Bhat, S. K. Chandrayan, S. Ahmed, S. Sharma, P. Kaur, T. P. Singh, and A. Srinivasan, "Inhibition of Protein Aggregation: Supramolecular Assemblies of Arginine Hold the Key," *PLoS ONE*, vol. 2, no. 11, p. e1176, Nov. 2007.
- [274] A. P. Golovanov, G. M. Hautbergue, S. A. Wilson, and L.-Y. Lian, "A Simple Method for Improving Protein Solubility and Long-Term Stability," *J. Am. Chem. Soc.*, vol. 126, no. 29, pp. 8933–8939, 2004.
- [275] L. Ito, K. Shiraki, and H. Yamaguchi, "Comparative analysis of amino acids and amino-acid derivatives in protein crystallization," *Acta Crystallogr. Sect. F Struct. Biol. Cryst. Commun.*, vol. 66, no. Pt 6, pp. 744–749, Jun. 2010.
- [276] W. N. Price II, Y. Chen, S. K. Handelman, H. Neely, P. Manor, R. Karlin, R. Nair, J. Liu, M. Baran, J. Everett, S. N. Tong, F. Forouhar, S. S. Swaminathan, T. Acton, R. Xiao, J. R. Luft, A. Lauricella, G. T. DeTitta, B. Rost, G. T. Montelione, and J. F. Hunt, "Understanding the physical properties that control protein crystallization by analysis of large-scale experimental data," *Nat Biotech*, vol. 27, no. 1, pp. 51–57, Jan. 2009.
- [277] L. Goldschmidt, D. R. Cooper, Z. S. Derewenda, and D. Eisenberg, "Toward rational protein crystallization: A Web server for the design of crystallizable protein variants," *Protein Science*, vol. 16, no. 8, pp. 1569–1576, 2007.
- [278] A. Dong, X. Xu, and A. M. Edwards, "In situ proteolysis for protein crystallization and structure determination," *Nat Meth*, vol. 4, no. 12, pp. 1019–1021, Dec. 2007.
- [279] A. Wernimont and A. Edwards, "In Situ Proteolysis to Generate Crystals for Structure Determination: An Update," *PLoS ONE*, vol. 4, no. 4, p. e5094, Apr. 2009.
- [280] A. Savchenko, A. Yee, A. Khachatryan, T. Skarina, E. Evdokimova, M. Pavlova, A. Semesi, J. Northey, S. Beasley, N. Lan, R. Das, M. Gerstein, C. H. Arrowmith, and A. M. Edwards, "Strategies for structural proteomics of prokaryotes: Quantifying the advantages of studying orthologous proteins and of using both NMR and X-ray crystallography approaches," *Proteins: Structure, Function, and Bioinformatics*, vol. 50, no. 3, pp. 392–399, 2003.
- [281] R. M. Jones, H. Wu, C. Wentworth, L. Luo, L. Collier-Hyams, and A. S. Neish, "Salmonella AvrA Coordinates Suppression of Host Immune and Apoptotic Defenses via JNK Pathway Blockade," *Cell Host & Microbe*, vol. 3, no. 4, pp. 233–244, Apr. 2008.
- [282] M. A. Larkin, G. Blackshields, N. P. Brown, R. Chenna, P. A. McGettigan, H. McWilliam, F. Valentin, I. M. Wallace, A. Wilm, R. Lopez, J. D. Thompson, T. J. Gibson, and D. G. Higgins, "Clustal W and Clustal X version 2.0," *Bioinformatics*, vol. 23, no. 21, pp. 2947–2948, Nov. 2007.
- [283] Z. Ben-Barak, W. Streckel, S. Yaron, S. Cohen, R. Prager, and H. Tschäpe, "The expression of the virulence-associated effector protein gene *avrA* is dependent on a *Salmonella enterica*-specific regulatory function," *International Journal of Medical Microbiology*, vol. 296, no. 1, pp. 25–38, Feb. 2006.

- [284] L. Zhan, L. Yang, L. Zhou, Y. Li, H. Gao, Z. Guo, L. Zhang, C. Qin, D. Zhou, and R. Yang, "Direct and negative regulation of the *sycO-ypkA-yopJ* operon by cyclic AMP receptor protein (CRP) in *Yersinia pestis*," *BMC Microbiology*, vol. 9, no. 1, p. 178, Aug. 2009.
- [285] M. Letzelter, I. Sorg, L. J. Mota, S. Meyer, J. Stalder, M. Feldman, M. Kuhn, I. Callebaut, and G. R. Cornelis, "The discovery of SycO highlights a new function for type III secretion effector chaperones," *EMBO J*, vol. 25, no. 13, pp. 3223–3233, Jul. 2006.
- [286] K. Trülsch, A. Roggenkamp, M. Aepfelbacher, G. Wilharm, K. Ruckdeschel, and J. Heesemann, "Analysis of chaperone-dependent Yop secretion/translocation and effector function using a mini-virulence plasmid of *Yersinia enterocolitica*," *Int. J. Med. Microbiol.*, vol. 293, no. 2–3, pp. 167–177, Jun. 2003.
- [287] S. Dittmann, A. Schmid, S. Richter, K. Trülsch, J. Heesemann, and G. Wilharm, "The *Yersinia enterocolitica* type three secretion chaperone SycO is integrated into the Yop regulatory network and binds to the Yop secretion protein YscM1," *BMC Microbiology*, vol. 7, no. 1, p. 67, 2007.
- [288] J. F. Ohren, H. Chen, A. Pavlovsky, C. Whitehead, E. Zhang, P. Kuffa, C. Yan, P. McConnell, C. Spessard, C. Banotai, W. T. Mueller, A. Delaney, C. Omer, J. Sebolt-Leopold, D. T. Dudley, I. K. Leung, C. Flamme, J. Warmus, M. Kaufman, S. Barrett, H. Tecle, and C. A. Hasemann, "Structures of human MAP kinase kinase 1 (MEK1) and MEK2 describe novel noncompetitive kinase inhibition," *Nat Struct Mol Biol*, vol. 11, no. 12, pp. 1192–1197, Dec. 2004.
- [289] T. O. Fischmann, C. K. Smith, T. W. Mayhood, J. E. Myers, P. Reichert, A. Mannarino, D. Carr, H. Zhu, J. Wong, R.-S. Yang, H. V. Le, and V. S. Madison, "Crystal Structures of MEK1 Binary and Ternary Complexes with Nucleotides and Inhibitors," *Biochemistry*, vol. 48, no. 12, pp. 2661–2674, Mar. 2009.
- [290] D. Busso, Y. Peleg, T. Heidebrecht, C. Romier, Y. Jacobovitch, A. Dantes, L. Salim, E. Troesch, A. Schuetz, U. Heinemann, G. E. Folkers, A. Geerlof, M. Wilmanns, A. Polewacz, C. Quedenau, K. Büsow, R. Adamson, E. Blagova, J. Walton, J. L. Cartwright, L. E. Bird, R. J. Owens, N. S. Berrow, K. S. Wilson, J. L. Sussman, A. Perrakis, and P. H. N. Celie, "Expression of protein complexes using multiple *Escherichia coli* protein co-expression systems: a benchmarking study," *J. Struct. Biol.*, vol. 175, no. 2, pp. 159–170, Aug. 2011.
- [291] "PeptideMass." [Online]. Available: http://web.expasy.org/peptide_mass/. [Accessed: 11-Aug-2013].
- [292] M. R. Wilkins, I. Lindskog, E. Gasteiger, A. Bairoch, J. C. Sanchez, D. F. Hochstrasser, and R. D. Appel, "Detailed peptide characterization using PEPTIDEMASS--a World-Wide-Web-accessible tool," *Electrophoresis*, vol. 18, no. 3–4, pp. 403–408, Apr. 1997.
- [293] H. Lineweaver and D. Burk, "The Determination of Enzyme Dissociation Constants," *J. Am. Chem. Soc.*, vol. 56, no. 3, pp. 658–666, Mar. 1934.
- [294] J. D. Thompson, D. G. Higgins, and T. J. Gibson, "CLUSTAL W: improving the sensitivity of progressive multiple sequence alignment through sequence weighting, position-specific gap penalties and weight matrix choice," *Nucleic Acids Res.*, vol. 22, no. 22, pp. 4673–4680, Nov. 1994.

- [295] J. D. Peterson, L. A. Umayam, T. Dickinson, E. K. Hickey, and O. White, "The Comprehensive Microbial Resource," *Nucleic Acids Res.*, vol. 29, no. 1, pp. 123–125, Jan. 2001.
- [296] S. C. Birtalan, R. M. Phillips, and P. Ghosh, "Three-dimensional secretion signals in chaperone-effector complexes of bacterial pathogens," *Mol. Cell*, vol. 9, no. 5, pp. 971–980, May 2002.
- [297] A. Shen, P. J. Lupardus, M. M. Gersch, A. W. Puri, V. E. Albrow, K. C. Garcia, and M. Bogyo, "Defining an allosteric circuit in the cysteine protease domain of *Clostridium difficile* toxins," *Nat Struct Mol Biol*, vol. 18, no. 3, pp. 364–371, Mar. 2011.
- [298] A. W. Puri, P. J. Lupardus, E. Deu, V. E. Albrow, K. C. Garcia, M. Bogyo, and A. Shen, "Rational Design of Inhibitors and Activity-Based Probes Targeting *Clostridium difficile* Virulence Factor TcdB," *Chemistry & Biology*, vol. 17, no. 11, pp. 1201–1211, Nov. 2010.
- [299] H. Yang, Y. Ke, J. Wang, Y. Tan, S. K. Myeni, D. Li, Q. Shi, Y. Yan, H. Chen, Z. Guo, Y. Yuan, X. Yang, R. Yang, and Z. Du, "Insight into Bacterial Virulence Mechanisms against Host Immune Response via the *Yersinia pestis*-Human Protein-Protein Interaction Network," *Infect. Immun.*, vol. 79, no. 11, pp. 4413–4424, Jan. 2011.
- [300] M. D. Dyer, C. Neff, M. Dufford, C. G. Rivera, D. Shattuck, J. Bassaganya-Riera, T. M. Murali, and B. W. Sobral, "The Human-Bacterial Pathogen Protein Interaction Networks of *Bacillus anthracis*, *Francisella tularensis*, and *Yersinia pestis*," *PLoS ONE*, vol. 5, no. 8, p. e12089, 2010.
- [301] N. A. Thomas, I. Ma, M. E. Prasad, and C. Rafuse, "Expanded Roles for Multicargo and Class 1B Effector Chaperones in Type III Secretion," *J. Bacteriol.*, vol. 194, no. 15, pp. 3767–3773, Jan. 2012.
- [302] C. Bieniossek, Y. Nie, D. Frey, N. Olieric, C. Schaffitzel, I. Collinson, C. Romier, P. Berger, T. J. Richmond, M. O. Steinmetz, and I. Berger, "Automated unrestricted multigene recombineering for multiprotein complex production," *Nat. Methods*, vol. 6, no. 6, pp. 447–450, Jun. 2009.
- [303] S. Stewart, M. Sundaram, Y. Zhang, J. Lee, M. Han, and K. L. Guan, "Kinase suppressor of Ras forms a multiprotein signaling complex and modulates MEK localization," *Mol. Cell Biol.*, vol. 19, no. 8, pp. 5523–5534, Aug. 1999.
- [304] H. Bisswanger, *Enzyme Kinetics*. John Wiley & Sons, 2008.
- [305] D. R. Alessi, Y. Saito, D. G. Campbell, P. Cohen, G. Sivanandam, U. Rapp, A. Ashworth, C. J. Marshall, and S. Cowley, "Identification of the sites in MAP kinase kinase-1 phosphorylated by p74raf-1," *EMBO J.*, vol. 13, no. 7, pp. 1610–1619, Apr. 1994.
- [306] "Kinexus | PhosphoNET." [Online]. Available: <http://www.phosphonet.ca/>. [Accessed: 10-Aug-2013].
- [307] R. Roskoski Jr, "MEK1/2 dual-specificity protein kinases: structure and regulation," *Biochem. Biophys. Res. Commun.*, vol. 417, no. 1, pp. 5–10, Jan. 2012.
- [308] D. F. Brennan, A. C. Dar, N. T. Hertz, W. C. H. Chao, A. L. Burlingame, K. M. Shokat, and D. Barford, "A Raf-induced allosteric transition of KSR stimulates phosphorylation of MEK," *Nature*, vol. 472, no. 7343, pp. 366–369, Apr. 2011.

- [309] J. E. Trosky, Y. Li, S. Mukherjee, G. Keitany, H. Ball, and K. Orth, "VopA inhibits ATP binding by acetylating the catalytic loop of MAPK kinases," *J. Biol. Chem.*, vol. 282, no. 47, pp. 34299–34305, Nov. 2007.
- [310] N. Shrestha, W. Bahnan, D. J. Wiley, G. Barber, K. A. Fields, and K. Schesser, "eIF2 signaling regulates pro-inflammatory cytokine expression and bacterial invasion," *J. Biol. Chem.*, Jul. 2012.
- [311] C. M. Sassetti and E. J. Rubin, "Genetic requirements for mycobacterial survival during infection," *PNAS*, vol. 100, no. 22, pp. 12989–12994, Oct. 2003.
- [312] C. M. Sassetti, D. H. Boyd, and E. J. Rubin, "Genes required for mycobacterial growth defined by high density mutagenesis," *Mol. Microbiol.*, vol. 48, no. 1, pp. 77–84, Apr. 2003.
- [313] S. Theroux, M. Pereira, K. S. Casten, R. D. Burwell, K. C. Yeung, J. M. Sedivy, and J. Klysik, "Raf kinase inhibitory protein knockout mice: expression in the brain and olfaction deficit," *Brain Res. Bull.*, vol. 71, no. 6, pp. 559–567, Mar. 2007.
- [314] B. Khatri, M. Fielder, G. Jones, W. Newell, M. Abu-Oun, and P. R. Wheeler, "High Throughput Phenotypic Analysis of Mycobacterium tuberculosis and Mycobacterium bovis Strains' Metabolism Using Biolog Phenotype Microarrays," *PLoS ONE*, vol. 8, no. 1, p. e52673, Jan. 2013.
- [315] M. Maestre-Reyna, R. Diderrich, M. S. Veelders, G. Eulenburg, V. Kalugin, S. Brückner, P. Keller, S. Rupp, H.-U. Mösch, and L.-O. Essen, "Structural basis for promiscuity and specificity during *Candida glabrata* invasion of host epithelia," *Proc. Natl. Acad. Sci. U.S.A.*, vol. 109, no. 42, pp. 16864–16869, Oct. 2012.

IV. Risk and Safety Statements

Table 17 List of potentially hazardous materials and respective hazard and precautionary statements

Compound	CAS -No.	Supplier	GHS hazard	Hazard Statement	Precautionary Statement
Arcylamide	79-06-1	Roth	07, 08	H340, H350, H361f, H372, H302, H312, H315, H319, H317	P281, P301+P312, P302+P352, P305+P351+P338, P308+P313, P405
Ethidiumbromide	1239-45-8	Roth	06, 08	331, 341	261, 281, 311
Carbenicillin	4800-94-6	Roth	08	H334, H317	P280, P302+P352, P304+P341, P333+P313, P342+P311
Cycloheximide	66-81-9	Roth	06, 08, 09	H300, H341, H360D, H411	P281, P273, P201, P301+P310, P308+P313, P405
Dimethylamineborane complex ABC	74-94-2	Fluka	01, 03	H228, H301 + H311,	P210, P280, P301 + P310, P312
DTT	3483-12-3	Roth	07	H302, H315, H319, H335	P280, P301+P312, P302+P352, P403+P233
EDTA	60-00-4	Roth	07	H319	P280, P264, P305+P351+P338, P337+P313,
Formaldehyde	50-00-0	Roth	05, 06, 08	H301+H311 +H331, H314, H317, H351, H370-H335	P281, P303+P361+P353, P304+P340, P305+P351+P338, P308, P310
HygB	31282-04-9	Roth	05, 06, 08	H301, H310, H330, H318, H334, H317	P280, P301+P310, P305+P351+P338, P342+P311, P405
Iodoacetamide	144-48-9	Sigma	06, 08	H301, H317, H334, H413	P261, P280, P301, P310, P342 + P311
Kanamycin	25389-94-0	Roth	08	H360D	P281, P260, P308+P313

Risk and Safety Statements

NaOH	131 0- 73-2	Roth	05	H290, H314	P280, P303+P361+P353, P301+P330+P331, P305+P351+P338, P310, P406
Ni(II)SO ₄	101 01- 97-0	Roth	07, 08, 09	H302, H332, H315, H334, H317, H341, H350i, H360D, H372, H410	P280, P201, P302+P352, P308+P313, P342+P311
TCEP	518 05- 45-9	Sigma		H314	P280, P305 + P351 + P338, P310
DTNB	69- 78-3	Sigma		H315, H319, H335	P261, P305 + P351 + P338

Table 18 Commercial protein crystallization screens and respective risk and safety phrases

Name	Supplier	Risk label	Safety phrases	Risk phrases
Classics suite	Qiagen	T, N	S53, S20, S26, S36/37/39, S45, S61	R45 R46 R60 R61 R10 R 23/25 R 36/37/38 R 48/20/22 R 51/53
Classics II	Qiagen	T, N	S53, S20, S26, S36/37/39, S45, S61	R45 R46 R60 R61 R10 R 23/25 R 36/37/38 R 48/20/22 R 51/53
pH clear	Qiagen	Xi	S26	R36/38
PEG	Qiagen	N	S61	R51/53
PEGII	Qiagen	T, N	S53, S13, S26, S36/37, S45, S61	R45, R10, R36, R51/53
Protein Complex	Qiagen	T	S20, S26, S36/37, S45, S61	R10, R23/25, R38, R41, R52/53

Risk and Safety Statements

OLD		NEW		
Symbols	Description	GHS-Symbols	Description	Hazard statement examples
	E Explosive		GH001 Exploding bomb	Explodes due to fire, shock, friction or heat; danger due to fire, blast and projectiles.
	F+ Extremely flammable F Highly flammable		GH002 Flame	Flammable; catches fire spontaneously if exposed to air; in contact with water releases flammable gases which may ignite spontaneously.
	O Oxidizing		GH003 Flame over circle	May cause fire or explosion; strong oxidizer.
No equivalent			GH004 Gas cylinder	Contains gas under pressure; may explode if heated; contains refrigerated gas; may cause cryogenic burns or injury.
	C Corrosive		GH005 Corrosion	May be corrosive to metals; causes severe skin burns and eye damage.
	T+ Very toxic T Toxic		GH006 Skull and crossbones	Small quantities are harmful or fatal.
	Xn Harmful	No direct equivalent		
	Xi Irritant			
No equivalent			GH007 Exclamation mark	Harmful; irritates eyes, skin or respiratory system; large quantities are fatal.
No direct equivalent			GH008 Health hazard	Causes allergic reactions; may cause cancer; may cause genetic defects; may damage fertility or the unborn child; causes damage to organs.
	N Dangerous for the environment		GH009 Environment	Harmful, toxic or very toxic to aquatic life with long lasting effects.

Figure 51 GHS pictograms (<http://www.mn-net.com/StartpageWaterAnalysisTesting/Customerservice/GHS/tabid/11572/language/en-US/Default.aspx>)

V. Appendix

Acknowledgements

First, I would like to thank Dr. Dr. Matthias Wilmanns for giving me the opportunity to work in his lab in the fascinating field of host-pathogen interactions and for many helpful and inspiring discussions, encouragement as well as for being the second referee of the thesis.

I am also very grateful to Prof. Dr. Dr. Christian Betzel for kindly offering the supervision of the thesis and for helpful discussions.

I am grateful to Prof. Bernd Meyer and Dr. Thomas Hackl for participating in the examination committee of the disputation.

The members of my PhD Thesis Advisory Committee, Dr. Anne-Claude Gavin, Dr. Rob Meijers, Prof. Martin Aepfelbacher and in particular P.D. Dr. Klaus Ruckdeschel I would like to thank for helpful discussions not only during the annual meetings and collaboration on the YopP project.

Moreover, I would like to thank the Heinrich Herz Stiftung for financial support of Hamburger Landesexzellenzinitiative (LEXI) and the graduate “School for Structure and Dynamics in infection” (SDI) along with P.D. Dr. Markus Perbandt for coordinating the schools efforts and for helpful discussions.

I am also grateful to Dr. Simon Holton for the successful collaboration on the Mtb project. I would also like to thank Dr. Dominik Oberthür for help during the DLS experiments.

I am particularly grateful to Drs. Florian Sauer, Felix List, Marie-Cécile Pelissier, Vivian Pogenberg, Spyros Chatziefthimiou, Morlin Milewski, Stephane Boivin, Annabel Parret, Victor Deineko and Matthew Groves for their continuous support in the daily lab work.

Madhankumar Anandakrishnan, Daniel Passon and the long row of visitors in our tiny office were always a good source to extend my horizon beyond Hamburg and Germany.

Last but not least, I am also grateful for the help and encouragement of my family. The support from my parents allowed me to follow my interests and to study the mysteries of chemistry. I owe also thanks to my siblings and their lovely spouses and children for reminding me that there is more than proteins and x-rays in the world.

Curriculum Vitae

Name	Georg Graf zu Eulenburg
Nationality	German
Date of Birth	17.09.1981
Place of Birth	Marburg/Germany
10/2009	Predocctoral Fellow at EMBL-Hamburg EMBL international PhD program/LEXI-SDI Supervisor: Dr. Matthias Wilmanns University Supervisor: Prof. Christian Betzel
10/2002-06/2009	Diploma Student, Philipps Universität Marburg Choice Subject: Biochemistry Diploma Thesis under Supervision of Prof. Dr. L.-O. Essen Titel: Strukturelle und funktionelle Charakterisierung von Adhäsinen von humanpathogen Candida spp.
2001-2002	National Service: Krankenhaus Sachsenhausen, Frankfurt/Main, Germany
1992-2001	High School (Gymnasium): Stiftsschule St. Johann, Amöneburg
1988-1992	Elementary School: Grundschule Kirchhain

Publications:

Parts of this thesis have already been published as:

Structural and biochemical characterization of Rv2140c, a phosphatidylethanolamine-binding protein from *Mycobacterium tuberculosis*

G. Eulenburg, V. A. Higman, A. Diehl, M. Wilmanns, S. J. Holton, *FEBS Lett.* **2013**, *587*, 2936–2942.

Other Publications:

Structural basis for promiscuity and specificity during *Candida glabrata* invasion of host epithelia

M. Maestre-Reyna, R. Diderrich, M. S. Veelders, G. Eulenburg, V. Kalugin, S. Brückner, P. Keller, S. Rupp, H.-U. Mösch, L.-O. Essen, *Proc. Natl. Acad. Sci. U. S. A.* **2012**, *109*, 16864–16869.

Conferences, Poster Presentations and Talks

1. Participation at the 12th International EMBL PhD Student Symposium in Heidelberg, Oct 21-23, 2010
2. Talk at the Institutseminar, Institut für Biochemie und Molekularbiologie, Universität Hamburg, Jul 11, 2011
Title: Understanding *Yersinia* Effector Protein YopP/J
Georg Eulenburg
3. Talk at the 5th International PhD Symposium at the Helmholtz Zentrum für Infektionsforschung, Dec 11, 2011
Title: Molecular Function of *Yersinia* Outer Protein P (YopP)
Georg Eulenburg, Matthias Wilmanns
4. Presentation of a Poster at the Gordon Conference on Microbial Toxins and Pathogenicity held in Waterville Valley, NH, July 8-13, 2012
Title: Structural and Functional Characterization of YopP
Georg Eulenburg, Klaus Ruckdeschel and Matthias Wilmanns

Erklärung

Hiermit erkläre ich, Georg Graf zu Eulenburg an Eides statt, die vorliegende Arbeit selbständig verfasst und keine anderen als die angegebenen Quellen und Hilfsmittel verwendet zu haben.

Diese Dissertation hat weder in gleicher, noch in ähnlicher Form in einem anderen Prüfungsverfahren vorgelegen.

Ich habe außer dieser Dissertation vorher keine weiteren Promotionsversuche unternommen oder an anderer Stelle vorgelegt und außer dem mit dem Zulassungsgesuch urkundlich vorgelegten Grad keine weiteren akademischen Grade erworben oder zu erwerben versucht.

Hamburg, den

Georg Graf zu Eulenburg